**Université de Montréal**

# Investigation of the Effect of Lymphocytic Microparticles on the Activity of Müller Cells in the Oxygen-Induced Retinopathy Mouse Model

**Par**

**ChenRongRong CAI**

**Département de pharmacologie et de physiologie**
**Faculté de médecine**

**Mémoire présenté à la Faculté des études supérieures en vue de l'obtention du grade de maîtrise en pharmacologie, option Générale**

**April 2020**

**Université de Montréal**

**Faculté des études supérieures**

Ce mémoire intitulé :

**Investigation of the Effect of Lymphocytic Microparticles on the Activity of Müller Cells in the Oxygen-Induced Retinopathy Mouse Model**

Présenté par : ChenRongRong Cai

A été évalué par un jury composé des personnes suivantes

Dr Christian Beauséjour

Président-rapporteur

Dr Hardy Pierre

Directeur de recherche

Dre Audrey Claing

Membre du jury

# RÉSUMÉ

La rétinopathie de la prématurité (ROP) est un trouble oculaire potentiellement aveuglant chez les nourrissons prématurés, qui est causé par la formation d'une néovascularisation rétinienne aberrante (NV). Des études récentes ont démontré que les cellules de Müller sont les principaux producteurs de cytokines inductrices d'inflammation et de facteurs de croissance dans des conditions pathologiques. Par ailleurs, le recrutement des macrophages est significativement augmenté au cours de la NV rétinienne, ce qui a un rôle proangiogénique dans la ROP. Par conséquent, nous avons émis l'hypothèse que les LMP inhibent la NV pathologique de la rétine en ciblant les cellules de Müller dans le modèle murin de rétinopathie induite par l'ischémie (OIR). Nous avons démontré que les microparticules lymphocytaires (LMP) dérivées de lymphocytes T CEM humains pendant l'apoptose possèdent une grande capacité angiostatique. Dans notre étude actuelle, nous avons étudié l'effet des LMP *in vitro* et *in vivo*. *In vitro*, l'influence des LMP sur les propriétés des cellules de Müller a été déterminée en utilisant des cellules de Müller de rat rMC-1 et des macrophages murins RAW 264.7. Les résultats ont révélé que les LMP étaient internalisées par rMC-1 et réduisaient la prolifération cellulaire de rMC-1 en fonction de la dose, sans induire l'apoptose cellulaire. Les LMP ont inhibé la capacité chimiotactique de rMC-1 sur RAW 264.7, ainsi que l'expression des chimiokines (VEGF et SDF-1) dans rMC-1. *In vivo*, l'injection intra-vitréenne de LMP a été internalisée par les cellules de Müller. Les LMP ont atténué la NV aberrante de la rétine et l'infiltration des macrophages en partie par l'expression réduite des chimiokines (VEGF et SDF-1). De plus, les LMP régulent la baisse d'expression de ERK1 / 2 et HIF-1α dans les cellules Müller.

Nos résultats actuels élargissent notre compréhension des effets des LMP, fournissant des évidences que les LMPs sont un traitement potentiel pour les maladies rétiniennes en lien avec la NV.

Mots-clés: LMP, effets anti-angiogéniques, cellules de Müller; macrophages, VEGF, SDF-1, le modèle de souris OIR; rétinienne NV

# ABSTRACT

Retinopathy of prematurity (ROP) is a potentially blinding ocular disorder in premature infants. It is caused by the formation of aberrant retinal neovascularization (NV). Recent studies have demonstrated that Müller cells are the primary producers of inflammation-inducing cytokines and growth factors in pathological conditions. Additionally, the recruitment of macrophages is significantly increased during retinal NV, which exerts a proangiogenic role in ROP. Lymphocytic microparticles (LMPs) are small membrane-wrapped vesicles released from human CEM T lymphocytes, which is a cell line of acute lymphoblastic leukemia. In our previous studies, we demonstrated that LMPs derived from apoptosis-induced human CEM T lymphocytes possess potent angiostatic capacities. Therefore, we hypothesized that LMPs inhibit pathological retinal NV via targeting Müller cells in an ischemia-induced retinopathy mouse model. In this study, we investigated the effect of LMPs both *in vitro* and *in vivo*. *In vitro*, we determined the influence of LMPs on Müller cell properties using rat Müller cells rMC-1 and murine macrophages RAW 264.7. The results revealed that LMPs were internalized and reduced cell proliferation of rMC-1 dose-dependently without inducing cell apoptosis. LMPs also inhibited the chemotactic capacity of rMC-1 on RAW 264.7, as well as the expression of the chemokines (VEGF and SDF-1) in rMC-1. *In vivo*, we intravitreally injected LMPs and found that LMPs was internalized by Müller cells. LMPs attenuated aberrant retinal NV and the infiltration of macrophages. LMPs also downregulated the expression of angiogenic factors/chemokines (VEGF and SDF-1) in Müller cells. Furthermore, LMPs downregulated the expression of ERK1/2 and HIF-1α in Müller cells. These findings expand our understanding of the effects of LMPs, providing evidence that LMPs are a potential treatment for retinal NV diseases.

**Keywords:** LMPs, anti-angiogenic effects, Müller cells; macrophages, VEGF, SDF-1, the OIR mouse model; retinal NV

# TABLE OF CONTENTS

# LIST OF TABLES



# LIST OF FIGURES

**Chapter 1: INTRODUCTION**

**Chapter 2: MATERIAL AND METHODS**



**Chapter 3: RESULTS**



**Chapter 4: DISCUSSION**

# LIST OF ABBREVIATIONS

| | |
|---|---|
| AMD | Age-related macular degeneration |
| BM | Basement membrane |
| BRB | Blood-retinal barrier |
| ECM | Extracellular matrix |
| ERK1/2 | Extracellular signal-regulated kinase 1/2 |
| EVs | Extracellular vesicles |
| GCL | Ganglion cell layer |
| GPCR | G-protein coupled receptor |
| GS | Glutamate synthetase |
| GFAP | Glial fibrillary acidic protein |
| HIF-1α | Hypoxia-induced factor 1α |
| IL | Interleukin |
| INL | Inner nuclear layer |
| IPL | Inner plexiform layer |
| ILM | Inner limiting membrane |
| LDLR | Low-density lipoprotein receptor |
| LMPs | Lymphocytic microparticles |
| MMPs | Matrix metalloproteinases |
| NO | Nitric oxide |
| NFL | Nerve fiber layer |
| NV | Neovascularization |
| OIR | Oxygen-induced retinopathy |
| ONL | Outer nuclear layer |
| OPL | Outer plexiform layer |

| | |
|---|---|
| OLM | Outer limiting membrane |
| ROP | Retinopathy of prematurity |
| ROS | Reactive oxygen species |
| RPE | Retinal pigment epithelium |
| VEGF | Vascular endothelial growth factor |

# ACKNOWLEDGEMENTS

First of all, I would like to express my deepest gratitude to my supervisor Dr. Pierre Hardy, for giving me the opportunity to pursue my master's degree. Thank you for letting me attend so many conferences and offering me the precious opportunities to learn and grow. I really appreciate your overwhelming support during the last three years. Without your persistent help, the goal of this project would not have been realized. Without your cultivation, I could not have become the person I am today.

A million times, thank you.

To Professor Beausejour, it was such a great pleasure to meet you in person. Thank you for coming to see my oral presentation, and thank you for your acknowledgment of my work. Thank you so much for all the supports and help.

To Professor Cardinal, thank you so much for all the document work, support, and academic suggestions. I would not have obtained the scholarship of tuition fee exemption without your help. Thank you for considering my situation and always trying to find solutions to my problem.

A million times, thank you.

To Professor Claing, it was such a great pleasure to attend your course. I still remember the day I went to your office asking questions about the course. You were so patient, friendly, and kind. Thank you for all the supports.

To Chun Yang, the most brilliant and kindest human being on earth. Thank you for the never-ending patience, caring, and support. Thank you for the things you taught me from your life

experience. Thank you for bringing the green lives to the lab; those beautiful little green plants lightened me up every single day.

To Carmen Gagnon, thank you for organizing the wet lab. Thank you for all the technical skills that you taught me. I really admire the way you work; you are the gold standard in the lab. Thank you for also sharing all those fun activities in Montreal, and for giving me the guidebook for Quebec city. Thank you as well for inviting me to the winter sports.

To Houda Tahiri, thank you for correcting my silly mistakes all the time, and thank you for all the computer skills you taught me. Without you, the lab would not have been well organized. Thank you for dedicating yourself to the lab.

I would also like to express my sincere appreciation to the Faculty of Medicine for offering me the international student tuition fee exemption and the MERIT scholarships. Without financial support, I could not have succeeded in my studies.

I would also like to thank my favorite people, my best friends, who are the most amazing people I have ever met in my entire life: Vitor, Gabrielle, Nissan, Angela, Nadine, Rasheda, Simon, Marie-Lyn, and Hyunyun. Thank you for the hugs, positive vibes, and never-ending supports. I also greatly appreciate the amazing teachers and other incredible people I have met at school during the class or at the research center. I am so blessed to meet you all during this journey.

Finally, I wish to acknowledge the support and great love of my family. Thank you for the unconditional support, love, and endless caring. You are the ones who kept me going, and I could not have make this far without them. Thank you for everything, I hope I can make you proud.

# Chapter 1
# INTRODUCTION

## 1.1 EYE

There is an old saying that eyes are the window to the souls. From the scientific perspective, eyes are the complex optical system responsible for receiving and processing visual details from the surrounding environment [1]. Eyes are endowed with the capacity for light-detection and the conversion of electrical-chemical impulses in the neurons [2]. It is essential to understand the constituents and the functions of each component of the eye to better comprehend their role in the pathogenesis of ocular diseases. The eye is composed of three distinct layers: (a) the outermost layer, which consists of the cornea and sclera; (b) the intermediate layer which is formed by the iris, ciliary body, and choroid; (c) and the retina, which forms the innermost layer. In addition, there are three transparent structures that are surrounded by these layers: aqueous, lens, and vitreous (see Figure 1) [3].

**Figure 1.** ***Components of the Human Eye***

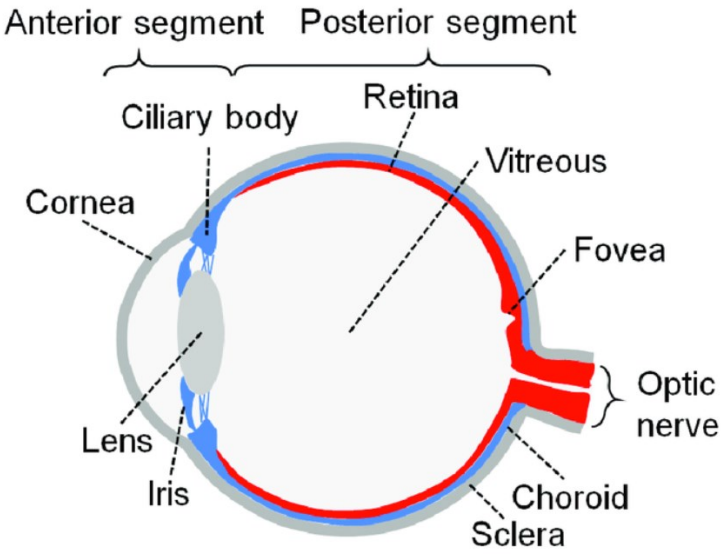

***Note***. The eye is composed of three distinct layers: the outermost layer: cornea and sclera; the intermediate layer: iris, ciliary body, and choroid; the innermost layer: retina. In addition, three transparent structures are surrounded by these layers: aqueous, lens, and vitreous. (reprinted from Katherine et al., 2017 [4]).

### 1.1.1 The Outermost Layer of the Eye

The outermost part of the eye is made up of the cornea and the sclera. The cornea is a transparent tissue that refracts and transmits light to the retina. In addition, it also protects the eyes against external insults, such as infections and mechanical injuries[5]. The sclera is connected with the cornea at the limbus, which is essential for preserving the configuration of the eye by forming connective tissues [5].

#### 1.1.1.1 Cornea

The human cornea is composed of five distinct layers (from the innermost to the outermost): the endothelium, Descemet's membrane, the stroma, Bowman's layer, and the epithelium (see Figure 2) [5].

**Figure 2.** ***The Diagram of Distinct Layers of the Cornea***

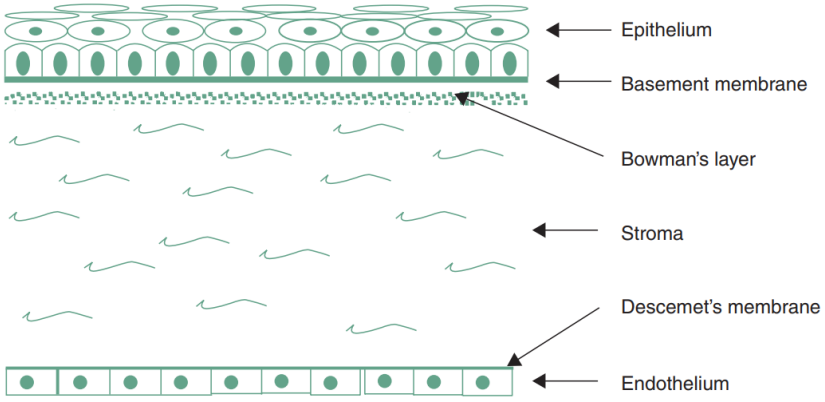


***Note.*** The cornea is composed of five distinct layers: the endothelium, Descemet's membrane, the stroma, Bowman's layer, and the epithelium. (reprinted from Collin et al., 2010 [3]).

The endothelium of the cornea is formed of a single layer of cuboid-shaped endothelial cells with a limited self-proliferating capacity. The endothelium is endowed with ion transport systems, which creates an osmotic difference between the stroma and aqueous. The osmotic gradient is vital for ensuring constant fluid in the stroma and is important for cornea transparency [3]. The Descemet's membrane is secreted by the cornea's endothelium cells and segregates the endothelium from the stroma [3].

The stroma of the cornea is a 500-µm-thickness tissue that is critical for maintaining the integrity of the cornea [5]. Keratocytes, the predominant cell types in the stroma, are an important source of proteoglycans and collagen productions. Keratocytes-secreted proteoglycans and collagens are fundamental for the structural maintenance and the clarity of the cornea [3]. The extracellular matrix (ECM) of the stroma is responsible for the flexibility of the cornea [3].

The outermost layer of the cornea, the epithelium, is separated from the stroma by Bowman's layer. The cornea epithelium is composed of layers of distinct cellular types: superficial cells, wing cells, and basal cells, which are supplemented by the pluripotent stem cells every 7 to 10 days [3].

The cornea epithelium is responsible for oxygen and nutrient absorption from the tear and also protects the eyes from exterior stimuli [6].

#### 1.1.1.2 Sclera

The outermost layer in the posterior segment of the eye is the sclera. The limbus is the margin between the cornea and the sclera [7]. The sclera is rich in fibrous tissues, which are critical for maintaining the structure of the eye, as well as protecting the eyes against interior and exterior insults [6].

### 1.1.2 The Intermediate Layer of the Eye

The intermediate layer of the eye is made up of the iris, ciliary body, and choroid.

#### 1.1.2.1 Iris

Human eye color is determined by a structure in the eye known as the iris. The iris is a small pigmented tissue that is in charge of the size and diameter of the pupil. The iris consists of five diverse layers (from the innermost to the outermost): the posterior pigmented epithelium layer, the dilator muscle layer, the sphincter muscle layer, the stroma, and the anterior border layer (see Figure 3) [8].

**Figure 3.** ***Different Layers of the Human Iris***

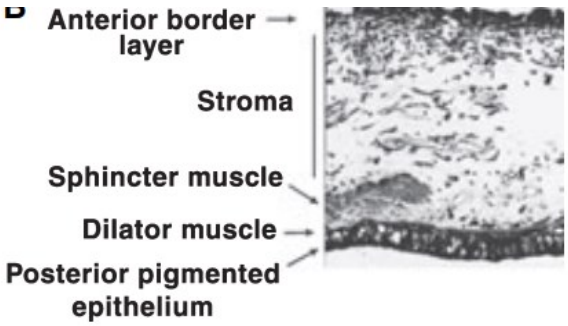


***Note***. The iris consists of five diverse layers (from the innermost to the outermost): the posterior pigmented epithelium layer, the dilator muscle layer, the sphincter muscle layer, the stroma, and the anterior border layer. (reprinted from Richard et al., 2009 [8]).

The innermost layer, the posterior pigmented epithelium, is highly pigmented, which is crucial for absorbing excessive lights [8]. The dilator muscle is implicated in pupil enlargement, whereas the sphincter muscle is in charge of pupil contraction [8]. In addition, the sphincter muscle layer is connected to the stroma, the thickest layer in the iris. The stroma and the anterior border layer account for the eye color determination, which stands out as the most critical component in the iris (see Figure 3) [1].

#### 1.1.2.2 Ciliary Body

The ciliary body is mainly composed of the ciliary muscles and the ciliary epithelium. It participates in aqueous production and reabsorption, as well as modulating the configuration of the lens [9].

The ciliary muscle is differentiated from the head mesenchyme [9]. It is composed of three distinct patterns of muscle fibers, from the innermost to the outermost: circular, oblique, and longitudinal [9]. The innermost circular muscle fibers are involved in controlling the axial diameter

of the lens. The oblique muscle fibers are bridges between circular muscle fibers and longitudinal muscle fibers. The outermost longitudinal muscle fibers link the anterior portion of the ciliary body to the sclera spur [9].

The ciliary epithelium originates from the optic cup. It is composed of two different types of epithelium: (a) the cuboidal pigmented epithelium, which makes up the outer part, and continues with the retinal pigment epithelium (RPE); and (b) the columnar non-pigmented epithelium, which constitutes the inner portion, which is in the immediate vicinity of the aqueous humor in the posterior chamber [7] and continues with the retina [10].

#### 1.1.2.3 Choroid

The choroid, a vascular-rich structure of the eye, is located amid the sclera and the retina [11]. The choroid is involved in multiple aspects, including providing oxygen and nutrition to the avascularized retina, controlling the temperature, as well as regulating intraocular pressure [12].

The choroid consists of five distinct layers: the Bruch's membrane, the choriocapillaris, two vascular layers, and the suprachoroid (see Figure 4) [11].

**Figure 4.** ***Schematic of Choroidal Structure***

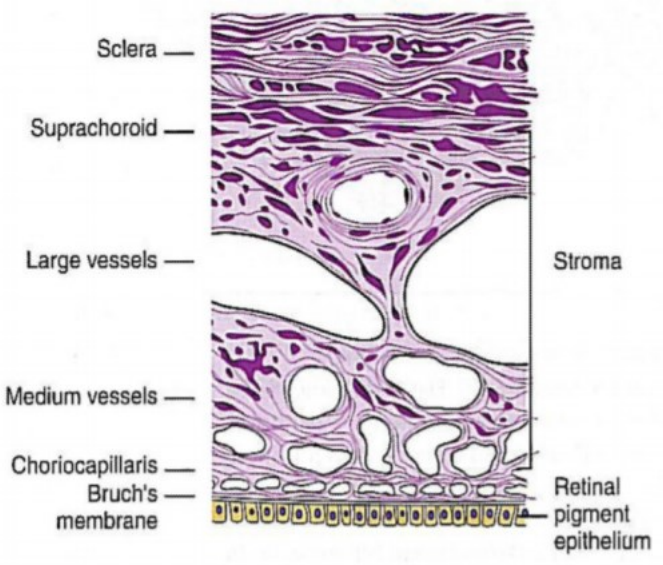


***Note.*** The choroid is made up of five layers: the Bruch's membrane, the choriocapillaris, the two vascular layers (the inner layer: Haller's; the outer layer: Sattler's), and the suprachoroid. (reprinted from Debora L et al., 2010 [11]).

The Bruch's membrane has three primary roles: (a) segregating the retina and the choroid, and restricting the retinal cell migration; (b) supporting the physiological function of RPE; (c) regulating molecule diffusion between RPE and the choroid [13]. The highly fenestrated choriocapillaris is permeable to large molecules that maintain pressure in the stroma [11]. The size of the choriocapillaris ranges from the center (10 μm) to the peripheral (7 μm) [11]. The choroid vascular layer contains two sublayers: the innermost vascular layer, Sattler's layer, is characterized by small and medium vessels, whereas the outermost vascular layer, Haller's layer, has a large vessel diameter [12]. The suprachoroid is adjacent to the sclera, which is composed of fibrous tissues and collagens [12].

### 1.1.3 The Innermost Layer of the Eye

### 1.1.3.1 Retina

The retina is a 200-μm-thick tissue that covers the inner surface of the eye [14]. The retina acts as a light acceptor, which transmits the light energy into neural signals [1]. The neural retina includes five main categories of neurons (see Figure 5A) that are well-arranged among the 10 parallel layers (see Figure 5B). The five main types of neurons are ganglion, amacrine, bipolar, horizontal cells, and photoreceptors.

**Figure 5.** ***The Cellular Components and Structure of the Retina***

**A.**

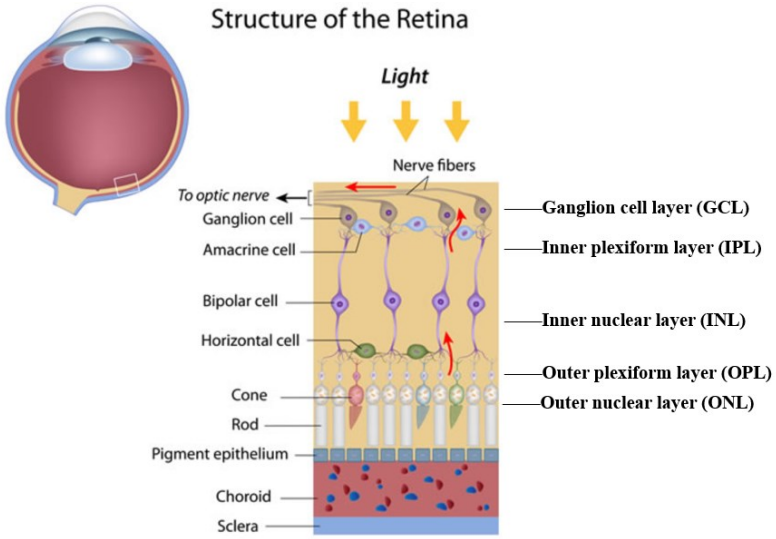


**B.**

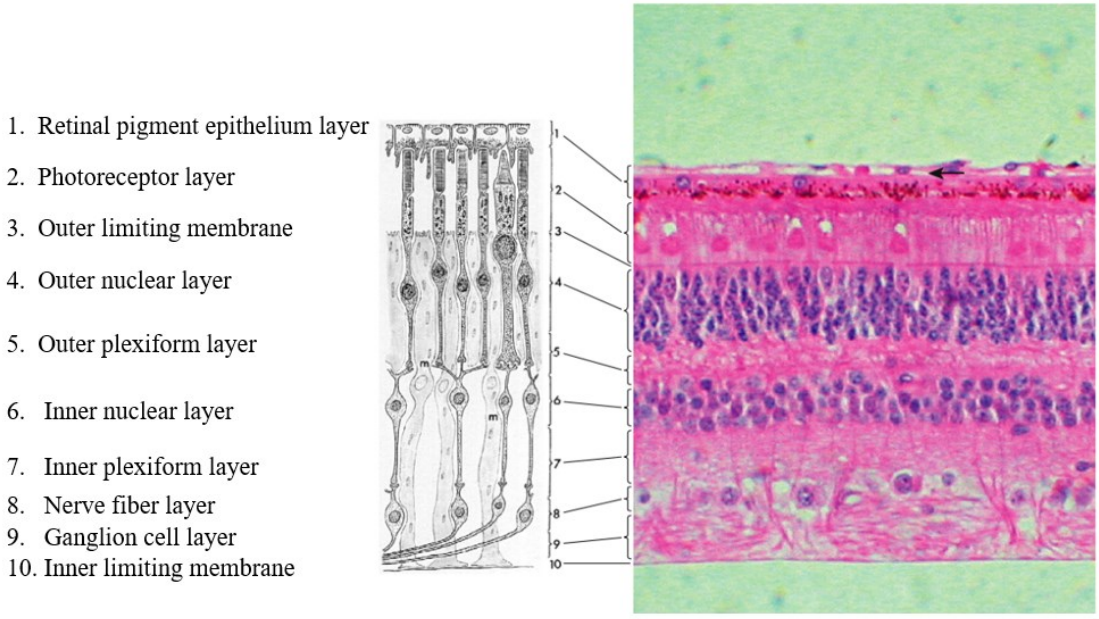


***Note.*** **A.** The retina comprises five main categories of neurons, which are ganglion, amacrine, bipolar, horizontal cells, and photoreceptors. (reprinted from Dr. Jin Huang (University of Sydney)). **B.** The retina is composed of ten parallel layers, as shown in the image. (reprinted from Reminton et al., 2012 [14]).

The cell bodies and synapse of the neurons are well organized in these parallel layers. Three layers within the retina contain neuron cell bodies make up the outer nuclear layer (ONL) that constitutes the cell bodies of the photoreceptors; the cell bodies of the internuncial neurons (amacrine, bipolar, and horizontal cells) are localized in the inner nuclear layer (INL); and the cell bodies of the retinal ganglion cells (RGCs) are located in the ganglion cell layer (GCL); The synapses connecting the photoreceptors and the interneurons are localized in the outer plexiform layer (OPL), whereas those between interneurons and RGCs are presented in the inner plexiform layer (IPL, see Figure 5A) [15].

RGCs are fundamental for visual information processing in the brain, which underlies the only optical signal transduction pathway for the central nervous system [16]. Even though there is a significant difference in morphology and functional properties of distinct types of RGCs, they still share a few similar characteristics [17], such as (a) the somata of RGCs are localized in the GCL; (b) the dendrites branch into the IPL; (c) the axons travel along the optic nerves toward the central nervous system [16].

The internuncial neurons comprise amacrine, bipolar, and horizontal cells. These interneurons are critical for processing and transducing the output visual signals to RGCs [15].

In general, amacrine cells play an inhibitory role in signal transduction, which intercepts signals between bipolar cells and RGCs [18]. At least 30 diverse subtypes of amacrine cells that differ in morphology and function have been identified [18]. The early expressed transcription factors determine the development of distinct subpopulations of amacrine cells [18]. In addition, the majority of synapses formed in the IPL, which connects with the synapse of RGCs, are attributed to amacrine cells [18].

The bipolar cells serve as a bridge connecting the outer and the inner retina (see Figure 5A). The bipolar cells possess two directional-opposite synapses. One moves upward toward the photoreceptors, whereas the other one goes downward, connecting with the RGCs [19]. More than 10 distinct types of bipolar cells have been confirmed in the mammalian retina [19]. The optimal indicators to identify the types of bipolar cells are the stratification level of the bipolar cells in the IPL and the cellular configuration [19]. Generally, bipolar cells are categorized into two kinds: ON and OFF, based on their different polarity in response to the light. The ON bipolar cells are deactivated (hyperpolarized) by glutamate secreted from the photoreceptors when it is dark, whereas the OFF bipolar cells are activated (depolarized), vice versa [19].

Horizontal cells play an inhibitory role in regulating the visual signal output from the photoreceptors. Furthermore, horizontal cells share similar molecular mechanisms at the transcriptional level with amacrine cells, which determine their development and differentiation [20].

Rods and cones are collectively termed photoreceptors. The human retina is composed of 120 million rods and 6 million cones [21]. They are specialized cells containing the photopigment rhodopsin that respond to the light [22]. Rods accumulate in the peripheral region of the retina, whereas cones mainly localize in the center and the macular zone of the retina [1]. Rods regulate the visual function during poor-lighting and are responsible for dark vision, whereas cones are in charge of color vision and visual acuity [21]

Although rods and cones differ in functions, they share a similar morphological construction. Rods and cones both comprise five main morphologically distinguishable compartments: (a) the outer segment, (b) the connective cilium, (c) the inner segment, (d) the cell body, and (e) the synaptic region (see Figure 6) [21]. The morphology of the outer segment is used to distinguish rods

from cones. Moreover, the outer segment is abundant in membrane discs that are composed of proteins essential for phototransduction [23]. The inner segment is where protein synthesis takes place [23]. The proteins synthesized in the inner segment must pass through the connective cilium to reach their active site, the outer segment [21]. Additionally, a great deal of mitochondria accumulates in the inner segment, which provides the energy required for protein synthesis, phototransduction, and protein transport [23]. The cell body is where the cell nucleus is located. The synaptic region can also be used to distinguish rods from cones, that the synaptic terminal of rods, also termed spherules, are smaller in size than the synaptic ending of cones, known as pedicles [21].

**Figure 6.** ***The Morphological Construction of Photoreceptors: Rods and Cones***

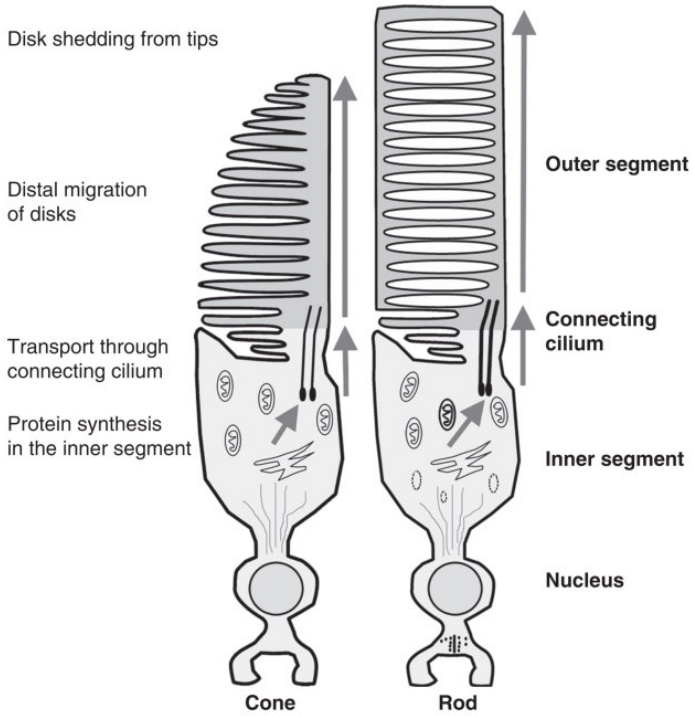


***Note.*** Rods and cones both comprise five main morphological distinguishable compartments. (reprinted from Perkin et al., 2010 [23]).

The retinal pigment epithelium (RPE) is a pigmented layer in the outermost layer of the retina, which is composed of a monolayer of cells that are cuboidal in the cross-sections and hexagonal when viewed from above. The RPE lies between the photoreceptors (rods and cones) of the retina and Bruch's membrane of the choroid (see Figure 7) [24].

In the cross-section, RPE is distinguished into apical and basal configurations. The apical surface of the RPE comprises two types of microvilli: one is the microvilli that maximize the surface area of the apical plasma membrane, and they are critical for transepithelial transport; the other is a specialized microvillus known as the photoreceptor sheath that envelops the photoreceptor outer segment [25]. The basal membrane is devoid of the microvilli; however, it has numerous infolds that increase the surface area, which is important for the absorption and secretion of materials (see Figure 7) [22]. The RPE also contains nucleus and organelles, such as the Golgi apparatus, mitochondria, endoplasmic reticulum, and lysosomes [25].

There are two major pigments in the RPE: melanin and lipofuscin. Melanin is concentrated in the cytoplasmic melanosomes, which resides in the apical side of the RPE. It participates in straight-light absorbing, scattered light minimizing, and free-radical stabilizing. Lipofuscin accumulates in RPE cells gradually with age; however, its role has yet to be determined [22].

RPE possesses multiple functions and is involved in several critical processes: (a) RPE is responsible for scattered-light absorbing, which is mediated by melanosomes; (a) RPE composes the outer blood-retinal barrier; (c) RPE provides nutrients for photoreceptors, which are critical for the maintenance of photoreceptor functions; and (d) RPE maintains the homeostasis of ions and water [24].

**Figure 7.** ***Structure of the Retinal Pigment Epithelium***

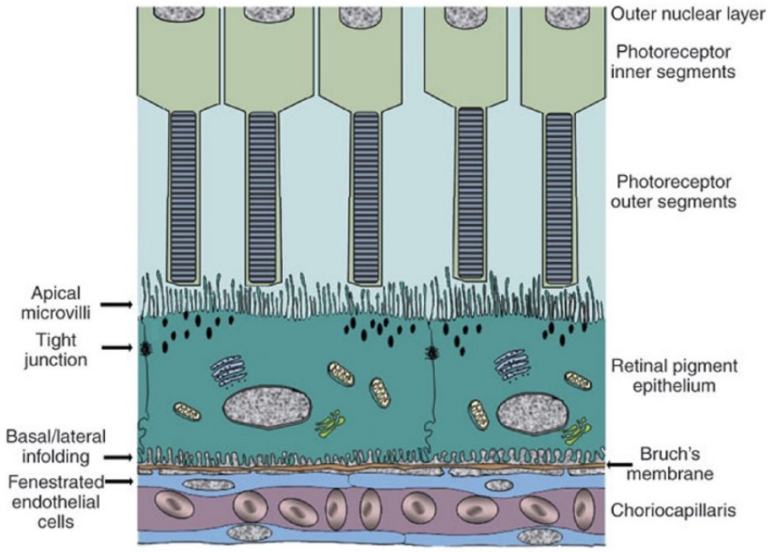


***Note.*** In the cross-section, RPE is distinguished into two configurations: the apical and basal structures. The apical of RPE contains two types of microvilli, and the basal RPE has numerous infolds. (reprinted from Fronk et al., 2016 [24]).

### 1.1.4 Structure Surrounded by the Ocular Layers

#### 1.1.4.1 Aqueous

The aqueous humor is a transparent fluid that replenishes the anterior and the posterior chamber of the eye [7]. The aqueous humor is an essential component of the eye that is involved in nutrition and neurotransmitter transportation, waste product removal, and the stabilization of the ocular structure [7]. Regulation of the dynamics of the aqueous humor is critical for maintaining the homeostasis and the function of the eye [7]. The dynamics of the aqueous humor is determined by the production and the absorption of the aqueous humor. The ciliary body controls the production

of aqueous humor, while the trabecular meshwork and the Schelemm's canal regulate the drainage of the fluid (see Figure 8) [7, 26].

**Figure 8.** ***Structures and Pathways that Regulate the Dynamics of Aqueous Humor***

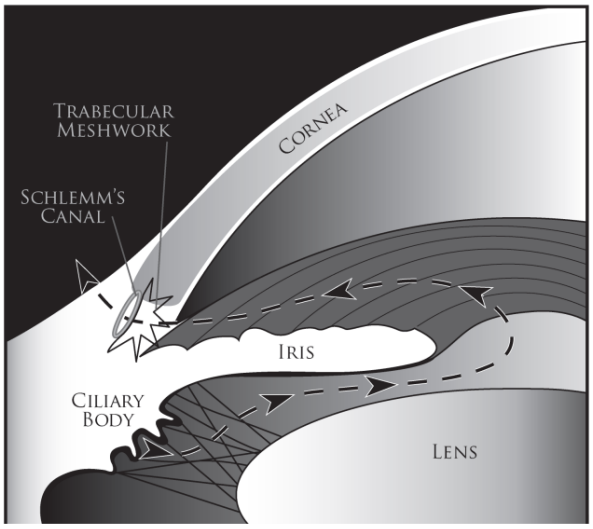


***Note.*** The aqueous humor is produced by the ciliary body and outflowed via the trabecular meshwork. (reprinted from Manik et al., 2010 [7]).

The trabecular meshwork, located at the transition zone of the sclera and the cornea, is mainly composed of connective tissues and various elastic components [26]. The Schelemm's canal is an endothelial-lined canal that is also a primary location of aqueous humor absorption [7].

The floating pathway of the aqueous humor initiates at the ciliary body, where it is produced. After replenishing the posterior chamber, it moves towards the anterior chamber and flows around the lens and the pupil (see Figure 8) [7]. There are two options for aqueous humor drainage: the

conventional means is mediated by the trabecular mesh and the Schelemm's canal, and the unconventional route is through the uveal meshwork and the ciliary muscles [7].

### 1.1.4.2 Lens

The lens is a transparent ellipsoid structure that is deficient in blood vessels, nerves, and connective tissues [9]. It lies behind the iris, and it cooperates with the cornea to adjust the light focused on the retina. The ciliary muscles regulate the configuration and the curvature of the lens via the zonules, a process called accommodation [27]. The human lens continues to grow throughout one's life, and the new cells are stored at the edge, whereas the older cells are accumulated in the center [28].

The lens has an active metabolism and requires nourishment to support its growth and transparency. Glucose serves as the primary energy source for the lens. In addition, the lens exchanges the waste components through the aqueous humor in a constant flow [2].

The lens comprises three major constituents: (a) the lens capsule, which is a transparent elastic basement membrane (BM) composed of collagens and glycans; (b) the lens epithelium which is a pack of cells that are essential for the maintenance of the lens homeostasis; (d) the lens fibers, which are derived from epithelial cells, are essential for minimizing light scattering and transparency improvement [28].

### 1.1.4.3 Vitreous Body

The vitreous body, also known as the vitreous humor, is an avascularized gel-like structure, mainly composed of water, protein, and a few cells [3]. It is located amid the lens and the retina [29].

Additionally, the viscous characteristic is attributed to the components of the vitreous humor: collagens and glycans [29].

## 1.2 VASCULAR DEVELOPMENT OF THE RETINA

Two disparate vascular systems support the nutrient and metabolic requirements of the retina: the non-fenestrated impermeable retinal vasculature supports the inner retina (2/3 of the retina); and the fenestrated highly-permeable choriocapillaris from the choroid supplies the outer retina (1/3 of the retina), which includes the RPE and photoreceptors (see Figure 9) [30].

**Figure 9.** ***The Retinal Vascular Systems***

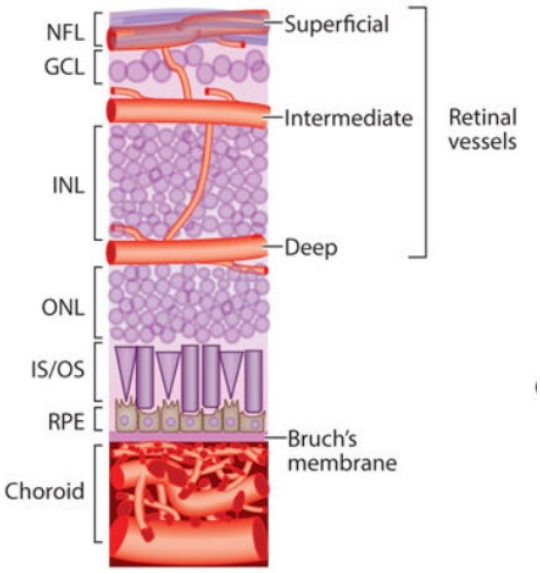


***Note.*** The retinal vasculature supports the inner retina (2/3 of the retina), whereas the choroidal vascular system supplies the photoreceptors and the RPE. (reprinted from Sun et al., 2018 [31]).

The growth of retinal vessels begins around 16 weeks of pregnancy through vasculogenesis, a process mediated by endothelial progenitor cells [30]. The development of retinal vasculature completes at approximately 38 ~ 40 weeks of gestational age [30]. Before the onset of retinal vascular growth, the hyaloid vessels temporarily support the inner retina, which degenerates by 20 weeks of gestational age when its place is taken by the inner retinal vessels [32]. Three parallel interconnected vascular networks constitute the retinal vascular system: the superficial, the intermediate, and the deep plexuses (see Figure 10) [31].

The first formed vascular layer is the superficial plexuses at 16 weeks of gestational age [31]. The superficial vascular layer originates from the capillaries at the optic nerve head and is localized above the GCL, where the nerve fiber layer (NFL) is (see Figure 10A). The superficial plexuses spread from the center to the peripheral in the inner retina and complete at approximately 36 ~ 40 weeks of gestation [30]. At 25 ~ 26 weeks, the deep plexuses are formed by vertically sprouting the superficial vascular layer from the NFL toward the OPL through a process known as angiogenesis (see Figure 10B). The intermediate plexuses are formed at the IPL (see Figure 10C) [30, 33]. Therefore, premature infants have an incomplete retinal vascular system [34].

**Figure 10.** ***The Growth of Retinal Vessels***

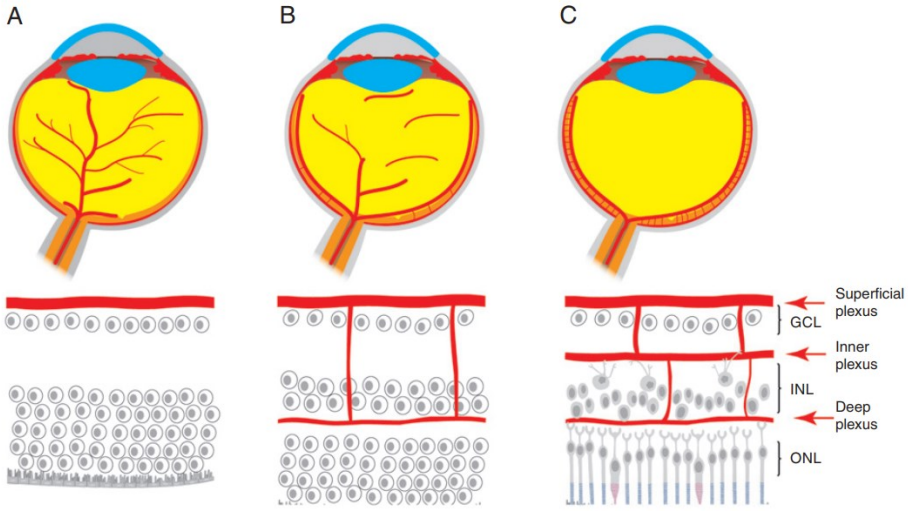

***Note.*** Three interconnected parallel vascular plexuses constitute the retinal vascular system: the superficial (at NFL), the intermediate (at IPL), and the deep (at OPL). **A:** The formation of the superficial retinal vascular layer. **B:** The formation of deep plexuses from the superficial vascular layer via angiogenic sprouting. **C:** The formation of intermediate plexuses. (reprinted from Nathan J Coorey et al., 2012 [35]).

In contrast to the development of retinal vasculature in humans that occurs before birth, retinal vascular growth in mice takes place after birth [36]. The superficial plexuses of the mice develop from postnatal day 1 (P1) to P7 (see Figure 11). The formation of deep and intermediate plexuses initiates similar to that in humans when the superficial vascular layer is complete [31]. The whole retinal vascular system in mice is completed in the third postnatal week (see Figure 11) [30].

**Figure 11.** ***The Timeline of Retinal Vascular Growth in Mice***

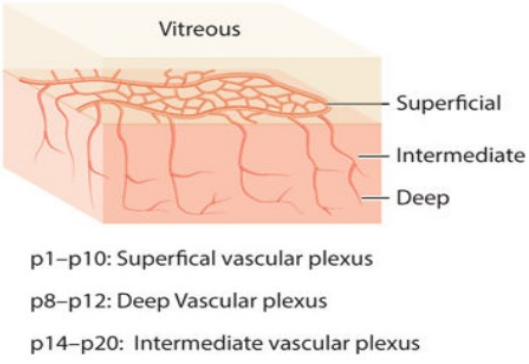


***Note.*** The growth of the retinal vascular system in mice initiates postnatally. The superficial vascular layer forms from P1 ~ P7, the deep vascular layer develops from P8 ~ P12, followed by the formation of the intermediate vascular layer (P14 ~P20; reprinted from Sun et al., 2018 [31]).

## 1.3 RETINOPATHY OF PREMATURITY

Retinopathy of prematurity (ROP), also termed retrolental fibroplasia, is an ocular disorder that is caused by the growth of aberrant retinal neovascularization (NV). ROP is the leading cause of visual damage and vision loss in premature infants [37].

The key risk factors for ROP include (a) supplemental oxygen therapy, (b) extremely-low gestational age, and (c) low birth weight [34]. As the medical care for the neonates has significantly improved, the survival rate of extremely-low gestational age as well as low birth weight neonates has also increased, which leads to the growing incidence of ROP [37].

### 1.3.1 Pathogenesis

ROP is a two-phase ocular disorder: phase I is called the vaso-obliteration phase, and phase II is known as the vaso-proliferation phase (see Figure 12) [34]. Three factors mainly cause the development of the first phase: (a) incomplete retinal vasculature in premature infants; (b) degeneration of pre-existing retinal vessels due to insufficient growth factors; and (c) relative hyperoxia caused by oxygen supplement supporting the immature respiratory system (see Figure 12A-B) [34]. The retina is one of the most metabolically active tissues, which consumes high levels of oxygen and nutrients [14]. Because the retina requires a high amount of the oxygen supplies, the microenvironment of the retina shifts from hyperoxia to hypoxia as the retina matures and initiates the second phase (see Figure 12C) [34]. Phase II is triggered by hypoxia, which induces the secretion of a large number of growth factors and results in pathological retinal NV (see Figure 12D) [34].

**Figure 12.** ***The Pathogenesis of ROP***

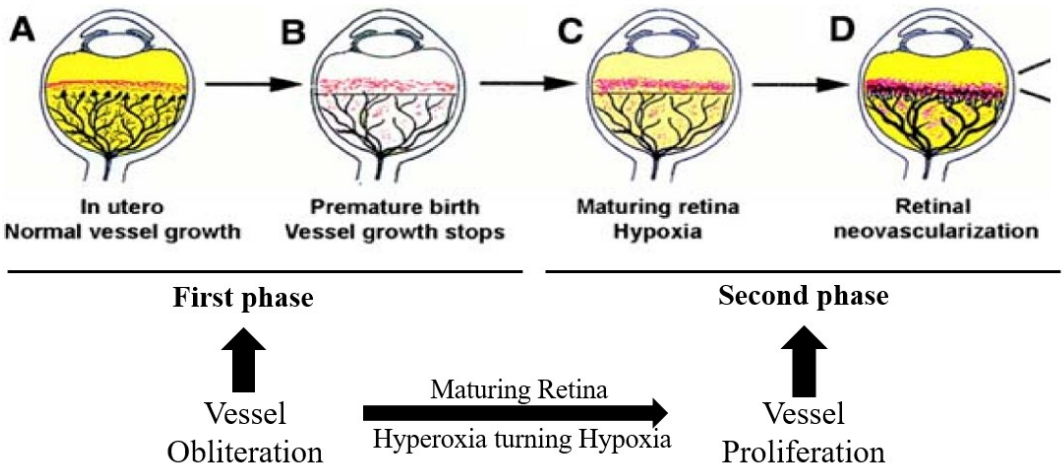


***Note.*** **A.** Vascular growth of the retina in the utero. **B.** Delayed retinal vessel growth and concomitant retinal vascular degeneration occur in premature births. This leads to phase I of ROP: the vaso-obliteration phase. **C.** The maturing retina turns hyperoxia into hypoxia, which initiates phase II of ROP. **D.** Retinal NV. Hypoxia triggers the secretion of growth factors, which induces the formation of pathological retinal neovessels. C and D together are known as the vaso-proliferation phase. (reprinted from Jing et al., 2007 [34]).

### 1.3.2 Classification

Three significant concepts are used to classify ROP: the zone, the extent, and the stage (see Figure 13) [38]. The retina is segmented into three major zones to assess the location (see Figure 13A): Zone I, Zone II, and Zone III. The optic nerve head is central to each zone. Zone I is the smallest circle, and the diameter is four times the distance between the optic nerve head and the

macula (see Figure 13A). The ring-shaped Zone II is concentric to Zone I, which extends from the edge of Zone I to the nasal side of the ora serrata, a serrated joint amid of the retina and the ciliary body (Figure 13A). Zone III is a crescent-shaped region (see Figure 13A) [39].

The extent of the disorder is recorded clock-wisely from 1 to 12 hr in a 1 hr segment manner (see Figure 13A) [39]. The severity of the disease is divided into five stages (see Figure 13B and13C): Stage I is characterized by the demarcation line, which forms at the interface of vascularized and avascularized retinal area, as shown in Figure 13B (the red line) and Figure 13C (the whitish line). Stage II features the visible ridge formed at the demarcation line, while Stage III is distinguished by the formation of pathological NV at the ridge. Stage IV is characterized by the retina partially separating from the underneath layer, whereas Stage V is the total retinal detachment [37-39].

**Figure 13.** ***The Classification of ROP***

**A.**

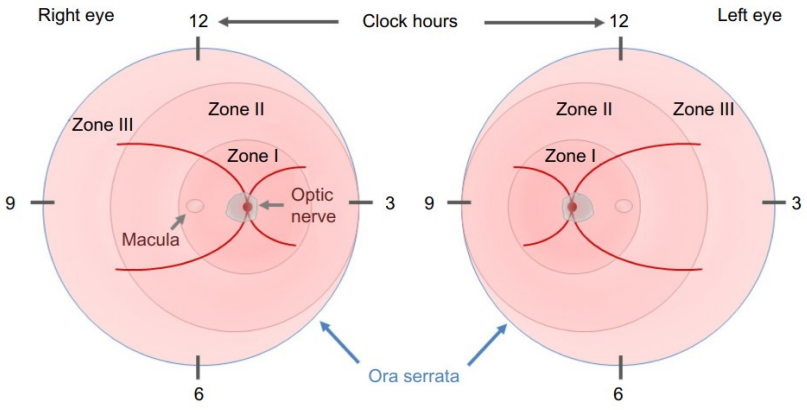

**B.**

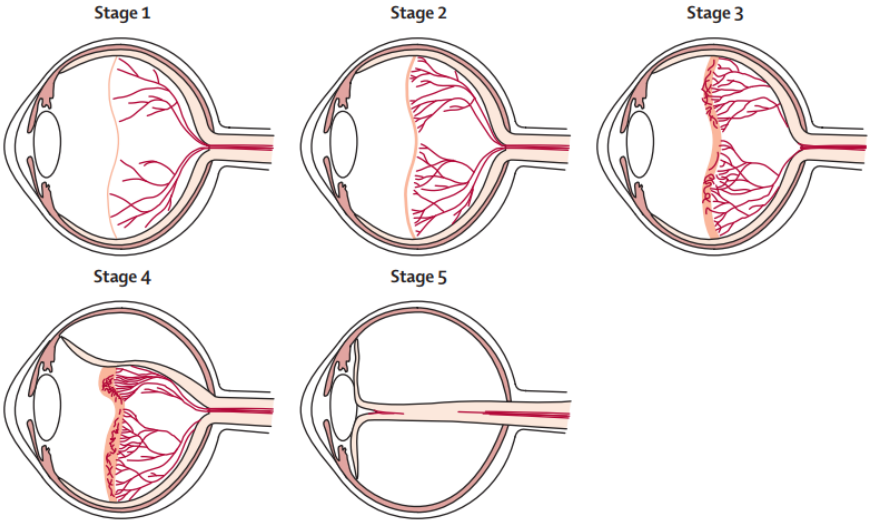
Stage 1
Stage 2
Stage 3
Stage 4
Stage 5

**C.**

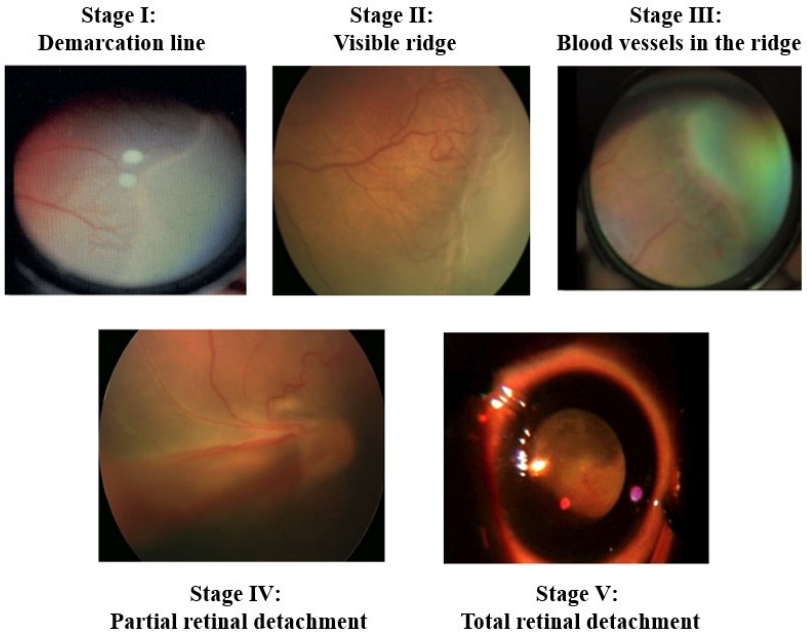
Stage I:
Demarcation line
Stage II:
Visible ridge
Stage III:
Blood vessels in the ridge
Stage IV:
Partial retinal detachment
Stage V:
Total retinal detachment

**Note. A.** Classification of ROP by the zone and the extent. The retina is segmented into three major zones to assess the location: Zone I, Zone II, and Zone III. The optic nerve head is central to each zone. Zone I is the smallest circle , and the diameter is four times the distance between the optic nerve head and the macula. The ring-shaped Zone II is concentric to Zone I, which extends from the edge of Zone I to the nasal side of the ora serrata. Zone III is a crescent-shaped region. The extent of the disorder is recorded clock-wisely from 1 to 12 hr in a 1 hr segment manner. (reprinted from Liegl et al., 2016 [40]). **B.** The five stages of ROP. Stage I: the demarcation line, which is shown as the red line; Stage II: the visible ridge formed at the demarcation line; Stage III: formation of the neovessels at the ridge; Stage IV: partial retinal detachment; Stage V: complete retinal detachment. (reprinted from Hellström et al., 2013 [37]). **C.** The five stages of ROP in the human eye; (reprinted from Komal et al., 2018 [39]).

### 1.3.3 Treatment and Challenges

There are two categories of treatment: one is to prevent the development of phase II ROP, and the other is to alleviate the progression of pathological retinal NV once phase II is initiated [40].

The preventive strategies are used against phase I ROP, which mainly involves growth factor supplementation (VEGF, erythropoietin, etc.) [41]. The current treatment available for phase II ROP includes laser-induced photocoagulation, cryosection, and intravitreal injection of anti-vascular endothelial growth factor (VEGF) [37].

Laser-induced photocoagulation attempts to burn away the peripheral avascular retina (see Figure 14A). With cryosection, the physician uses an instrument to generate freezing temperatures and quickly touches the spot of the avascular retina. Both treatments destroy the areas of the retina without vascularization, which reduces signals for pathological retinal NV. However, the procedures are invasive and also destroy the side visions [40].

Anti-VEGF therapy was one of the top 10 discoveries in 2006 and is a promising treatment for cancer [42]. It has revolutionized the treatment for ocular NV diseases (see Figure 14B). The currently used anti-VEGF drugs include bevacizumab, ranibizumab, pegaptanib, and aflibercept [43]. Clinical trials have revealed the advantage of these drugs in that they have successfully prevented the ongoing pathological retinal NV, controlling the leaking vasculature, and preserving the central vision [42]. One of the disadvantages of these regimens is that they all require repeated and long-term injections, which increase the risks of post-injection and drug-related ocular and systemic side effects. The ocular adverse events include intraocular inflammation, rhegmatogenous retinal detachment, intraocular pressure elevation, ocular hemorrhage, and endophthalmitis [43]. Not all the abovementioned anti-VEGF drugs elicit system complications. Clinical reports have shown that pegaptanib has an excellent safety profile with no systemic complication observed [43]. Additionaly, the intraocular injection of ranibizumab significantly increases non-ocular hemorrhage events [43]. In comparison with pegaptanib and ranibizumab, bevacizumab has significant more systemic side effects, including blood pressure elevation, cerebrovascular complications, myocardial infarctions, and iliac artery aneurysms [43]. Despite the superior efficiency of treating patients with severe ocular NV, the unwanted side effects have held back its effectiveness [44].

None of them have achieved the expectations, and they are not appropriate for the long-term treatment of ROP. Therefore, there is an urgent need to discover long-term therapeutic strategies targeting retinal NV with superior efficiency but with fewer side-effects.

**Figure 14.** ***Treatment for Phase II ROP***

**A.** **B.**

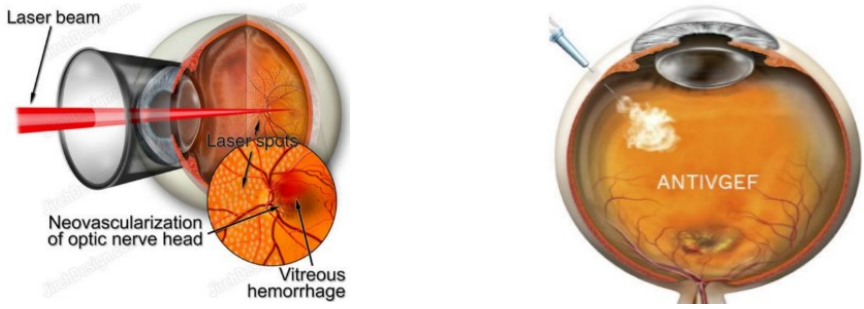


***Note.*** **A.** Laser-induced photocoagulation. **B.** Anti-VEGF intravitreal injection. (reprinted from Southern Vitreoretinal Associates).

## 1.4 MULLER CELLS

### 1.4.1 Morphology

Müller cells are the major glial cells that extend from the inner retina (NFL) to the outer retina (the basal side of the ONL; see Figure 15) [45]. Five distinguishable morphological compartments constitute the configuration of Müller cells: the somata, the inner process, the outer process, the endfoot, and the microvilli (see Figure 15). The polygonal-shaped somata of Müller cells are localized in the INL. Müller cells have two main trunks extending in the opposite direction, known as the inner process and the outer process. In the IPL, Müller cells narrow to a slender stalk-like process (inner process) that can vary in diameter from 0.5 to 15 μm, depending on the species [45]. The basal end of each inner process spans through the GCL and terminates into an endfoot expansion, which lies adjacent to the NFL [46]. The outer process extends from the INL upwards to the outer limiting membrane, where the apex locates and forms the microvilli (see Figure 15) [45].

**Figure 15.** ***The Morphology of Müller Glial Cells***

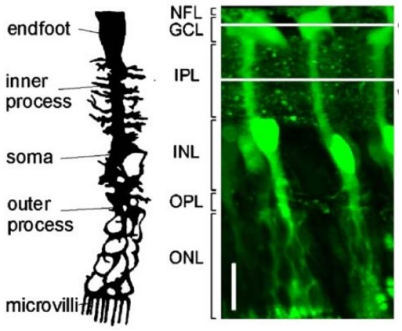


***Note.*** Müller cells comprise five distinguishable morphological compartments: the somata (INL), the inner process (IPL), the outer process (OPL), the endfoot (NFL), and the microvilli (the basal ONL; reprinted from Bringmann et al., 2006 [45]).

### 1.4.2 Functions in the Healthy Retina

Due to the geographic advantage, Müller cells have connections with almost all types of cells within the retina (see Figure 16). Müller cells are endowed with critical functions that are essential for maintaining retinal homeostasis [45]. Müller cells are necessary for several processes, including the metabolism of glucose, the modulation of retinal circulation, the recycling of neurotransmitters, the maintenance of the blood-brain barrier (BRB), the production of growth factors, and the maintenance of ion and water homeostasis [45].

**Figure 16.** ***Retinal Cells That Contact with Müller Cells***

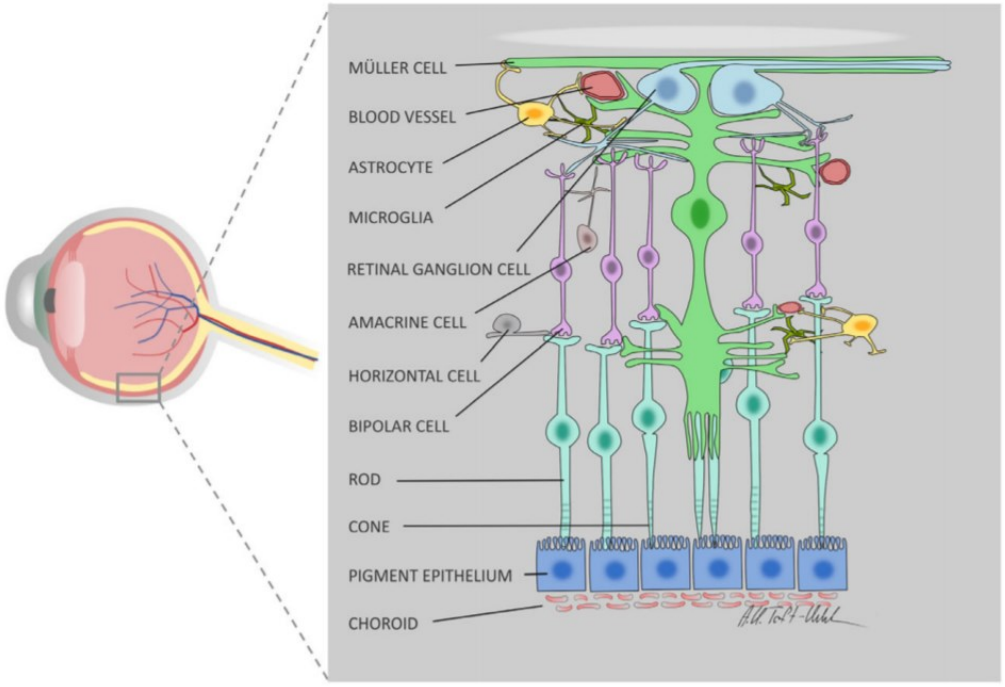


***Note.*** Müller cells extend from the inner retina (NFL) to the outer retina (the basal ONL). They are in contact with almost all types of cells, including (a) RGCs, (b) astrocytes, (c) microglia, (d) interneurons (amacrine, bipolar, and horizontal cells), and (e) photoreceptors (rods and cones; reprinted from Kolko et al., 2017 [47]).

The activity of Müller cells mainly relies on anaerobic glycolysis due to the fact that Müller cells require little oxygen consumption [48]. Müller cells can generate lactate through glycolytic metabolism. Lactate is converted into pyruvate, which is further utilized by neurons as a substrate for the Krebs cycle [45]. In addition, Müller cells are essential for the maintenance of internal homeostasis of the neurons [45]. The membrane of Müller cells expresses transmitter uptake systems for glutamate. The recycling of excessive glutamate protects the neurons from overexcitation-induced toxicity [45, 47].

Müller cells are also an essential source of ATP, in which the production is stimulated by extracellular glutamate [45]. The ATP-generated by Müller cells also provides energy for residential

microglia cells [49]. Additionally, Müller cells are involved in the regulation of the physiological conditions as well as the activity of photoreceptors, in which specific depletion of VEGF from Müller cells reduces the thickness of the photoreceptor layer and ONL [50].

### 1.4.3 Functions in the Pathological Retina

In contrast to retinal neurons, which are highly susceptible to various injuries, Müller cells are quite resistant to most pathological conditions, due to their peculiar energy metabolism (glycolytic metabolism) [45]. Therefore, they survive most of their injuries and remain an active player in pathological events.

The reactions of Müller cells in response to damages can be classified into two major types: the non-specific responses, which are stimulus-independent, and the specific reactions which are determined by the stimulus [45].

Enhanced proliferation and upregulation of intermediate filament glial fibrillary acidic protein (GFAP) are two significant characteristics of non-specific reactions of Müller cells [48].

The specific reactions of Müller cells are stimulus-dependent. For example, in response to hypoxia, Müller cells express an inducible form of nitric oxide synthase, which increases the expression of nitric oxide (NO) [35]. Low levels of NO have a beneficial effect, in which it counteracts hypoxia by dilating the blood vessels and protects neurons from glutamate toxicity [48]. Nevertheless, overexpression of NO is detrimental, which causes the formation of excessive free nitrogen radicals that are toxic to neurons [48].

In addition, Müller cells are an essential source of pro-inflammatory cytokines and growth factors in pathological conditions [51]. Müller cells have been implicated in pathological retinal NV, retinal inflammation, and the breakdown of the BRB [52 53].

## 1.5 MACROPHAGES

Macrophages are important phagocytes that belong to the mononuclear phagocyte system (see Figure 17) [54]. Macrophages are widely distributed in all organs and connective tissues [55]. In the steady-state, the monocyte-macrophage lineage is generated from the blood stem cell in the bone marrow. They are driven to the circulation via the monocyte-stimulating factor, where they further mature into monocytes. During an inflammatory response, monocytes migrate to the inflamed tissues following the chemokine gradients, where they further differentiate into macrophages [54, 56].

**Figure 17.** ***The Morphology of Macrophages***

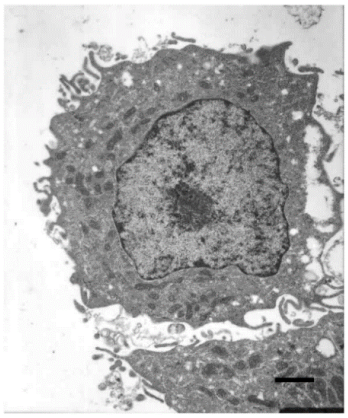

***Note.*** Transmission electron microscope image of macrophages. (reprinted from Sarah et al., 2012 [57]).

### 1.5.1 The General Functions of Macrophages

Macrophages are the first line of host defense against microbes that breach epithelial barriers. A major function of macrophages in host defense is to ingest microbes through the process of phagocytosis [58].

During an acute inflammatory response, macrophages differentiated from blood-derived monocytes elicit phagocytic function [55]. Phagocytosis is an active, energy-dependent process that invaginates large particles (> 0.5 μm in diameter) into vesicles via different membrane receptors expressed on the cell surface [59]. The phagocyted vesicles, named phagosome, contain the ingested microbes fused with lysosomes, and these subsequently form the phagolysosome where the foreign matters within are degraded [59]. Activated macrophages kill phagocytosed microbes by the action of microbicidal factors within the phagolysosomes [59]. The activated macrophages generate microbicidal factors via converting molecular oxygen into reactive oxygen species (ROS), which are highly oxidizing reagents with unpaired electrons that damage microbes [55]. In addition to ROS, activated macrophages also produce reactive nitrogen species [58].

In addition to engulfing external materials, macrophages can ingest necrotic host cells, including cells that die in tissues due to the effects of injuries, toxins, or interrupted blood supply [56]. Macrophages also recognize and phagocytize apoptotic cells in advance of releasing harmful contents and inducing inflammatory response by the apoptotic cells [58].

Besides the function of phagocytosis, macrophages are capable of releasing various types of cytokines or chemokines that recruit more monocytes and other leukocytes from the blood circulation into the site of inflammation [60, 61].

Macrophages also serve as antigen-presenting cells [62]. Foreign microorganisms that are degraded within macrophages produce antigens, which are further presented on the cell surface of macrophages to activate T lymphocytes [62]. This process is critical to the initiation of T cell-mediated adaptive immune response [58].

Macrophages also have the capacity to promote the repair of damaged tissues by stimulating neovessel growth as well as synthesizing the collagen-riched extracellular matrix [61]. This effect is mediated by the cytokines secreted by macrophages [63].

### 1.5.2 Macrophage Recruitment

The general process of macrophages leaving the blood circulation toward a particular site of inflammation or injury is termed recruitment or migration [64]. The migration of macrophages to the sites of infection or tissue injury form a major part of the process of inflammation [64]. Chemokines, which are a contraction of chemotactic cytokines, are responsible for regulating the recruitment of macrophages during an inflammatory response [65].

#### 1.5.2.1 Chemokines

Chemokines belong to a large cytokine family with a molecular mass of 8 ~ 10 kD [66]. They participate in cell motility functions in the development and maintenance of tissue architecture, and inflammatory response [65]. Chemokines share a similar three-dimensional structure : (a) a three-strand of anti-parallel β-sheets, (b) a C-terminal domain containing an α-helix, and (c) the disulfide bridges linking the conserved cysteine residues (see Figure 18A) [67]. They are also categorized into four main subclasses based on the arrangement of two of four conserved cysteine residues [67]: (a) the CC family, in which there is no amino acid located amid the two cysteine residues; (b) the CXC

family, in which the two cysteine residues are apart from each other with one amino acid in between; (c) the CX3C family, in which three amino acids separate the two cysteine residues; and (d) the particular C family which has only one conserved cystines residue (see Figure 18B) [68].

**Figure 18.** ***Structure and Subfamily of the Chemokines***

**A.**

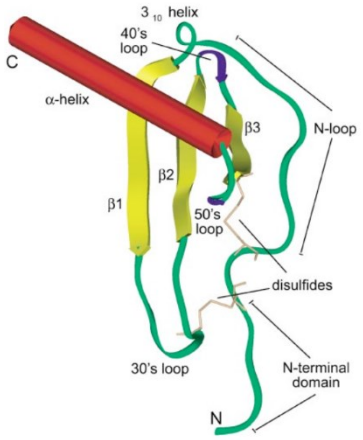


**B.**

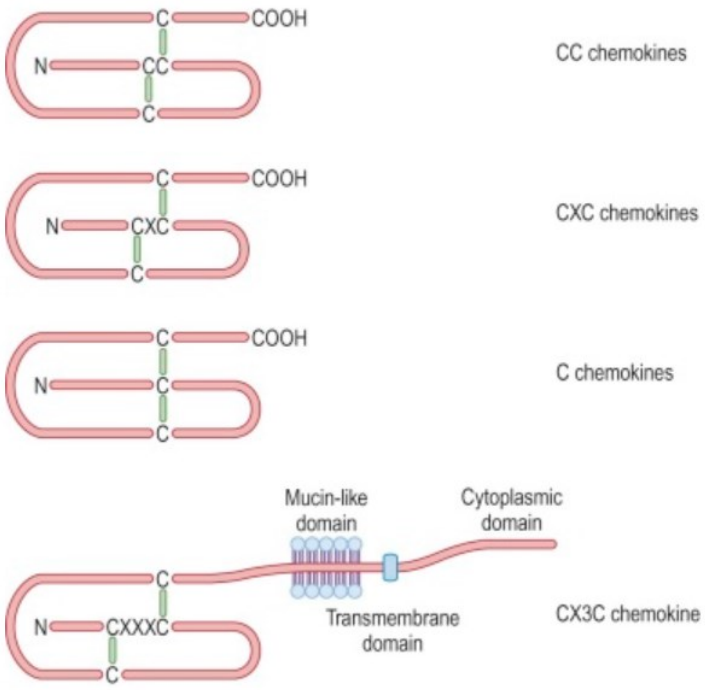


***Note.*** **A.** Chemokines share a similar three-dimensional structure : (a) a three-strand of anti-parallel β-sheets, (b) a C-terminal domain containing an α-helix, and (c) the disulfide bridges linking the conserved cysteine residues. (reprinted from Fernandez et al., 2002 [67]). **B.** Chemokines are categorized into four main subclasses based on the arrangement of two of four conserved cysteine residues: CC, CXC, C, and CX3C family. (reprinted from Middleton's Allergy, 2014).

Chemokines are generated by several kinds of cells, including leukocytes, epithelial cells, endothelial cells, resident macrophages, fibroblasts, and other stromal cells. Additionally, pro-inflammatory cytokines are capable of inducing chemokine production [68].

Chemokines exert recruitment effect via chemokine receptors, which belong to the superfamily of seven-transmembrane domain receptors, named the G-protein coupled receptor [65]. The receptors of chemokines initiate intracellular responses through associated trimeric G proteins. All chemokine receptors mediating cell migration share an amino acid sequence motif (DRYLAIV) at

the terminal of the third transmembrane domain, which is vital for interactions with G proteins [65]. The G proteins stimulate the signaling events that cause cytoskeletal changes and polymerization of actin and myosin filaments, resulting in increased cell motility [68].

### 1.5.3 Subsets of Macrophages

Macrophages are characterized by plasticity and functional heterogeneity, which are environmental stimuli-dependent [54]. Macrophages are generally categorized into two main groups based on the related functions (see Figure 19) [69].

The classically activated macrophages (M1 macrophages) are stimulated by cytokines such as interferon-γ [55]. M1 macrophages express transcription factors, which results in increased microbicidal functions and the secretion of pro-inflammatory cytokines (see Figure 19) [55]. In addition to the pro-inflammatory role, M1 macrophages also exert an anti-angiogenic effect [70].

Distinct from M1 macrophages, M2 macrophages are mainly stimulated by IL-4 together with IL-13 [55]. They produce cytokines that terminate inflammation and initiate tissue repair. M2 macrophages have wound-healing, pro-angiogenic, and anti-inflammatory properties (see Figure 19) [70, 71].

**Figure 19.** ***The Subsets and Related Functions of Macrophages***

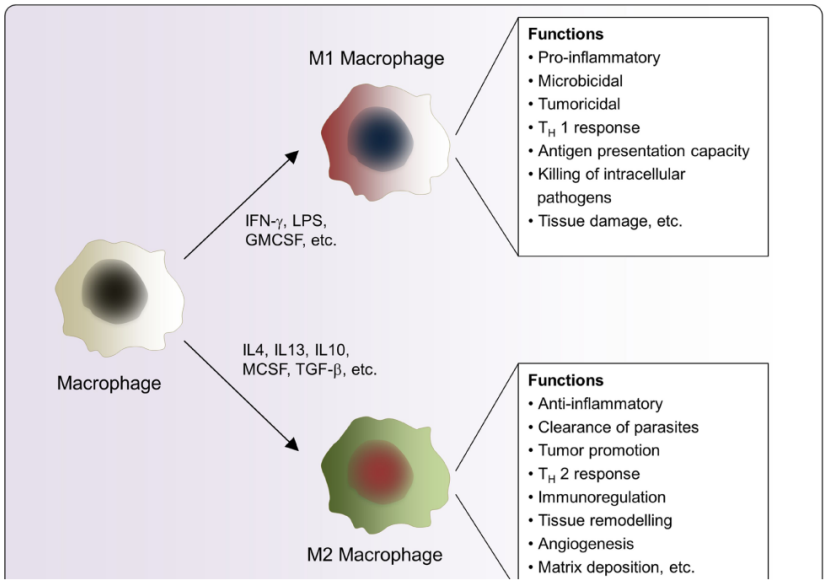


***Note.*** Macrophages are categorized into two main classes: M1 and M2, according to the stimuli they received. Different phenotypes of macrophages have their specific functions. (reprinted from Uzma et al., 2018 [71]).

### 1.5.4 Macrophages in ROP

An increasing body of evidence has demonstrated a pro-angiogenic role of macrophages in the pathogenesis of aberrant retinal vascular formation [72-74]. Studies have shown that the number of macrophages substantially increases during retinal NV, which is mainly attributed to the recruitment of monocyte-derived macrophages [75, 76]. The migration of macrophages initiates around P14 in the OIR mouse model [77]. The depletion of monocyte-derived macrophages significantly attenuates pathological retinal NV [78]. Moreover, studies have pointed out that M2 macrophages, rather than M1, promote aberrant retinal vascular formation [73].

## 1.6 ANGIOGENESIS-RELATED FACTORS

Vascular development is vital for physiological processes as well as disease progression [79, 80]. There are two types of vascular formation: (a) *de novo* vascular development, also named vasculogenesis, in which endothelial progenitor cells mediate the process; and (b) angiogenesis, where neovessels sprout from the pre-existing vasculature (see Figure 20A) [81].

The angiogenesis is an elaborately regulated stepwise process, which involves (a) protease secretion, (b) extracellular matrix (ECM) and BM degradation, (c) endothelial cell proliferation, (d) endothelial cell migration, (e) vascular tube formation, (f) vascular fusion, and (g) vascular maturation and stabilization (see Figure 20B) [81].

The process of angiogenesis involves not only endothelial cell activity, but also comprises various angiogenesis factors contributing to this complex and dynamic process.

**Figure 20.** ***Angiogenesis***

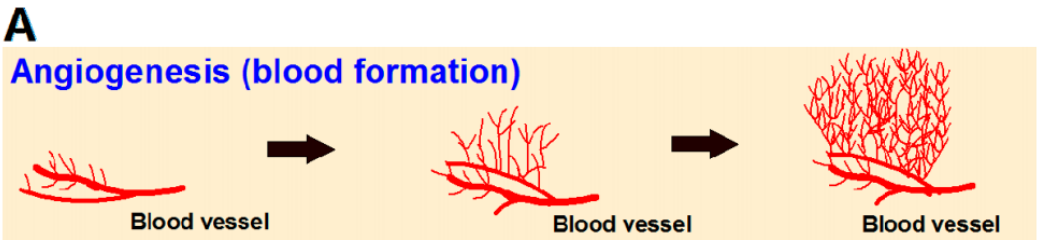

**B.**

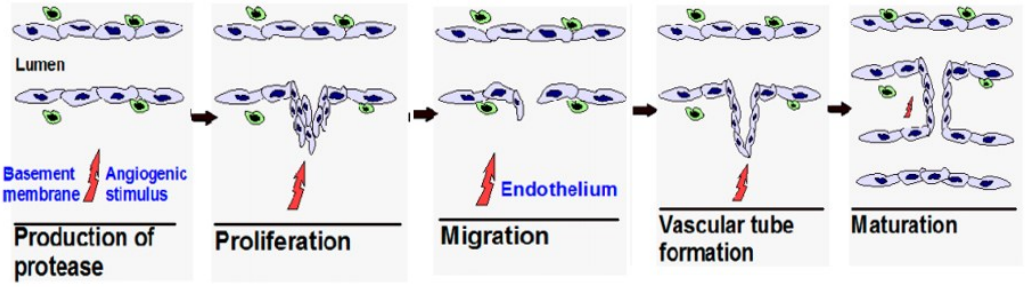


***Note.*** **A**. Angiogenesis, a process that neovessels sprout from the pre-existing vessels. **B.** The angiogenic process involves (a) protease secretion which causes (b) ECM and BM degradation, (c) endothelial cell proliferation, (d) endothelial cell migration, (e) vascular tube formation, (f) vascular fusion, and (g) vascular maturation and stabilization (new BM synthesis; pericyte and smooth muscle cell stabilization). (reprinted from Rajabi et al., 2017 [82]).

### 1.6.1 Vascular endothelial growth factor (VEGF)

VEGF, a family of heparin-binding homodimeric glycoproteins containing seven members, is essential for orchestrating the formation of neovessels [83]. They exert effects via binding to tyrosine kinase receptors expressed on the membrane and transducing the signal intracellularly [84].

VEGF-A, the most extensively studied pro-angiogenic protein, participates in physiological vascular formation and pathological NV [50, 85]. In addition to its angiogenesis-inducing function, VEGF-A also acts as a chemoattractant for monocytes/macrophages[86].

#### 1.6.1.1 VEGF-A in Angiogenesis

In response to hypoxia, parenchymal cells secrete the key pro-angiogenic factor, VEGF-A, which activates the quiescent endothelial cells [81]. The activated endothelial cells increase the

secretion of the proteolytic enzymes that degrade ECM and BM (see Figure 21A) [87]. In the angiogenic process, there are two distinct cellular phenotypes of endothelial cells involved, which are known as the tip cells and the stalk cells [88]. Endothelial tip cells that are heavily endowed with VEGF-receptor 2 guide angiogenic sprouting following the VEGF-A concentration gradient (see Figure 21B), whereas endothelial stalk cells proliferate and elongate the sprouting (see Figure 21C) [88]. The newly formed sproutings fuse to form the lumen (see Figure 21D), which allows blood perfusion and oxygen delivery (see Figure 21E). Pericytes and smooth muscle cells are recruited to stabilize the neovessels (see Figure 21F) [87].

**Figure 21.** ***VEGF-A in Angiogenesis***

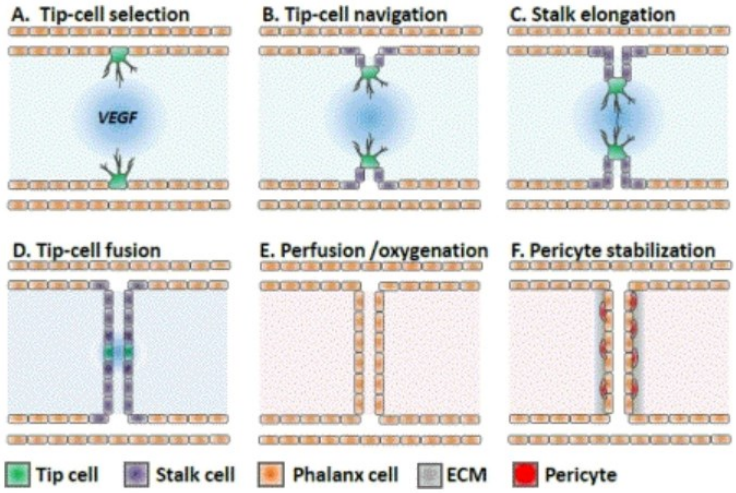


***Note.*** **A.** VEGF activates quiescent endothelial cells. The activated endothelial cells adopt a specific phenotype; this process is known as tip cell selection. **B.** Endothelial tips cells guide angiogenic sprouting following the VEGF-A concentration gradient. **C.** The other distinct phenotype of endothelial cells is stalk cells, which proliferate and elongate the sprouting. **D.** The newly formed vessels fuse. **E.** Blood perfusion and oxygen delivery occur in the neovessels. **F.** Neovessel maturation and stabilization via pericytes. (reprinted from Adair TH et al., 2010 [81]).

### 1.6.1.2 VEGF-A in ROP

The growth of normal retinal blood vessels is VEGF-A-dependent [30]. The neural retina develops prior to retinal vascular development and creates physiological hypoxia due to increased oxygen demand [89]. In retinal vascular development, VEGF-A is produced locally by astrocytes, which guides the vessel growth in the superficial layer (NFL). In the INL, VEGF-A is produced by Müller cells to form deep plexuses [89]. Once the vascular development in the retina is complete, VEGF-A is downregulated to an average level by the oxygen delivered via the neovessels [30].

In phase I of ROP, VEGF expression and VEGF-A-driven vessel growth are suppressed by hyperoxia [90]. Because VEGF-A is essential for endothelial cell survival, the reduced level of VEGF-A causes vascular endothelial cell apoptosis, which results in the degeneration of the pre-existing retinal vessels [81].

In phase II of ROP, hyperoxia turns into hypoxia due to the increased demand for oxygen by the maturing retina. Hypoxia subsequently stimulates the production of VEGF-A from various types of cells [91], which contributes to the formation of aberrant retinal NV [92]. Moreover, the significantly increased VEGF-A level has been identified in the vitreous humor of patients with retinal NV [93].

### 1.6.2 Stromal Cell-Derived Factor (SDF-1)

Stromal cell-derived factor-1 (SDF-1), also termed C-X-C motif chemokine 12 (CXCL12), is a chemotactic factor that belongs to the CXC chemokine group [94]. SDF-1 exerts an effect exclusively through the activation of G-protein-coupled receptor CXCR4, which exists as a membrane receptor on mononuclear and endothelial cells [95]. Several tissues within the body have been shown to produce SDF-1, including the brain, bone marrow, kidney, lung, lymph node, liver,

and muscle [95]. SDF-1 is implicated in the homing and recruitment of lymphocytes, monocytes/macrophages, and stem/progenitor cells [94-96].

#### 1.6.2.1 SDF-1 in Angiogenesis

In addition to the well-known chemotactic effect, SDF-1 also serves as a potent angiogenesis-inducing factor. SDF-1 can directly stimulate angiogenesis via the activation of CXCR4 expressed on the endothelial cells [97]. The CXCR4-expressing endothelial cells migrate following the SDF-1 chemokine gradient and subsequently form neovessels [97]. Furthermore, the increased angiogenic factors, such as VEGF and basic fibroblast growth factor, enhance the expression of CXCR4 on endothelial cells [98], which further promote the angiogenic process.

Additionally, the interaction of SDF-1 with CXCR4-expressing cells leads to the activation of NF-kB, which results in increased secretion of matrix metalloproteinases (MMPs), NO, and angiogenic factors (e.g., VEGF) [95] that are critical modulators in the angiogenic process.

#### 1.6.2.2 SDF-1 in ROP

An increased SDF-1 level has been detected in the vitreous humor of ROP patients with vascular complication [93]. The expression of SDF-1 increases under hypoxia, which impairs the gap junctions of retinal endothelial cells [99]. Moreover, inhibition of SDF-1 significantly prevents pathological retinal NV [99]. In addition to the direct effect on angiogenesis, SDF-1 also indirectly regulates retinal NV via the recruitment of pro-angiogenic monocyte-derived macrophages [78]. Abrogation of SDF-1 drastically suppresses the infiltration of peripheral macrophages as well as the recruitment of the bone marrow-derived cells (e.g., endothelial progenitor cells) involved in the retinal angiogenic process [78]

### 1.6.3 Hypoxia-Inducible Factor-1 α

Hypoxia-inducible factor-1 (HIF-1) is recognized as a master regulator of transcription in response to hypoxic stress. HIF-1 is a heterodimeric protein composed of an oxygen-regulated subunit (HIF-1α,120 kD) and a stably-expressed subunit (HIF-1β, 94 kD) [100].

Although transcription of HIF-1α mRNA continuously takes place under normoxia, the protein is rapidly degraded by the proteasome [100]. Generally, the degradation of HIF-1α is initiated by the interaction of Von Hippel-Lindau (VHL) with Elongin C protein, which recruits an E3 ubiquitin-protein ligase complex. HIF-1α is quickly ubiquitinated by the complex, followed by recognization and degradation by the 26 S proteasome [101]. The binding activity of VHL is dependent on hydroxylation of either proline residue 402 or 564, which are mediated by a dioxygenase known as prolyl hydroxylase [102]. However, the activity of hydroxylase is inhibited under hypoxia, which results in increased protein expression of HIF-1α [100]. The stabilized HIF-1α then dimerizes with HIF-1β and forms a complex which subsequently translocates into the nucleus and binds to the hypoxia-responsive elements (HREs) in the promoter region of the target genes [103]. HIF-1 regulates the transcription of hundreds of genes in a cell-type-specific manner, in which the protein expression of HIF-1α determines the functional activity of HIF-1 [100]. The stability of the HIF-1α protein is highly regulated at the posttranscriptional level by phosphorylation, acetylation, hydroxylation, and ubiquitination [103].

#### 1.6.3.1 HIF-1α in Angiogenesis

Angiogenesis is a complex process that is regulated by multiple gene products, and many of these genes are regulated in an oxygen-dependent manner [87]. HIF-1α almost regulates at every step

of the angiogenic process via modulating the transcription of multiple genes under hypoxic stimulus [103]. The degradation of the extracellular matrix, the first step of angiogenesis, is mediated by the upregulated MMPs [81], which are direct targets of HIF-1α [103]. The master regulator of angiogenesis VEGF, another direct target of HIF-1α under hypoxia, promotes angiogenesis via increasing endothelial cell proliferation and directing endothelial cell migration [101]. Furthermore, the vessel branching regulated by Notch signaling is targeted by HIF-1α as well, in which HIF-1α directly binds to the Notch intracellular domain and enhances the transcriptional activity [104].

#### 1.6.3.2 HIF-1α in ROP

Considering that hypoxia plays a pivotal role in the pathogenesis of ROP, especially in the development of the second phase, the vaso-proliferation phase, it should not be surprising that HIF-1α participates during pathological retinal NV.

In a mouse model of oxygen-induced ischemic retinopathy, which mimics the pathogenesis of ROP, the expression of HIF-α displays a temporal and spatial correlation with VEGF mRNA expression, which is suppressed in the vaso-obliteration phase and upregulated in the vaso-proliferation phase [105]. In addition to VEGF, several other pro-angiogenic factors, such as erythropoietin, SDF-1, and platelet-derived growth factor B, are under the control of HIF-1α, which further contributes to pathological retinal NV [106, 107]. Moreover, pharmacological inhibition of HIF-1α reduces pathological retinal NV without affecting physiological NV and also prevents the impaired visual function [108].

## 1.7 EXTRACELLULAR VESICLES

In general, all types of cells are able to secrete membrane-wrapped vesicles named extracellular vesicles (EVs) [109]. EVs are critical mediators of intercellular communications [110]. They are released into the extracellular microenvironment when parental cells undergo apoptosis or activation [109]. The secreted-EVs contain distinct biological components (proteins, lipids, and nucleic acids) that are determined by the stimulus and the cell types (see Figure 22A). EVs target recipient cells and release their contents, which elicit functional changes in the targeted cells (see Figure 22A) [111].

EVs are mainly grouped into two classes: microvesicles and exosomes, according to the generation process [112]. Exosomes (30 ~ 100 nm) are intraluminal vesicles that are formed by inward budding of the endosomal membrane [111]. Exosomes are released upon the fusion of multivesicular endosomes with the plasma membrane (see Figure 22B) [112]. Microvesicles also named microparticles, which range from 100 ~ 1000 nm, are small membrane vesicles produced by outward budding of the cell membrane (see Figure 22B) [111].

**Figure 22.** ***Nature and The Generation Process of EVs***

**A.**

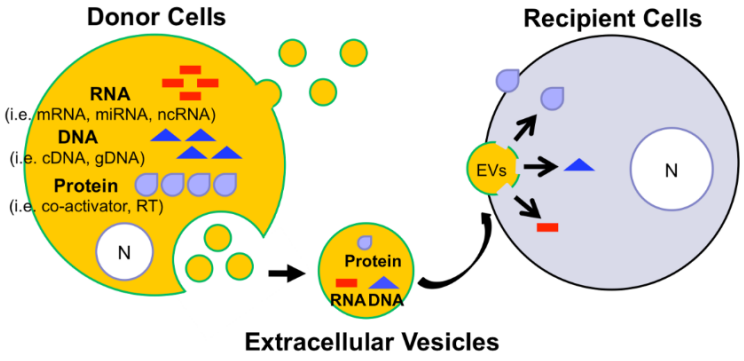


**B.**

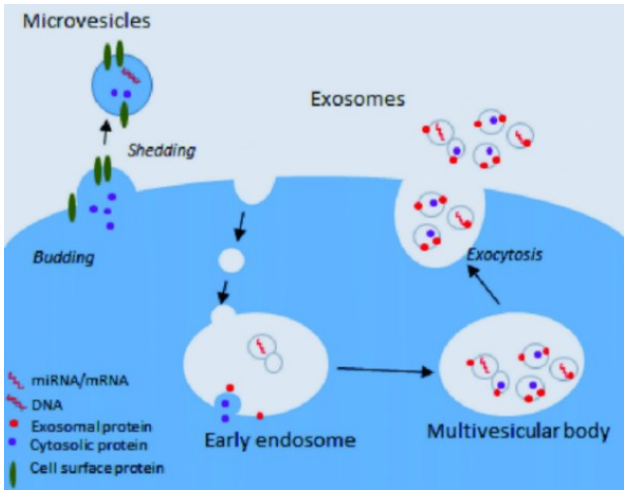


***Note.*** **A.** The critical role of EVs in intercellular communication. **B.** The generation processes of two main subgroups of EVs: microvesicles and exosomes. (reprinted from Charlotte et al., 2017 [109]).

### 1.7.1 The Functions of EVs

EVs released into the extracellular fluid have been implicated in multiple processes, including (a) intercellular communication, (b) angiogenesis, (c) cell survival, and (d) inflammation [113].

EVs play an essential role in intercellular communication by transferring biological components from the parental cells to the recipients and therefore regulate the components and functions of the recipient cells. Microparticles released from platelets transfer the platelet fibrinogen receptor to cancer cells, thereby increasing the adhesion of cancer cells to endothelial cells [110]. Activated platelet-derived microparticles contain activated caspase 3 and serve as a messenger that induce macrophage apoptosis [114]. Additionally, exosomes excreted from tumor cells transfer mutant epidermal growth factor receptor RNA to platelet [113].

EVs have pro- and anti-angiogenic properties. Microparticles released from apoptotic endothelial cells contain MMP-2 and MMP-9 that promote angiogenesis via matrix degradation [110].

Moreover, activated platelet-derived microparticles also contribute to the formation of neovessels via promoting the proliferation, survival, migration, and tube formation of endothelial cells [114]. In addition to pro-angiogenic effects, microparticles released from endothelial cells are capable of suppressing angiogenesis through the production of ROS [115].

Studies showed that cancer cells received chemotherapy treatment increase the secretion of EVs, which contain accumulated chemotherapeutic drugs [113, 116]. These suggest that cancer cells release EVs might support cancer cell survival by removing the chemotherapeutic drugs, which in turn reduce the intracellular drug concentration. Additionally, EVs can transfer multidrug transport. Microparticles secreted from drug-resistant cancer cells transfer P-glycoprotein to drug-sensitive cancer cells [117].

EVs can also affect inflammation. Microparticles released from neutrophils containing anti-inflammatory protein annexin 1 inhibit the inflammatory reaction of macrophages in response to bacterial lipopolysaccharide [118]. Additionally, these microparticles also trigger the secretion of transforming growth factor β1, which inhibits the activation of macrophages and elicits an anti-inflammatory response [119].

### 1.7.2 Lymphocytic Microparticles

Microparticles have been implicated in the pathogenesis of inflammatory and cardiovascular diseases that are associated with vascular damage or impaired angiogenesis [120]. In particular, elevated levels of microparticles originated from lymphocytes have been detected in human atherosclerotic plaque [121] and patients with preeclampsia [122]. Moreover, microparticles generated from apoptotic T lymphocytes or the plasma of diabetic patients impair vascular endothelial function via the modulation of the NO pathway and activation of NF-kB [123].

Lymphocytic microparticles (LMPs) are small membrane-wrapped vesicles derived from apoptotic human CEM T lymphocytes, which is a human cell line generated from acute lymphoblastic leukemia [124]. We have demonstrated that LMPs possess potent anti-angiogenic and anti-tumor effects [125-128].

### 1.7.3 The Angiogenesis-Inhibiting Capacities of LMPs

The angiogenesis-inhibiting capacities of LMPs have been confirmed in several models: (a) in the aortic ring model, LMPs drastically suppresses the formation of neovessels after 48 h (see Figure 23A) [125]; (b) in the corneal angiogenesis model, LMPs causes a 23% reduction of angiogenesis (see Figure 23B) [125]; (c) in the Lewis lung carcinoma model, LMPs reduce the microvascular density in the tumor model by 40% (see Figure 23C) [128]; and (d) in the laser-induced choroidal NV mouse model, LMPs attenuate pathological choroidal NV by 75% (see Figure 23D) [126].

**Figure 23.** ***The Angiogenesis-Inhibiting Capacities of LMPs.***

**A.** **B.**

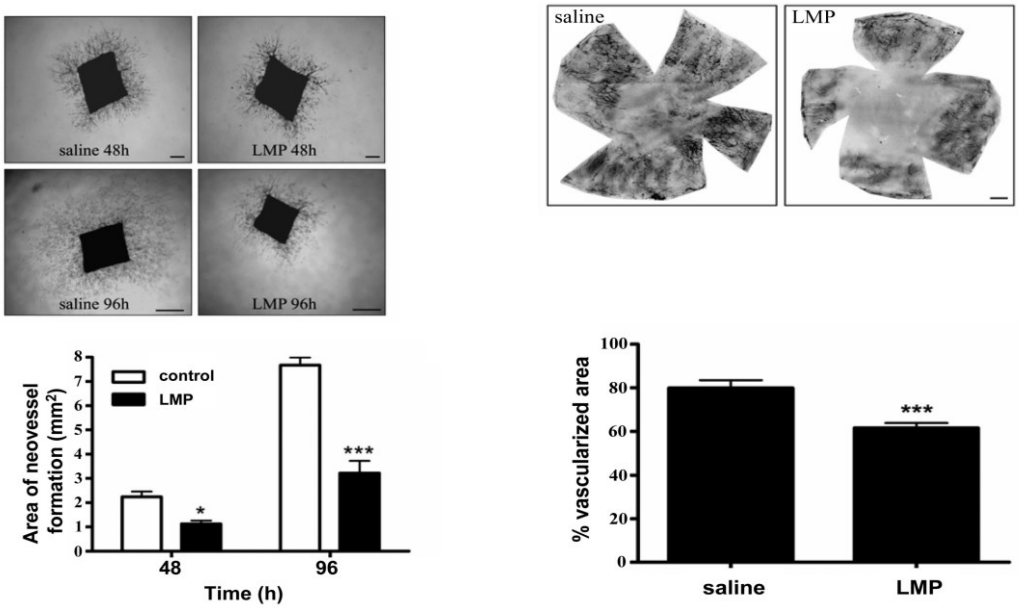
saline 48h
LMP 48h
saline 96h
LMP 96h
saline
LMP
control
LMP
Area of neovessel formation (mm²)
Time (h)
48
96
*
***
% vascularized area
saline
LMP
***

**C.**

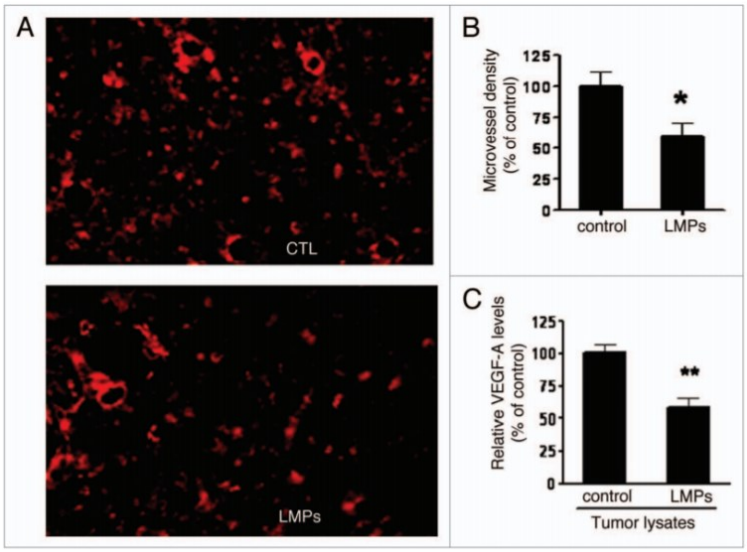
A
CTL
LMPs
B
Microvessel density (% of control)
control
LMPs
*
C
Relative VEGF-A levels (% of control)
control
LMPs
Tumor lysates
**

**D.**

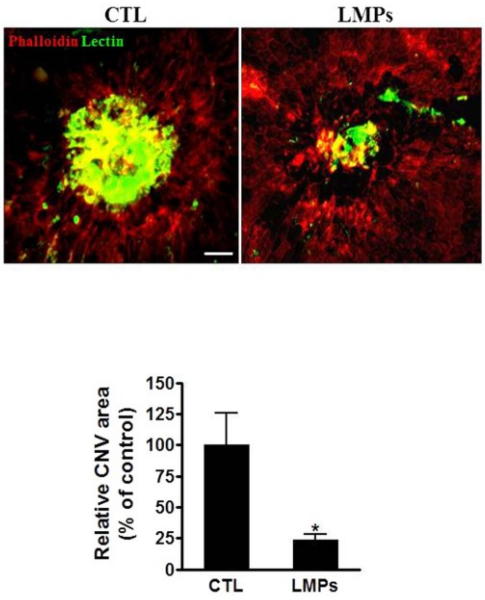


***Note.*** **A.** LMPs inhibit the formation of neovessels in the aortic ring model. (reprinted from Chun Yang et al., 2008 [125]). **B.** LMPs inhibit retinal angiogenesis in the hypoxia-induced retinopathy rat model. (reprinted from Chun Yang et al., 2012 [129]). **C.** LMPs reduce the microvessel density in the Lewis lung carcinoma mouse model. (reprinted from Chun Yang et al., 2014 [128]**). D.** LMPs suppress choroidal NV in the laser-induced choroidal NV mouse model. (reprinted from Tahiri Houda et al., 2016 [126]).

The molecular mechanisms affected by the angiostatic LMPs have also been extensively studied, showing that LMPs inhibit the activities of endothelial cells (migration and proliferation) by modifying the NADPH oxidase (NOX) pathway [125]. In addition, LMPs target VEGF-related signaling pathways in different types of endothelial cells [129] and Lewis lung carcinoma cells [128].

## 1.8 RESEARCH PROJECT

In our previous studies, we demonstrated that LMPs suppress pathological retinal NV in a rat model of ischemic retinopathy via affecting the proliferation and migration as well as ERK pathway in the retinal endothelial cells [129]. In this study, we set out to gain a better insight into the angiogenesis-inhibiting effects of LMPs in a mouse model of ischemic retinopathy. Considering Müller cells' anatomical and functional importance in the retina as well as the pathogenesis of ROP, it is hypothesized that LMPs target Müller cells. LMPs reduce the expression of angiogenic/chemotactic factors VEGF and SDF-1 in Müller cells, which reduce the recruitment of monocyte-derived macrophages. All this can lead to the attenuation of pathological retinal NV.

The main objectives of this work are to investigate the angiostatic capacities of LMPs and the possible mechanisms affected by LMPs. For this purpose, the influence of LMPs is studied *in vitro, ex vivo,* and *in vivo.* The objectives are as follows:

1: To study the impact of LMPs on Müller cell proliferation and apoptosis *in vitro*.

2: To examine the influence of LMPs on the chemoattraction of macrophages mediated by Müller cells *in vitro* and *ex vivo.*

3: To confirm the angiostatic effect of LMPs *in vivo.*

4: To dissect the molecular mechanisms affected by LMPs *in vitro* and *in vivo*.

# Chapter 2:

# MATERIAL AND METHODS

## 2.1 THE PRODUCTION OF LYMPHOCYTIC MICROPARTICLES

Human CEM T lymphocytes were purchased from American Type Culture Collection (ATCC) and grown in X-VIVO medium (Cambrex). Briefly, human CEM T lymphocytes were incubated with 0.5 μg/mL apoptotic reagent actinomycin D (Sigma Aldrich) for 24 h. The medium was processed through multistep centrifugation as follows to obtain the pellet containing microparticles: (a) the medium was centrifuged at 750 g for 15 min to remove large cells; (b) followed by centrifugation at 1,500 g for 5 min to remove cell debris, and apoptotic bodies; and (c) the last centrifugation of the supernatant containing microparticles was conducted at the speed of 12,000 g for 50 min to obtain the pellets. The sedimented pellet containing LMPs were washed twice and recovered in phosphate buffer saline (PBS) (see Figure 24A). We utilized the last washing medium as a negative control. The characterization of LMPs was determined by Annexin-V staining via flow cytometry analysis (see Figure 24B), and the concentration of LMPs was assessed by Bradford protein assay (Sigma Aldrich).

**Figure 24.** ***The Production Process of LMPs***

**A.**

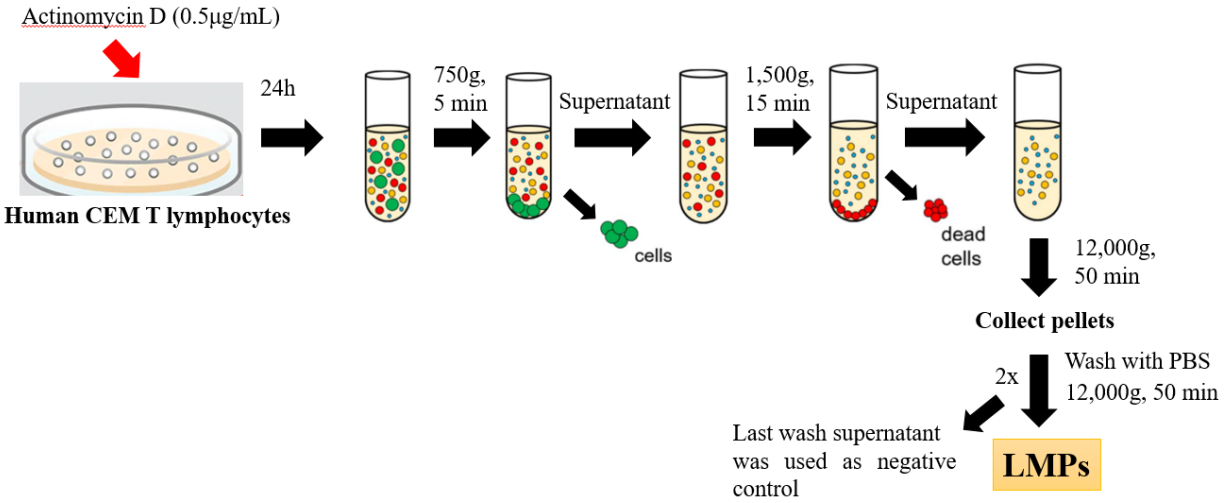

**B.**

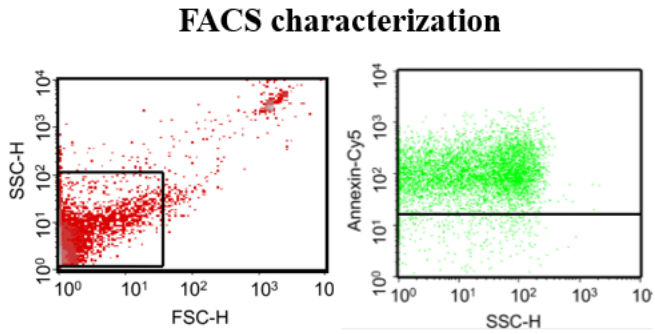


***Note.*** **A.** Human CEM T lymphocytes were treated with an apoptosis-inducing reagent actinomycin D (0.5 µg/mL) for 24 h. Cell medium containing microparticles proceeded for multiple-step centrifugation at different speeds. **B.** Characterization of LMPs by flow cytometry analysis. 1 µm beads were used to gate LMPs. The gated events of LMPs were further subjected to Annexin-V-Cy5 staining to exclude the electronic noise.

## 2.2 CELL CULTURE

### 2.2.1 rMC-1 Cells

Rat Müller cell line (rMC-1, Kerafast) was obtained from Dr. Sylvain Chemtob (CHU Sainte-Justine Research Center, Montreal, QC). rMC-1 cells were grown in Dulbecco's Modified Eagle's Medium (DMEM, Gibco) supplemented with 10% fetal bovine serum (FBS, Gibco) and 1% penicillin/streptomycin (Gibco). Cells were cultured in a humidified incubator under standard conditions (37°C, 5% $CO_2$, and 21% $O_2$). Cells were passaged at the confluency of 70 ~ 80%, and the culture medium was replaced every 2 ~ 3 days.

### 2.2.2 RAW 264.7 Cells

Macrophage cell line (RAW 264.7) was purchased from ATCC, and cells were grown in DMEM (Gibco) supplemented with 10% FBS (Gibco) and 1% penicillin/streptomycin (Gibco). Cells were cultured in a humidified incubator under standard conditions (37℃, 5% $CO_2$, and 21% $O_2$). Cells were passaged at the confluency of 70 ~ 80%, and the culture medium was replaced every 2 ~ 3 days.

## 2.3 DIL-LMPs UPTAKE EXPERIMENT

### 2.3.1 Generation of Dil-LMPs

Because the lipophilic fluorescent dye dialkylcarbocyanines, in particular Dil (1,1′-Dioctadecyl-3,3,3′,3′-Tetramethylindocarbocyanine Perchlorate, Molecular Probes), does not affect cell viability, development, and physiological properties [130]. Therefore, we used Dil to label LMPs to trace the distribution of LMPs *in vitro* and *in vivo*. Dil was dissolved in ethanol (5 mg/mL). Dil-LMPs were generated by incubating the lipophilic fluorescent dye Dil (5 mg/mL) with human CEM T lymphocytes for 24 h before actinomycin D treatment.

### 2.3.2 Dil-LMPs Uptake Assay

For the Dil-LMPs uptake experiment, rMC-1 Müller cells were seeded in the 96-well plate overnight, followed by incubating with Dil-LMPs (10 μg/mL) for 1, 4, 8, and 24 h. Cells were washed three times with PBS after reaching the incubation time point, respectively, followed by

subjecting them to spectrofluorometer readings (fluorescent excitation: 600 nm, emission: 665 nm; Clariostar) to assess the uptake by determining the mean fluorescent intensity (MFI).

## 2.4 CELL EVENT EXPERIMENTS

### 2.4.1 Hypoxia Induction by Cobalt Chloride in rMC-1

The hypoxic condition of rMC-1 was stimulated by the chemical reagent cobalt chloride ($CoCl_2$, Sigma Aldrich). $CoCl_2$ was diluted in 2% FBS DMEM (Gibco) and filtered with a 0.2 μm syringe filter (Sigma Aldrich). rMC-1 were either incubated with 50 μM or 100 μM of $CoCl_2$ for 24 h. The optimal concentration of $CoCl_2$ was determined by the cell proliferation of rMC-1 and the mRNA expression level of VEGF in rMC-1, which were assessed by [$^3$H]-thymidine incorporation and real-time PCR, respectively.

### 2.4.2 Cell Proliferation via [$^3$H]-Thymidine Incorporation Assay

rMC-1 at approximately 60% confluency were incubated with $CoCl_2$ (100 μM) and indicated concentrations of LMPs (5, 10, 20, and 30 μg/mL) for 24 h. Cell proliferation was determined by [$^3$H]-thymidine (Perkin Elmer). Briefly, cells were incubated with 1 Ci/mL of [$^3$H]-thymidine reagent for 24 h, and the cell proliferation was assessed by scintillation counting.

### 2.4.3 Cell Apoptosis via Flow Cytometry

rMC-1 at the confluency of 60% were treated with $CoCl_2$ (100 μM) and LMPs (10 μg/mL) for 24 h, followed by incubation with reagents from FITC Annexin V/Dead Cell Apoptosis Kit (Invitrogen)

according to the manufacture's protocol. Staurosporine (1 μg/mL) was used as a positive control. rMC-1 were incubated with staurosporine (1 μg/mL) and $CoCl_2$ (100 μM) for 6 h. Apoptosis was determined by flow cytometry analysis via FacsCalibur (BD Biosciences) and expressed as the percentage of cells undergoing early and late apoptosis over the total number of cells per condition.

## 2.5 TRANSWELL MIGRATION ASSAY

The chemotactic capacity of rMC-1 was determined by transwell migration assay with RAW 264.7 murine macrophages (see Figure 25). The 24-well plate with the transwell inserts of 5.0 μm pore size (Costar) was used for the migration assay. The supernatant was collected from the following three conditions: rMC-1 without any treatment (NOR), rMC-1 treated with $CoCl_2$ (100 μM), and rMC-1 incubated together with $CoCl_2$ (100 μM) and LMPs (10 μg/mL). The collected supernatant (600 μL) was added to the lower chamber. RAW 264.7 cells (1 x $10^5$ cells, 100 μL) were seeded in the insert of the upper chamber. The plate was incubated in a humidified incubator under standard conditions (37°C, 5% $CO_2$, and 21% $O_2$) for 2 h to allow the cells to migrate. After 2 h, the medium in the upper chamber was discarded. The membrane of the insert was washed S and fixed with 4% paraformaldehyde (PFA). The cell nucleus on the membrane was identified by DAPI (1:5000). The membrane was then carefully cut, transferred onto a slide, mounted with a drop of Mountant PermaFluor medium (Thermo Scientific), and covered with a coverslip. Images (4 images/condition) were taken by the DMi8 Leica microscope (Concord).

**Figure 25.** ***Transwell Migration Assay of RAW 264.7***

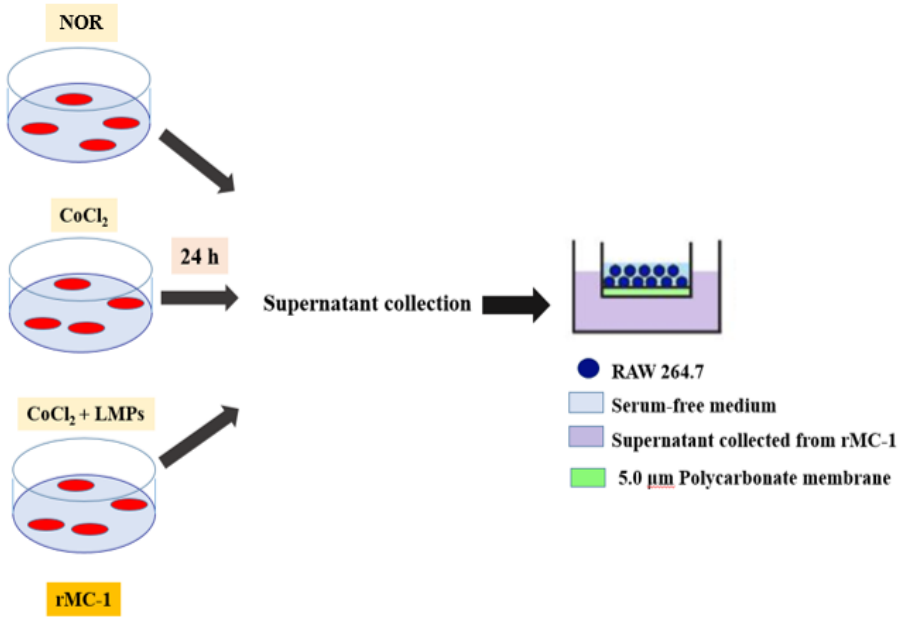


***Note.*** The supernatant was collected in the following three different conditions after 24 h incubation: NOR (without any treatment), $CoCl_2$ (100 μM)-treated, and $CoCl_2$ (100 μM) together with LMPs (10 μg/mL). The supernatant was subjected to transwell migration assay with RAW 264.7 cells.

## 2.6 THE ANIMAL MODEL OF ISCHEMIC RETINOPATHY

### 2.6.1 Animal

The animal protocol (#686) was approved by the CHU Sainte-Justine Research Center Animal Welfare Committee CIBPAR. C57BL/6J mice at postnatal (P) day 5 (P5), along with their mothers, were purchased from Charles River (St. Constant, QC, CA).

### 2.6.2 Mouse Model Establishment

The effect of LMPs was investigated *in vivo* using the mouse model of oxygen-stimulated ischemic retinopathy (OIR), as described by Smith et al., [131]. Briefly, P7 mice pups, along with their breeding mothers, were exposed to 75% $O_2$ (Oxycycler A820CV; BioSpherix Ltd.) for five days until P12. Mice were relocated back to room air (21% $O_2$) at P12 and kept in the room air until P17 (see Figure 26). Mice were supplied with sufficient food and water and kept under 12 h daylight and 12 h dark cycle. A control group of mice was kept in the room air from P7 to P17.

**Figure 26.** ***The Timeline of The Animal Model Establishment***

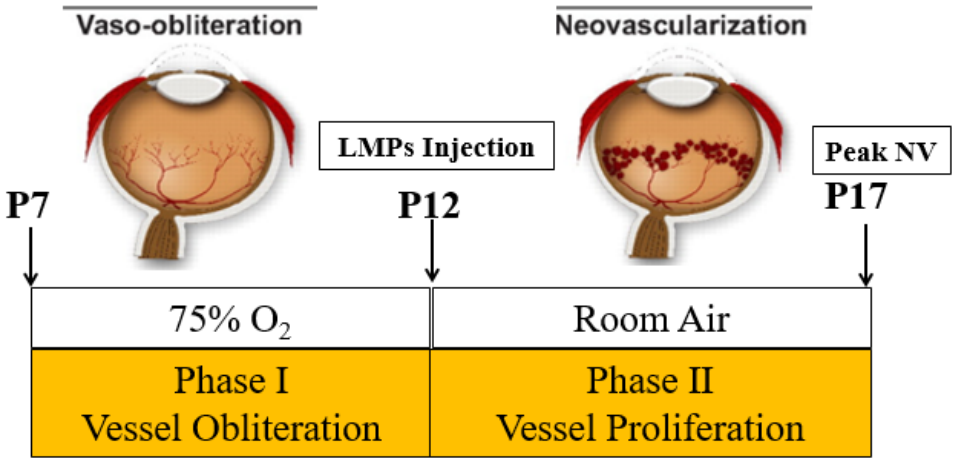


***Note.*** C57BL/6J mice pups and the breeding mothers underwent a duration of hyperoxia (75% $O_2$) from P7 to P12. After P12, the mice were relocated back to room air (21% $O_2$). Mice received a single intravitreal injection of LMPs (10 μg/μL) in one eye and the same volume of sterile PBS (vehicle) in the contralateral eye at P12. Hyperoxia from P7 ~ P12 initiated phase I of ROP: vessel

obliteration phase. The relative hypoxia from P12 ~ P17 developed phase II of ROP: vessel proliferation phase.

### 2.6.3 Mice Weight Monitoring

The weight of the pups was measured on P7, P12, and P17 before the onset of experiments. Mice weight between 5.5 g ~ 7 g on P12 and between 7 g ~ 8.5 g on P17 were included for the following experiments.

### 2.6.4 Intravitreal Injection of LMPs or Dil-LMPs

LMPs (10 μg/μL, 1 μL/eye) were intravitreally injected in the right eye of P12 mice once. The same volume of sterile PBS was injected in the contralateral eye (n = 5 mice/group; 5 eyes/condition). Dil-LMPs (10 μg/μL, 1 μL/eye) were intravitreally injected on P12 to track the distribution of LMPs in the retina. The same volume of sterile PBS was injected in the contralateral eye (n = 5 mice/group; 5 eyes/condition).

### 2.6.5 *Ex Vivo* Retinal Explants Model

To mimic the *in vivo* microenvironment, we established the *ex vivo* retinal explants model. The model established procedure was based on our previous publication [126], with minor modifications. Briefly, P14 OIR mice were anesthetized; eyes were collected and dissected under the microscopy (Olympus SZ61) in a Petri dish filled with 1X Hank's Balanced Salt Solution (HBSS, Thermo Scientific). Retinas (3 retinas/condition) were incubated in a 24-well plate with LMPs (50 μg/mL) or sterile PBS for 24 h. The dish was cultured in a humidified incubator under standard conditions

(37°C, 5% $CO_2$, and 21% $O_2$). Retinas were collected after 24 h and subjected to RNA extraction. The supernatant was collected and subjected to the transwell migration assay

## 2.7 RNA EXTRACTION

### 2.7.1 Retinal Tissue RNA Extraction

The P14 retinas from the mice-received an intravitreal injection and *ex vivo* retinal explant model were used for total RNA extraction (3 retinas/condition). Briefly, the P14 retinas in the respective condition were pooled in the RLT buffer (350 µL) supplemented with β-mercaptoethanol (β-ME, 1:100, Sigma Aldrich) for sonication. RNAs were extracted with RNeasy®Mini Kit (QIAGEN) according to the manufacture's protocol. Briefly, after sonication, 70% ethanol (350 µL) was added to the buffer RLT. The whole volume (700 µL = 350 µL buffer RLT + 350 µL 70% ethanol ) was transferred to the RNeasy Mini spin column and underwent multistep centrifugation with different mediums. The initial centrifugation was conducted at the speed of 10,000 g for 15 s, followed by the same spinning speed and time with buffer RW1 (700 µL). The last two centrifugations were conducted with buffer RPE (500 µL) at the same rate for 15 s and 2 min, respectively. RNeasy column was then placed in a new 2 mL collection tube and centrifuged at full speed for 1 min to dry the column. The RNAs were eluted by spinning at the maximum speed for 1 min with RNase-free water (30 µL), and the concentration was measured by Nanodrop™ 2000/2000c (Thermo Scientific).

### 2.7.2 rMC-1 RNA Extraction

Total RNA was extracted from rMC-1 in the following three conditions after 24 h of incubation: rMC-1 without any treatment (NOR), rMC-1 incubated with $CoCl_2$ (100 µM), and rMC-1 treated

with $CoCl_2$ (100 μM) and LMPs (10 μg/mL). The RNAs were extracted with RNeasy®Mini Kit following the procedures as abovementioned, and the concentration was measured by NanodropTM 2000/2000c.

## 2.8 REAL-TIME PCR

### 2.8.1 cDNA Synthesis

The extracted RNAs that met the requirements of $A_{260}/A_{280}$ between 1.8~2.1 and $A_{260}/A_{230}$ above 2.0 were included for the following real-time PCR experiments. DNase-treated RNA was converted into cDNA for PCR analysis via iScript Advanced cDNA synthesis kit (Bio-Rad) according to the manufacturer's protocol. Briefly, 1 μg of RNA was converted into cDNA via preparing a 20 μL mixture containing 5x iScript Advanced Reaction Mix (4 μL), iScript Advanced Reverse Transcriptase (1 μL), the volume of RNA that reached the total amount (1 μg), and nuclease-free water. The mixtures were incubated at 46℃ for 20 min, followed by inactivation at 95 ℃ for 1 min. The cDNA was diluted 1/10 and stored at -20℃.

### 2.8.2 RT-PCR

Primers were designed via Primer3 (version 4.0; http://bioinfo.ut.ee/primer3-0.4.0/) according to requirements: the size of (minimum: 20; optimal: 24; maximum: 26), the GC% of the primer (minimum: 40; maximum: 60), the max-self complementarity (4.00), and the product size (ranging from 100 ~ 200 bp). Primers were synthesized by Alpha DNA (Montreal, QC, CA), as indicated in table 1.

**Table 1. The Primers Used for Real-Time PCR**

| Gene Target | Primer Sequence (5' ——> 3') |
|---|---|
| VEGF (rat) | F: 5'-GACAGAACAAAGCCAGA-3' |
| | R: 5'-CACCGCCTTGGCTTGTCAC-3' |
| VEGF (mouse) | F: 5'-GACTTGTGTTGGGAGGAGGA-3' |
| | R: 5'-TCTGGAAGTGAGCCAATGTG-3' |
| ERK1 (rat) | F: 5'-ACCACATCTGCTACTTCCTCTACC-3' |
| | R: 5'-ATTGGCCGAGTGTATGTACTTGAG-3' |
| ERK2 (rat) | F: 5'-GTCTCAGCTTACCCACTCTTGACT-3' |
| | R: 5'-ATAAAAGCCACTACGACCAGAACT-3' |
| HIF-1α (rat) | F: 5'-CTTCTGATGGAAGCACTAGACAAA-3' |
| | R: 5'-GAATACATTGACCATATCGCTGTC-3' |
| β-actin (rat) | F: 5'-CACTGGCATTGTGATGGACT-3' |
| | R: 5'-CTCTCAGCTGTGGTGGTGAA-3' |
| HPRT (mouse) | F: 5'-GGACCTCTCGAAGTGTTGGATA-3' |
| | R: 5'-GCGCTCATCTTAGGCTTTGTAT-3' |
| SDF-1 (rat) | F: 5'-AACTCCTTTACTCAAATGGGACAG-3' |
| | R: 5'-ACAACAGACACTTCCTTTTCCTTC-3' |
| SDF-1 (mouse) | F: 5'-GCTTGGGAGGAAACAAATACAG-3' |
| | R: 5'-GAGAATGGGGGATTAAGGTAGG-3' |

Quantitative analysis of gene expression was performed on the LightCycler 96 sequence detection system with SYBR Green Master Mix Kit (Bio-Rad). PCR protocol involved a preincubation step at 95℃ for 600 s (1 cycle), followed by a 3-step amplification: denaturation at 95℃ for 10 s, 60℃ for 60 s, and 72℃ for 60 s (40 cycles), and a melting step at 95℃ for 10 s, 65℃ for 60 s, and 97℃

for 1 s (1 cycle). Each sample was analyzed in triplicate. Gene expressions of the OIR retinas and retinal explants were normalized to HPRT. Gene expressions of rMC-1 were normalized to β-actin.

## 2.9 WESTERN BLOT

rMC-1 at the confluency of 60% were incubated with $CoCl_2$ (100 μM) and LMPs (10 μg/mL) for 24 h. Soluble proteins were extracted using Mammalian Protein Extraction Reagent (M-PER, Thermo Fisher) supplemented with proteinase inhibitor Cocktail Halt Reagent (1:100, Thermo Fisher) and the concentration was determined by Bradford protein assay (Sigma Aldrich). Proteins (30 μg) were separated by SDS-PAGE using 12% gel and transferred onto a polyvinylidene difluoride membrane (Bio-Rad). The membranes were blocked in PBS with 0.05% Tween 20 (Bio-rad) containing 3% milk or 3% bovine serum albumin (BSA) for 1 h at room temperature. The membranes were then incubated at 4°C overnight with a monoclonal antibody against VEGF-A (1:1000, mouse, Abcam), a polyclonal antibody against HIF-1α (1:500, rabbit, Abcam), or a polyclonal antibody against ERK1/2 (1:1000, rabbit, Abcam). Finally, the membranes were incubated with horseradish peroxidase-linked anti-rabbit IgG (1:3000, Santa Cruz) or horseradish peroxidase-linked anti-mouse IgG (1:3000, Santa Cruz) for 1 h at room temperature. β-actin was used as an internal control (1:5000, Novus Biologicals). The signals were visualized via ECL Western blot detection system (Perkin Elmer). ImageJ software was used to analyze the densitometry values in terms of pixel intensity.

## 2.10 IMMUNOFLUORESCENT STAINING

### 2.10.1 rMC-1 Cells

For the detection of Dil-LMPs uptake by rMC-1, an ethanol-sterilized coverslip was plated in the 24-well plate before seeding the cells. rMC-1 were treated with Dil-LMPs (10 μg/mL) for 8 and 24 h. After incubation, cells were washed, fixed with 4% PFA, and followed by 1 h blocking at room temperature with medium containing 0.3% TritonX-100/PBS, 0.3M Glycine, 10% normal goat serum (NGS), and 3% BSA. Primary and secondary antibodies were diluted in PBS that contained 0.3% TritonX-100/PBS and 3% BSA. Cells were incubated with a monoclonal antibody against glutamate synthetase (1:500, mouse, Millipore) for 2 h at room temperature, followed by incubation with goat-anti-mouse AlexaFluor 488 (1:1000, Life Technologies) for 2 h at room temperature. Cells nucleus was identified by DAPI (1:5000). Coverslips were then transferred onto a slide, mounted with Mountant PermaFluor medium (Thermo Scientific), and imaged with the DMi8 Leica microscope (Concord).

### 2.10.2 Retinal Whole-Mounts

Eyes from P17 mice were collected, fixed with 4% PFA, and dissected under the microscope (Olympus SZ61). The intact retinas were blocked for 1 h at room temperature with the medium containing 0.3% TritonX-100/PBS, 0.3M Glycine, 10% NGS, and 3% BSA. Primary and secondary antibodies were diluted in PBS that included 0.3% TritonX-100/PBS and 3% BSA.

To assess macrophage recruitment, we incubated retinas at 4℃ overnight with a monoclonal antibody against F4/80, which is conjugated with FITC (1:50, rat, Thermo Fisher) or a monoclonal antibody against TMEM119 (1:100, rabbit, Abcam). Then the retinas were incubated with goat-anti-rabbit AlexaFluor 594 (1:1000, Thermo Scientific) for 1 h at room temperature. Retinas were then carefully transferred onto a slide, cut into a flower shape, and mounted with Mountant PermaFluor medium (Thermo Scientific). Images (3 images/condition) were taken by the SP8 Leica confocal microscopy (Concord).

To quantify the retinal neovascular tuft formation, we incubated the retinas with Rhodamine Lectin I (1:100, VECTOR) at 4℃ overnight. Retinas were then carefully transferred onto a slide, cut into a flower shape, and mounted with Mountant PermaFluor medium (Thermo Scientific). Images (3 images/condition) were taken by the SP8 Leica confocal microscopy (Concord). SWIFT_NV ImageJ software was used to quantify the neovascular tuft area by comparing the number of pixels in the neovessel area to the total number of that in the retinal flatmount in a blind fashion. Adobe Photoshop CS5 was used to adjust the brightness and contrast of the images.

### 2.10.3 Retinal Cryosections

Eyes from P17 mice were immersed in 30% sucrose for cryoprotection and followed by embedded in Tissue-Tek®O.C.T compound (Sakura Finetek) for freezing. Eyes were cut into 10-μm-thick sections, and three serial sections were collected on one slide and stored at -20℃. The slides were dried, washed, fixed with 4% PFA, and blocked 1 h at room temperature with medium containing 0.3% TritonX-100/PBS, 0.3M Glycine, 10% NGS, 3% BSA. Primary and secondary antibodies were diluted in PBS that included 0.3% TritonX-100 and 3% BSA. The slides were incubated for 2 h at room temperature with a monoclonal antibody against glutamate synthetase (1:500, mouse, Millipore), a monoclonal antibody against VEGF-A (1:500, mouse, Abcam), a polyclonal antibody against SDF-1 (1:100, rabbit, Abcam), a polyclonal antibody against ERK1/2 (1:200, rabbit, Abcam), or a polyclonal antibody against HIF-1α (1:500, rabbit, Abcam). After the primary incubation, slides were incubated for 2 h at room temperature with secondary antibodies conjugated with fluorochrome: goat-anti-rabbit AlexaFluor 594 (1:1000, Life Technologies), or goat-anti-mouse AlexaFluor 488 (1:1000, Life Technologies). The cell nucleus was identified by DAPI (1:5000). Sections were mounted with the Mountant PermaFluor medium (Thermo Scientific),

covered with a coverslip, and imaged (3 images/section; 3 section/condition) with the SP8 Leica confocal microscopy (Concord).

## 2.11 DATA ANALYSIS

The experiments conducted in this study were all repeated at least three times. Values were presented as means ± SEM. Data were analyzed by Prism 5 via t-test or one-way ANOVA. The P-value less than 0.05 ($p \leq 0.05$) was considered statistically significant.

# Chapter 3:
# RESULTS

## 3.1 THE INFLUENCE OF LMPS ON MULLER CELL *IN VITRO*

Previously, we observed that LMPs exert anti-angiogenic properties predominantly through affecting VEGF signaling pathways in different cell types [125, 128, 129]. Mounting evidence indicates that Müller cell-derived VEGF significantly contributes to the formation of aberrant retinal

neovessels in both ROP and diabetic retinopathy [52, 132, 133]. Here, we investigated whether LMPs were internalized by Müller cells and whether LMPs influenced Müller cell proliferation and apoptosis.

### 3.1.1 The Internalization of LMPs by rMC-1

To mimic the *in vivo* hypoxic milieu, we used cobalt chloride ($CoCl_2$) to induce hypoxia in rMC-1. $CoCl_2$ is a chemical compound that induces hypoxia via stabilizing transcription factor HIF-1α, and it consequently increases VEGF expression [134].

We determined the optimal concentration of $CoCl_2$ by rMC-1 cell proliferation and the relative mRNA level of VEGF in rMC-1. We incubated rMC-1 with different concentrations of $CoCl_2$ (50 μM and 100 μM) for 24 h. We assessed the cell proliferation of rMC-1 via [$^3$H]-thymidine incorporation assay. The results indicated that $CoCl_2$ (50 μM) did not significantly inhibit rMC-1 cell proliferation. However, at the concentration of 100 μM, $CoCl_2$ significantly reduced cell proliferation ($P < 0.05$) (see Figure 27A). Next, we evaluated VEGF mRNA expression in $CoCl_2$-induced cells. The results of real-time PCR showed that 100 μM of $CoCl_2$ substantially upregulated the mRNA level of VEGF ($P < 0.001$), whereas 50 μM of $CoCl_2$ did not significantly increase VEGF mRNA expression compared with the control (NOR indicates normoxia) (see Figure 27B). Therefore, we chose 100 μM of $CoCl_2$ as the optimal concentration to induce hypoxia in rMC-1 for the following *in vitro* experiments.

Next, we studied whether rMC-1 internalized LMPs. For this purpose, we generated the lipophilic dye-labeled LMPs (Dil-LMPs). The lipophilic dye Dil, which has no cytotoxic effect on cell development, viability, and physiological properties [130], has been broadly used as a marker to trace the living cells. Here, we utilized two methods to determine the uptake of Dil-LMPs by rMC-

1. First, we measured the fluorescent intensity of rMC-1 at different time points (1, 4, 8, and 24 h) due to the uptake of Dil-LMPs. The results revealed that Dil-LMPs were internalized by rMC-1 time-dependently (see Figure 27C).

Next, we utilized immunofluorescent staining to confirm that Dil-LMPs were indeed within the cytoplasm instead of residing on the plasma membrane. We captured the immunofluorescent staining images of rMC-1 treated with Dil-LMPs at 8 h and 24 h. The fluorescent staining results exhibited the uptake of Dil-LMPs by rMC-1. Dil-LMPs (red) was observed within the cytoplasm of rMC-1 at 8 h (see Figure 27D). When the cells were co-stained with glutamate synthetase (GS, green), an enzyme exclusively expressed by Müller cells [46], the internalized Dil-LMPs by rMC-1 was merged into yellow. Consistent with the previous intensity measurement results, the uptake of Dil-LMPs by rMC-1 notably increased at 24 h, as evidenced by the increased intensity and extent of the merged color yellow (see Figure 27D).

**Figure 27.** ***The Internalization of LMPs by rMC-1***

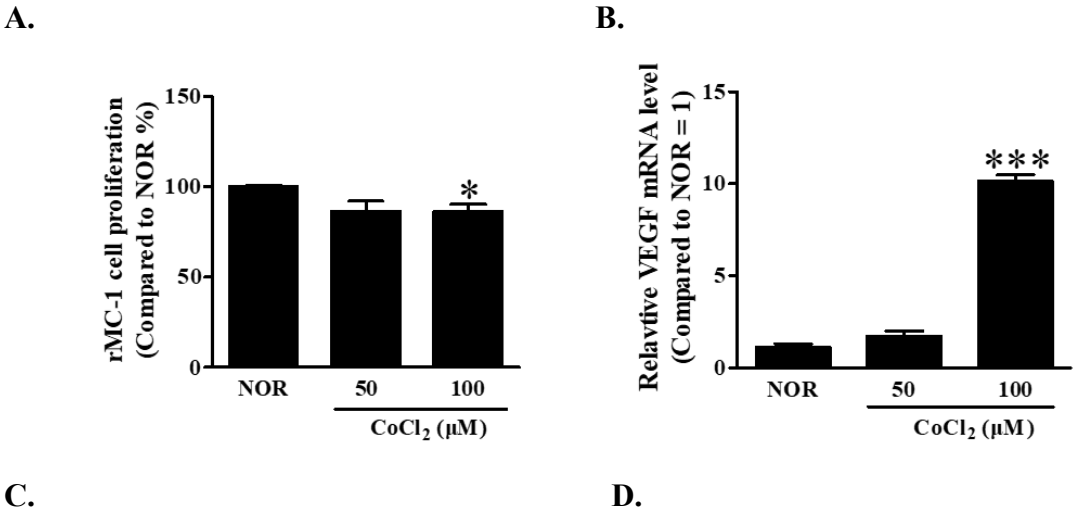

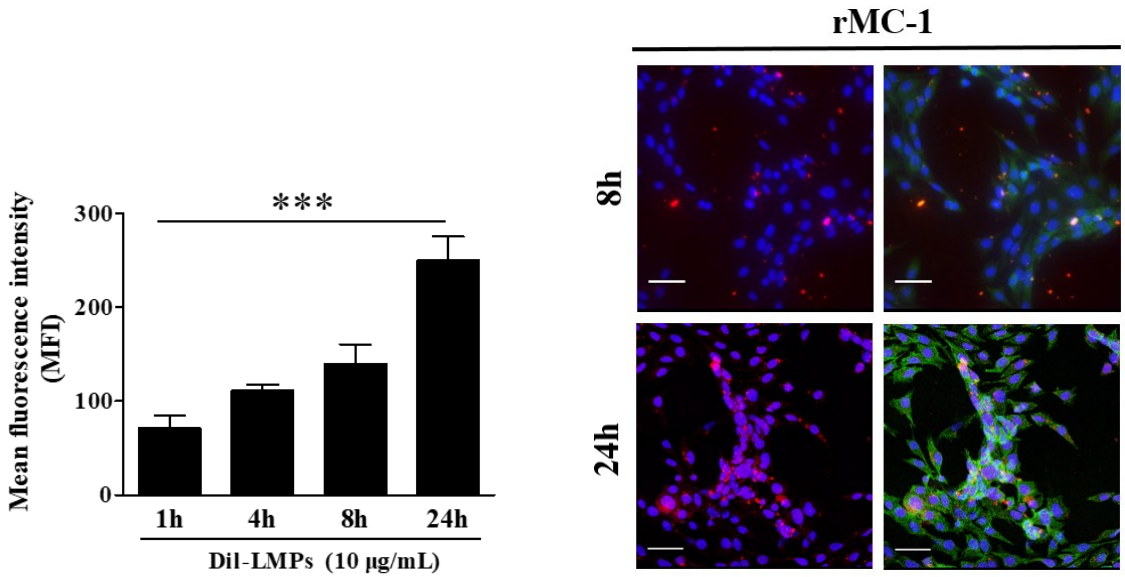


***Note.*** To find the optimal condition of $CoCl_2$ to induce hypoxia in rMC-1, we conducted cell proliferation (A) and real-time PCR (B). **A.** Cell proliferation of rMC-1 was assessed after 24 h of incubation with $CoCl_2$ (50 μM or 100 μM). The abbreviation NOR indicates as normoxia. $^*P < 0.05$ vs. NOR **B.** Relative mRNA level of VEGF in rMC-1 treated with different concentrations of $CoCl_2$ (50 μM or 100 μM). $^{***}P < 0.001$ vs. NOR. **C.** Measurement of the fluorescent intensity of rMC-1 at different time points (1, 4, 8, and 24 h), due to the uptake of lipophilic dye Dil labeled-LMPs (Dil-LMPs). The fluorescent intensity (indicates Dil-LMPs uptake) of rMC-1 was determined by spectrofluorometer reading and presented as mean fluorescent intensity (MFI). $^{***}P < 0.001$ vs. 1 h. **D.** Representative images of the uptake of Dil-LMPs (red) by rMC-1 at 8 h and 24 h. rMC-1 were stained with glutamate synthetase (GS, green). The cell nucleus was identified by DAPI (blue). Original magnification: x 400. Scale bars = 20 μm.

### 3.1.2 LMPs Dose-Dependently Inhibit rMC-1 Cell Proliferation and Prevent Cell Apoptosis

Under normal conditions, Müller cells are essential for the maintenance of retinal homeostasis, as well as the protection of neural functions [45]. However, they are overactivated during pathological conditions, characterized by increased cell proliferation, which subsequently release various factors that contribute to the pathogenesis of diseases [45, 48]. Having demonstrated the uptake of

LMPs by rMC-1 (see Figure 27C-D), we wondered whether LMPs could inhibit Müller cell proliferation without inducing cell apoptosis.

We determined the impacts of LMPs on hypoxic rMC-1 cell proliferation and apoptosis by [$^3$H]-thymidine incorporation and flow cytometry analysis, respectively. We showed that LMPs dose-dependently suppressed hypoxic rMC-1 cell proliferation. The cell proliferation of hypoxic rMC-1was reduced by 13.12%, 16.91%, 27.84%, and 44.52% at the concentration of 5, 10, 20, and 30 μg/mL of LMPs, respectively, compared with the hypoxic condition (see Figure 28A). We wondered whether the observed decreased cell proliferation of rMC-1 (see Figure 28A) was a result of the increased cell apoptosis. Therefore, to determine whether LMPs induced rMC-1 cell apoptosis, we chose to assess the lowest concentration of LMPs (10 μg/mL) that already had a significant impact ($P < 0.001$) on rMC-1 cell proliferation. We used Annexin-V/PI binding assay via flow cytometry to determine rMC-1 cell apoptosis. The apoptotic cells were indicated as Annexin-V positive, in which there were 32.7% apoptotic cells in the $CoCl_2$-stimulated group (hypoxic condition) and 24.4% apoptotic cells in the LMPs-treated condition (see Figure 28B-C). LMPs significantly prevented rMC-1 cell apoptosis, which was induced by $CoCl_2$ (see Figure 28B-C). These results suggest that 10 μg/mL of LMPs decreased rMC-1 cell proliferation without inducing cell apoptosis. Therefore, we chose 10 μg/mL of LMPs as the optimal concentration for the following *in vitro* experiments.

**Figure 28.** ***LMPs Dose-Dependently Inhibit rMC-1 Cell Proliferation And Prevent Cell Apoptosis***

**A.**

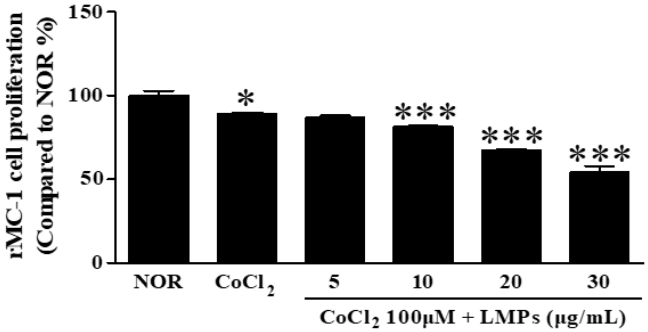


**B.**

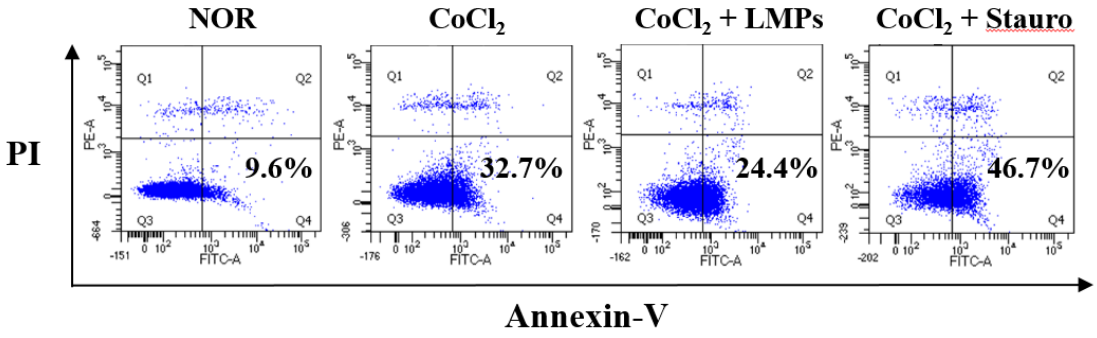


**C.**

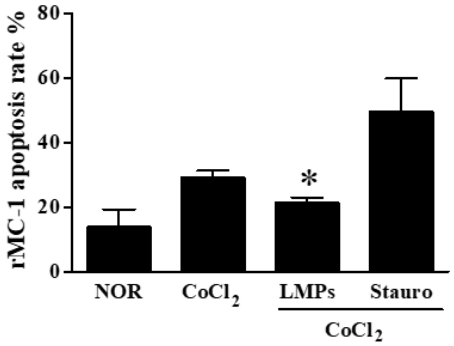


***Note.*** **A.** Cell proliferation of rMC-1 in different conditions: NOR, $CoCl_2$ (100 μM), $CoCl_2$ (100 μM) together with different concentrations of LMPs (5, 10, 20 and 30 μg/mL). rMC-1 cell proliferation was determined by [$^3$H]-thymidine incorporation assay, and the relative proliferation rates of rMC-1 were presented as the percentage of NOR. *$P < 0.05$ vs. NOR; ***$P < 0.001$ vs. $CoCl_2$. **B.** Representative images of rMC-1 cell apoptosis determined by flow cytometry analysis. Cell apoptosis of rMC-1 at different conditions: NOR, $CoCl_2$ (100 μM), $CoCl_2$ (100 μM) together

with LMPs (10 μg/mL) were assessed by Annexin V/PI staining. Staurosporine (1 μg/mL) was used as a positive control, and rMC-1 was incubated with staurosporine and $CoCl_2$ (100 μM) together for 6 h. **C.** The apoptotic rates were performed as the percentage of cells undergoing apoptosis over the total number of cells. *$P < 0.05$ vs. $CoCl_2$.

## 3.2 LMPS ALTER THE MIGRATION OF RAW 264.7 MEDIATED BY rMC-1 AND RETINAL EXPLANTS

Müller cells are the major producers of proinflammatory cytokines and growth factors under pathological conditions [51]. Studies have demonstrated that macrophages are recruited to the hypoxic retina following the chemokine gradients during the second phase of ROP, and they exert a pro-angiogenic effect [72]. Therefore, we investigated whether LMPs affected the recruitment of macrophages mediated by Müller cells.

We conducted the transwell migration assay to determine the chemotactic capacity of Müller cells. We performed the migration assay with RAW 264.7 and supernatant, which was collected from three conditions of rMC-1 after 24 h of incubation. The fluorescent staining images revealed that $CoCl_2$ increased the cell migration of RAW 264.7, and the phenomenon was attenuated by LMPs (see Figure 29A). Furthermore, we counted the migration number in each condition, and the counting results indicated that $CoCl_2$ significantly increased 240% of RAW 264.7 cell migration ($P < 0.05$), which was suppressed by LMPs by more than 150% (see Figure 29B).

To obtain a better insight into the effect mediated by LMPs, we established an *ex vivo* retinal explant model to mimic the *in vivo* microenvironment. The mouse model of OIR has been proven to mimic the pathogenesis of ROP [131]. The increased infiltration of monocyte-derived macrophages is observed two days after the onset of hypoxia (P12) [135]. Therefore, we collected the retinas from P14 OIR mice to establish the *ex vivo* retinal explant model. Based on our previous publication [126]

with a minor modification, we incubated the hypoxic retinas (n = 3 retinas/condition) from P14 OIR mice with 50 μg/mL of LMPs for 24 h. After 24 h, we collected the supernatant from each condition and subjected it to the migration assay with RAW 264.7. The fluorescent staining images revealed a considerable decline in cell migration in the LMPs-treated group in comparison to the control (see Figure 29C). The counting results indicated that LMPs suppressed RAW 264.7 cell migration by more than 50% ($P < 0.05$; see Figure 29D).

**Figure 29.** ***LMPs Alter The Recruitment of Macrophages Mediated by rMC-1 And Retinal Explants***

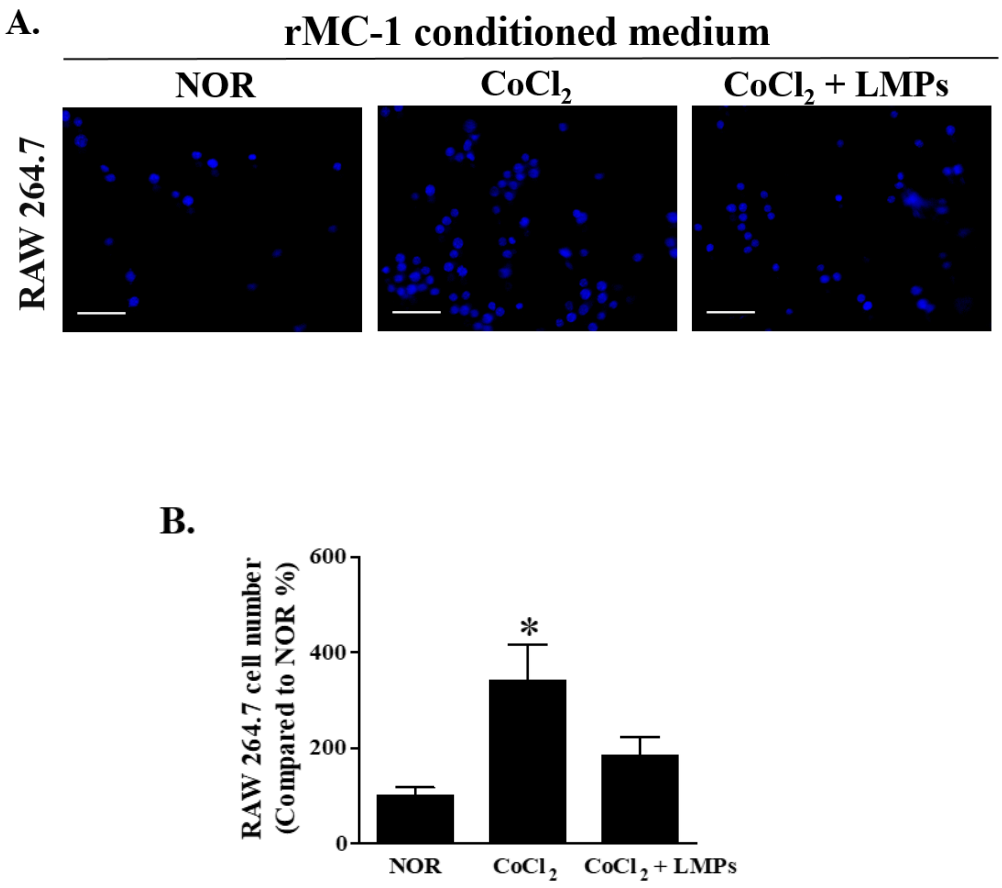

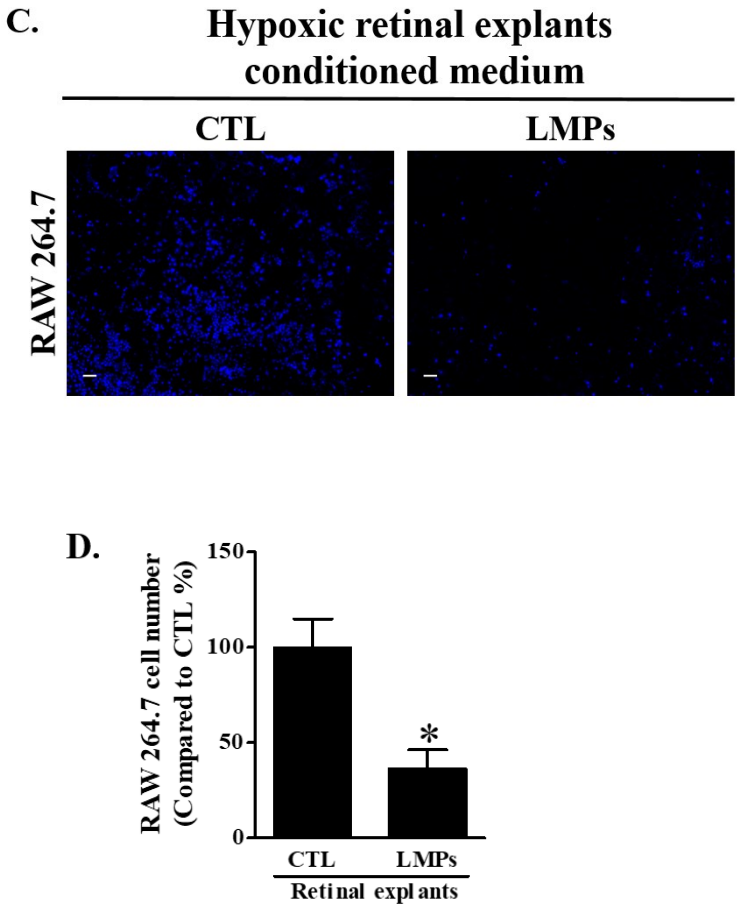


***Note.*** **A.** Representative fluorescent staining images of RAW 264.7 cell migration conducted with rMC-1 supernatant from different conditions. The supernatant was collected from the following three conditions: rMC-1 without any treatment (NOR), rMC-1-stimulated with $CoCl_2$ (100 μM), and rMC-1-incubated together with $CoCl_2$ (100 μM) and LMPs (10 μg/mL). The cell nucleus of RAW 264.7 was stained with DAPI (blue). **B.** RAW 264.7 migration number was counted in each condition (three images/condition) and was performed as the percentage of NOR. **P* < 0.05 vs. NOR. **C.** Representative fluorescent staining results of RAW 264.7 cell migration conducted with supernatant collected from the following conditions. The supernatant was collected from hypoxic retinal explants or hypoxic retinal explants incubated with LMPs (50 μg/mL). The cell nucleus was identified by DAPI (blue). **D.** RAW 264.7 cell migration number was counted in each condition (three images/condition) and was presented as the percentage of CTL. **P* < 0.05 vs. CTL. Original magnification for A: x 400. Original magnification for C: x 100. Scale bars = 50 μm.

## 3.3 LMPS REDUCE CHEMOKINE EXPRESSION *IN VITRO* AND *EX VIVO*

Having observed that LMPs altered the migration of RAW 264.7 mediated by rMC-1 and the retinal explant model (see Figure 29), we questioned whether LMPs reduced the expression of chemokines in rMC-1 and the retinas from the *ex vivo* retinal explant model.

### 3.3.1 LMPs Reduce VEGF Expression

In addition to the extensively studied pro-angiogenic effect, VEGF also serves as an essential chemoattractant for monocyte/macrophage recruitment [136]. Thus, we surmised that LMPs affected the expression of VEGF in rMC-1. Several previous studies corroborated this hypothesis, finding evidence showing that LMPs affect VEGF expression in several kinds of cells [125, 126, 128, 129].

We first quantified the mRNA level of VEGF in rMC-1. The results of real-time PCR exhibited a 6.9-fold increase of VEGF expression in the $CoCl_2$-induced group in comparison to NOR (see Figure 30A). In the LMPs-treated condition, there was a 21.9-fold reduction compared with the hypoxic condition (see Figure 30A). We further determined the effect of LMPs on VEGF expression at the protein level in the three conditions. The Western blot results indicated that VEGF was expressed higher in the $CoCl_2$-stimulated group and lowered in the LMPs-treated condition (see Figure 30B). Moreover, we measured the mRNA expression of VEGF in hypoxic retinal explants. The real-time PCR results revealed a 1.4-fold decrease of VEGF mRNA expression in the LMPs-treated hypoxic retinal explants compared with the control (see Figure 30C).

**Figure 30.** ***LMPs Reduce VEGF Expression In Vitro And Ex Vivo***

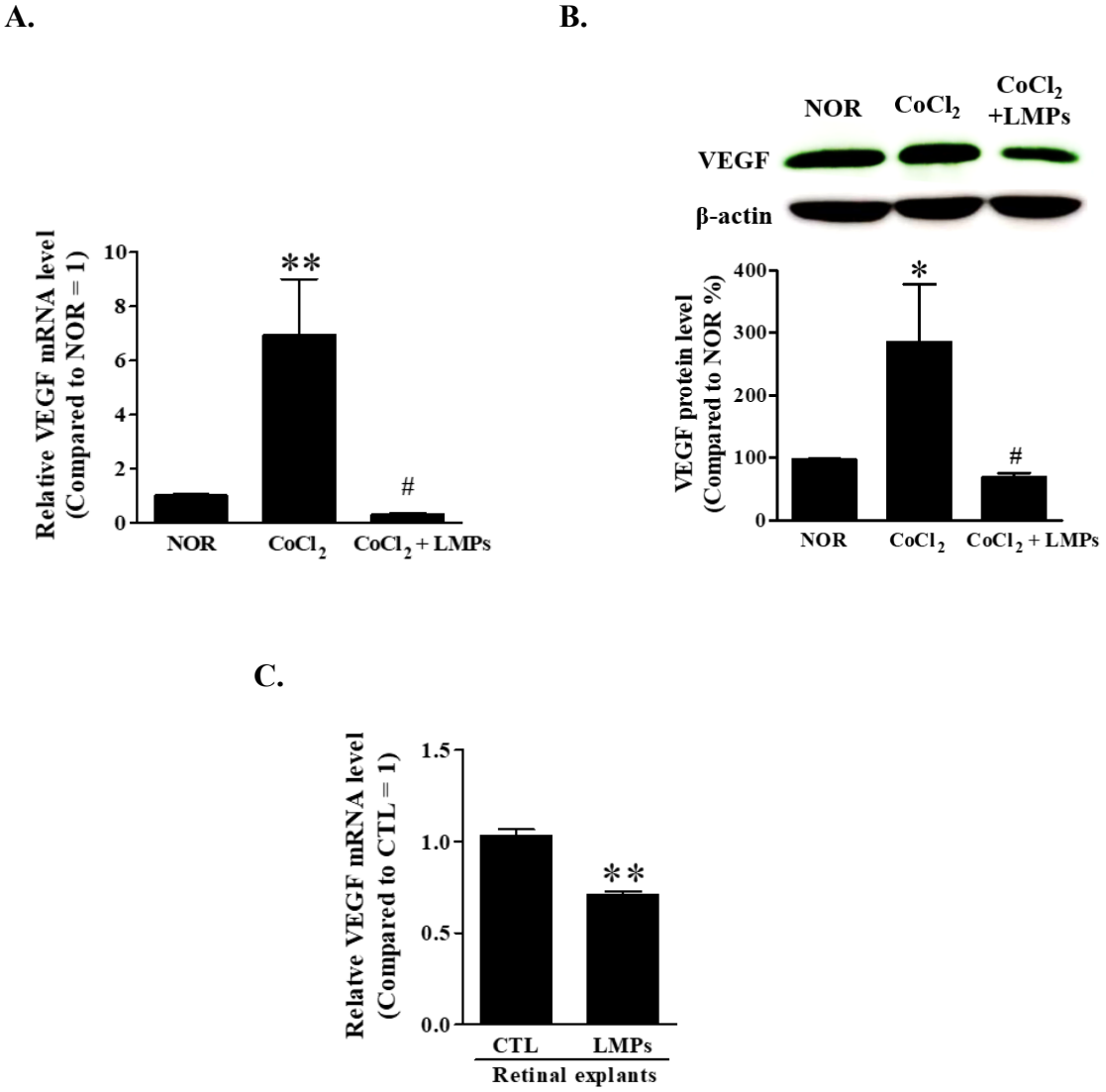


***Note.*** **A.** Relative VEGF mRNA level of rMC-1 in NOR, $CoCl_2$ (100 μM)-induced hypoxia, and $CoCl_2$ (100 μM) together with LMPs (10 μg/mL). $^{**}P < 0.01$ vs. NOR; $\#P < 0.01$ vs. $CoCl_2$. **B.** Total VEGF protein level of rMC-1 in the abovementioned three conditions. VEGF protein level was normalized to β-actin and presented relative to NOR. $^{*}P < 0.05$ vs. NOR; $\#P < 0.05$ vs. $CoCl_2$. **C.** Relative VEGF mRNA level in hypoxic retinal explants of control or LMPs (50 μg/mL) treated retinal explants. $^{**}P < 0.01$ vs. CTL.

### 3.3.2 LMPs Reduce the mRNA Expression of SDF-1

The potent chemoattractant, stromal cell-derived factor-1 (SDF-1), plays an essential role in macrophage recruitment [61, 96]. In addition, SDF-1 also contributes to pathological retinal NV [99]. Therefore, we analyzed the mRNA expression of SDF-1 in rMC-1 and retinal explants.

The results of real-time PCR indicated a 43-fold increase of SDF-1 mRNA expression in the $CoCl_2$ stimulated group compared with NOR, and a 124-fold decrease of that in the LMPs-treated group as compared with $CoCl_2$ condition (see Figure 31A). Furthermore, we determined the mRNA expression of SDF-1 in the retinas of hypoxic retinal explants. The results indicated that there was a 1.3-fold reduction of SDF-1 mRNA expression in the LMPs-treated group (see Figure 31B).

**Figure 31.** ***LMPs Reduce The mRNA Expression of SDF-1 In Vitro And Ex Vivo***

**A.**

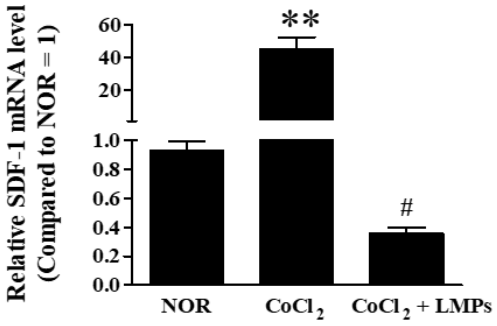


**B.**

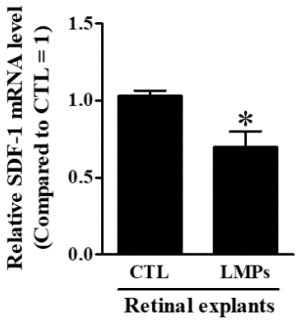


***Note.*** **A.** Relative SDF-1 mRNA level of rMC-1 in NOR, $CoCl_2$ (100 μM)-induced hypoxia, and $CoCl_2$ (100 μM) together with LMPs (10 μg/mL). $^{**}P < 0.01$ vs. NOR; $\#P < 0.01$ vs. $CoCl_2$. **B.** Relative SDF-1 mRNA level in hypoxic retinal explants of control and LMPs (50 μg/mL) treated hypoxic retinal explants. $^{*}P < 0.05$ vs. CTL.

### 3.4 LMPS DOWNREGULATE ERK1/2 AND HIF-1A EXPRESSION *IN VITRO*

Next, we set out to dissect the molecular mechanisms underlying the previously observed effects of LMPs. Studies have shown that extracellular signal-regulated kinases 1/2 (ERK1/2) regulate the proliferation of Müller cells [137] and participate in VEGF secretion from Müller cells [138]. VEGF and SDF-1 both contain HREs in their promoter region, which can be regulated by transcription factor hypoxia-induced factor-1 (HIF-1) [101, 139]. Because we demonstrated that LMPs dose-dependently decreased the cell proliferation (see Figure 28A) as well as reduced the expression of the chemokines in rMC-1 (see Figures 30 and 31), we surmised that LMPs affected the expression of ERK1/2 and HIF-1α in rMC-1.

First, we measured the expressions of ERK1/2 and HIF-1α at the mRNA level. The results of real-time PCR showed that $CoCl_2$ increased ERK1 5-fold, ERK2 1.5-fold, and HIF-1α mRNA expression 18.6-fold (see Figure 32A). The effect of $CoCl_2$ was suppressed by LMPs, in which LMPs decreased 3.4-fold of ERK1, 1.8-fold of ERK2, and 19.3-fold of HIF-1α mRNA expression (see Figure 32A). Next, we determined the effect of LMPs on the protein expressions of ERK1/2

and HIF-1α. The results of the Western blot demonstrated that LMPs decreased ERK1/2 protein expression by approximately 75% (see Figure 32B) and HIF-1α protein expression by approximately 60% (see Figure 32C) compared with the $CoCl_2$-stimulated group.

**Figure 32.** ***LMPs Downregulate ERK1/2 and HIF-1α Expression In Vitro***

**A.**

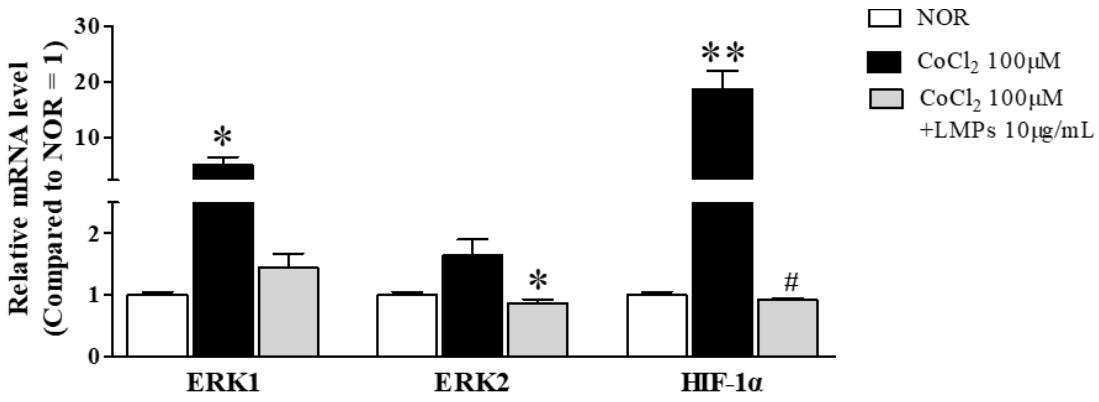


**B.**

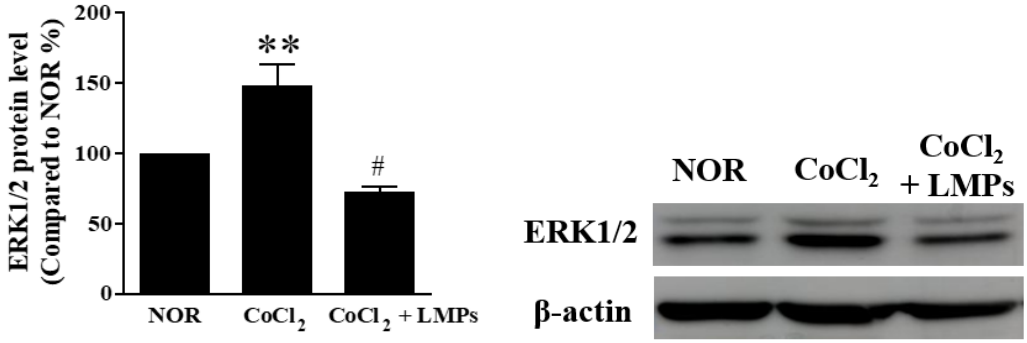


**C.**

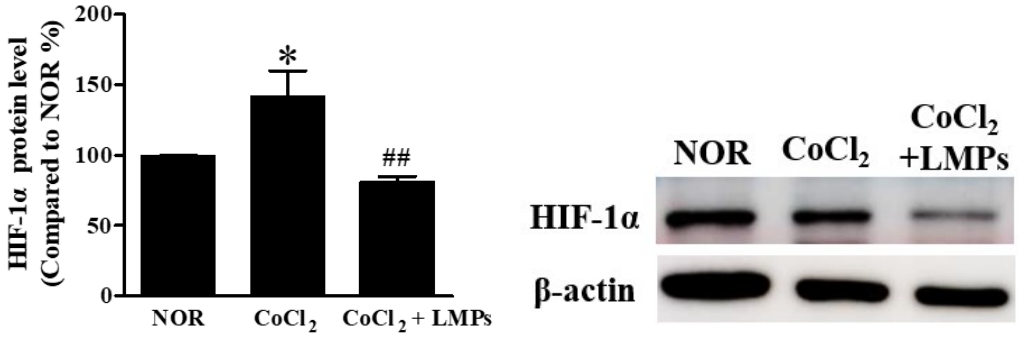


***Note.*** **A.** Relative ERK1/2 and HIF-1α mRNA levels in NOR, $CoCl_2$ (100 μM), and $CoCl_2$ (100 μM) together with LMPs (10 μg/mL). **P* < 0.05 , ***P* < 0.01 vs. NOR; **P* < 0.05 vs. CoCl2; #*P* < 0.01 vs. $CoCl_2$. **B.** Total protein level of ERK1/2 in the abovementioned three conditions. ERK1/2 protein level was normalized to β-actin and presented as the percentage of NOR. ***P* < 0.01 vs. NOR; #*P* < 0.01 vs. $CoCl_2$. C. Total protein level of HIF-1α in the abovementioned three conditions. The protein level of HIF-1α was normalized to β-actin and presented as the percentage of NOR. **P* < 0.05 vs. NOR; ##*P* < 0.01 vs. $CoCl_2$.

### 3.5 THE IMPACTS OF LMPS *IN VIVO*

Previously, we showed that LMPs elicit anti-angiogenic effects in different models, [125, 126, 128, 129]. The influence of LMPs on aberrant retinal angiogenesis and the related mechanisms, however, remained unclear.

In this study, we used an OIR mouse model [131] to study the effect of LMPs *in vivo*. As reported by Andreas et al., [140], the postnatal weight gain of the mice affects the severity of retinal NV in the OIR mouse model. Additionally, to make sure the mice were in good shape before and after the treatment, we weighed the mice before the initiation of the experiments. We included the weight

of the mice between 5.5 g ~ 7 g at P12 for the intravitreal injection. We intravitreally injected LMPs (10 μg/μL; 1 μL/eye) into the right eye and the same volume of sterile PBS (1 μL) into the contralateral eye at P12. We included the mice weight between 7 g ~ 8.5 g at P17 for the following experiments. The average weight of mice at different time points was summarized in table 2.

Table 2. The average weight of mice pups at different time points.

| Postnatal time point (P) | The average weight of mice pups (g) |
|---|---|
| P7 | 3.3 ± 0.5 |
| P12 | 6.0 ± 0.5 |
| P17 | 7.5 ± 0.5 |

### 3.5.1 LMPs Inhibit Pathological Retinal NV *In Vivo*

To determine the influence of LMPs on aberrant retinal NV, we analyzed the neovascular tuft formation at P17. We collected the eyes and carefully dissected under the microscope to obtain the intact retinas.

We stained the P17 retinal flatmounts in NOR, OIR vehicle, and OIR LMPs with lectin, which is the most widely used marker to visualize blood vessels by binding to the glycoprotein localized in the basal membrane of the endothelial cells [141]. Confocal immunofluorescent staining exhibited the vascular structure of retinas at P17 in three different conditions (see Figure 33A). As shown in Figure 33A, the superficial plexuses in the NOR were well-organized and covered almost the entire surface of the retina. However, in the OIR vehicle, the vascular structure was significantly disrupted, and the neovessels were densely formed instead of having a fine structure and a clear gap between the neighboring vessels. The neovascular tufts could also be detected at the interface of the

avascular and vascularized region, presented as increased intensity of red fluorescence. As expected, in the LMPs-intravitreal injected group, the neovessels were less densely formed. Furthermore, there were less apparent neovascular tufts forming in the LMPs-injected group (see Figure 33A). We further quantified the neovascular tuft area in the OIR vehicle and the OIR LMP. Results indicated that LMPs attenuated retinal neovascular tuft area by 55% (see Figure 33B). These results suggest that LMPs can alleviate aberrant retinal NV in the ischemic retinopathy mouse model.

**Figure 33.** ***LMPs Inhibit Pathological Retinal NV In Vivo***

**A.**

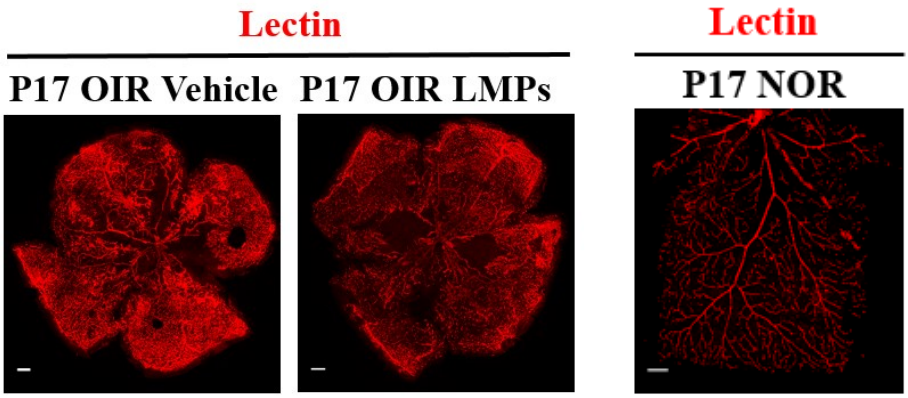


**B.**

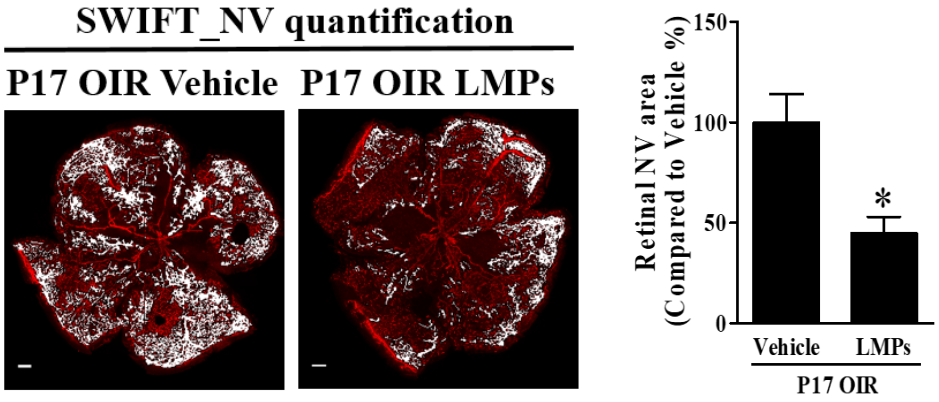


***Note.*** **A.** Representative confocal immunofluorescent staining of P17 retinal flatmounts of OIR Vehicle, OIR LMPs, and NOR. The retinal flatmounts were stained with lectin (red). **B.** Quantification of retinal neovascular tuft area in the OIR Vehicle and OIR LMPs. Images were quantified blindly by comparing the pixels in the neovascular tuft area to the total pixels in the whole retinal flatmount via SWIFT_NV Image J software. Quantification results were expressed as the percentage of OIR Vehicle. *$P < 0.05$ vs. OIR Vehicle. Original magnification for OIR Vehicle and OIR LMPs: x 100. Scale bars = 200 μm. Original magnification for NOR: x 630. Scale bar: 50 μm.

### 3.5.2 LMPs Suppress Macrophage Recruitment *In Vivo*

Earlier, we showed the indirect anti-migratory effect of LMPs on RAW 264.7 macrophages (see Figure 29). We also demonstrated that LMPs reduced the expression of chemokines (VEGF and SDF-1) in the hypoxic retinal explants (see Figures 30 and 31). However, whether LMPs affected the migration of macrophages *in vivo* remains unknown.

Considering the fact that LMPs were intravitreally injected at P12, and the infiltration of monocyte-derived macrophages initiate around P14 [77], we hypothesized that LMPs could inhibit the recruitment of macrophages *in vivo*. To address our hypothesis, we stained the P17 retinal flatmounts of the OIR vehicle, OIR LMPs, and NOR with FITC-conjugated F4/80 antibody, a

broadly used marker for murine macrophage identification [142]. The immunofluorescent staining images indicated that only a small number of F4/80 positive cells were presented in the NOR retina, which was attributed to the presence of residential microglia (see Figure 34A). In the OIR vehicle, the cells that were positive with F4/80 were substantially increased in comparison to NOR; however, this phenomenon was inhibited by LMPs (see Figure 34A), as evidenced by the significantly less F4/80 positive cells stained in the retinal flatmount. We counted the F4/80 positive cell number in each condition, and the results showed that LMPs reduced the number of F4/80 positive cells by 55% (see Figure 34B).

Residential macrophages termed microglia share a considerable number of surface markers with monocyte-derived macrophages, including F4/80 [142, 143]. To exclude the possibility that LMPs could diminish the density of residential microglia, which is present in the retina during development [75], we used two markers to stain the retinal flatmounts of the OIR vehicle and OIR LMPs at P17: (a) TMEM119, which is a specific microglia surface marker [144], and (b) F4/80, which stains both macrophages and microglia [142]. The staining results revealed that the majority of the cells that were positive with F4/80 were not stained positive with TMEM119, which indicated that most of the F4/80 positive cells were macrophages recruited from the peripheral instead of residential microglia (see Figure 34C). Besides, we did not observe an apparent reduction of TMEM119 positive cells in the OIR LMPs as compared with the OIR vehicle (see Figure 34C). We also analyzed the mRNA expression of the chemokines (VEGF and SDF-1) at P14 after a single intravitreal injection. The results of the real-time PCR revealed a threefold increase of VEGF in the OIR vehicle, and an eightfold decrease in the OIR LMPs (see Figure 34D). Similarly, there was a 6.2-fold upregulation of SDF-1 mRNA expression in OIR vehicle and a 57.2-fold reduction in OIR LMPs (see Figure 34E). These results suggest that LMPs suppressed the recruitment of monocyte-derived macrophages *in vivo*.

**Figure 34.** ***LMPs Suppress Macrophage Recruitment In Vivo***

**A.**

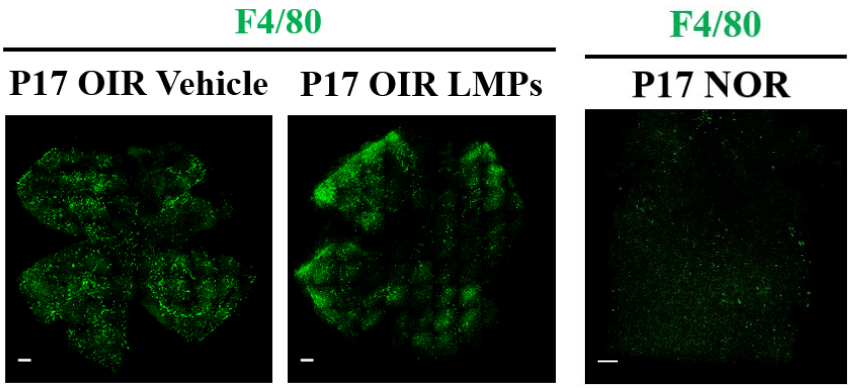


**B.**

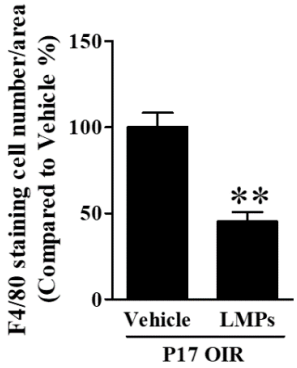


**C.**

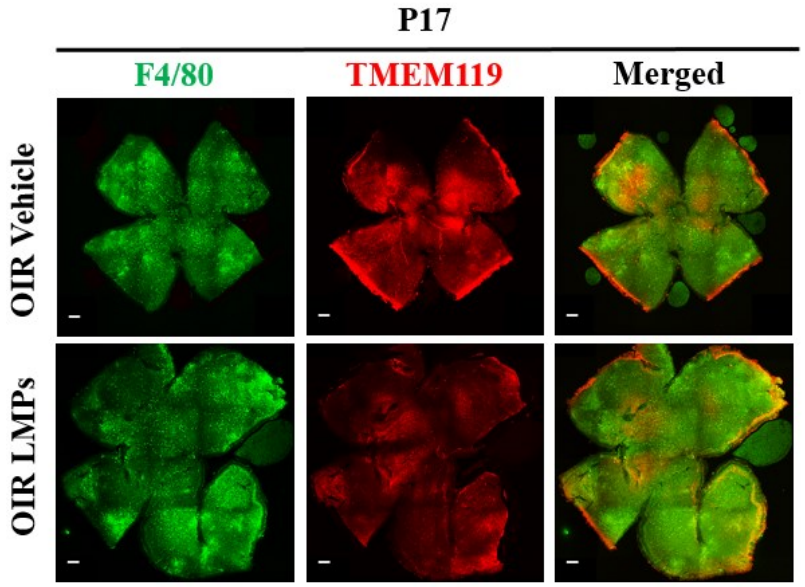


**D.**

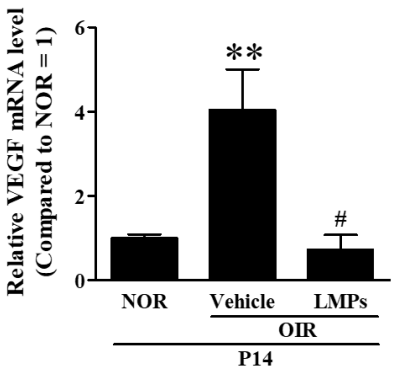


**E.**

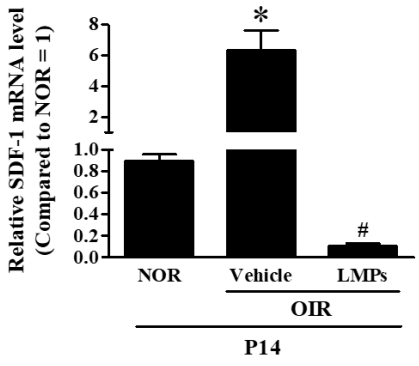


***Note.*** **A.** Representative immunofluorescent staining of the P17 retinal flatmounts of the OIR Vehicle, OIR LMPs, and NOR. The retinal flatmounts were stained with FITC-conjugated F4/80 (green). **B.** The number of F4/80 positive cells was counted in the OIR Vehicle and OIR LMPs and expressed as the percentage of OIR Vehicle. $^{**}P < 0.01$ vs. OIR Vehicle. **C.** Representative images of the P17 retinal flatmounts of the OIR Vehicle and OIR LMPs. The retinal flatmounts were stained with F4/80 (green) and TMEM119 (red). **D.** Relative mRNA level of VEGF in NOR, OIR Vehicle, and OIR LMPs at P14 (n = 3 retinas (eyes)/condition). $^{**}P < 0.01$ vs. NOR; $\#P < 0.01$ vs. OIR Vehicle. **E.** Relative mRNA level of SDF-1 in NOR, OIR Vehicle, and OIR LMPs at P14. $^{*}P < 0.05$ vs. NOR; $\#P < 0.01$ vs. OIR Vehicle. Original magnification for A (OIR Vehicle and OIR

LMPs), x 100. Scale bars = 200 μm. Original magnification for A (NOR): x 630. Scale bar: 50 μm. Original magnification for C: x 100. Scale bars: 200 μm.

## 3.6 LMPS TARGET MULLER CELLS *IN VIVO*

Considering that most of the results were conducted *in vitro,* which was different from the *in vivo* microenvironment, we questioned whether LMPs targeted Müller cells *in vivo.*

### 3.6.1 Müller Cells Internalize LMPs

To determine the uptake of LMPs by Müller Cells *in vivo*, we intravitreally injected Dil- LMPs at P12 to track the distribution of LMPs in the retina. As shown in Figure 35A, Dil-LMPs (red fluorescence) reached the inner and outer retina, and they seemed mainly localized in the INL and ONL. When retinal sections were co-stained with GS, most of the Dil-LMPs were colocalized with GS, as indicated by the presence of the merged color yellow (see Figure 35A). To exclude the possibility that the backgrounds caused the red signals, we stained the P17 retinal section of OIR CTL without Dil-LMPs injection. As shown in Figure 35B, there was no red fluorescent background in the OIR CTL. These data suggest that Dil-LMPs were internalized by Müller cells.

### 3.6.2 LMPs Inhibit VEGF and SDF-1 Expressed in Müller Cells

Having demonstrated the uptake of LMPs by Müller cells, we subsequently investigated whether LMPs reduced the expression of VEGF and SDF-1 in Müller cells *in vivo*.

First, to determine whether LMPs reduced the expression of VEGF in Müller cells, we stained the P17 retinal sections of NOR, OIR vehicle, and OIR LMPs with VEGF and GS. As indicated in

Figure 35C, VEGF was expressed at a modest level in the INL and displayed as straight lines in the OPL in the normoxic retina (see Figure 35C). The intensity of VEGF expression was substantially enhanced in the OIR vehicle, which was mainly localized in the INL and OPL (see Figure 35C). This phenomenon was weakened by LMPs in the INL and OPL (see Figure 35C). When retinal sections were co-stained with GS, the majority of VEGF was colocalized with GS, especially with Müller cell somata (INL) and outer processes (OPL) (see Figure 35C).

Next, we determined whether LMPs suppressed the expression level of SDF-1 in Müller cells. We stained the P17 retinal sections of NOR, OIR vehicle, and OIR LMPs with SDF-1 and GS. The immunofluorescent staining results revealed that SDF-1 was hardly detectable under normoxia (see Figure 35D). However, the expression intensity of SDF-1 was drastically enhanced in the IPL, INL, and OPL in the OIR vehicle (see Figure 35D). And the phenomenon was weakened by LMPs (see Figure 35D). When sections were co-stained with GS, the majority of SDF-1 was colocalized with GS, mainly in the IPL (Müller cell inner processes) and INL (Müller cell somata) (see Figure 35D). The VEGF and SDF-1 staining intensities in NOR retinal sections were similar to that in the OIR vehicle and the OIR LMPs.

**Figure 35.** ***LMPs Are Internalized by Müller Cells and Inhibit VEGF and SDF-1 Expressed in Müller Cells In Vivo***

**A.**

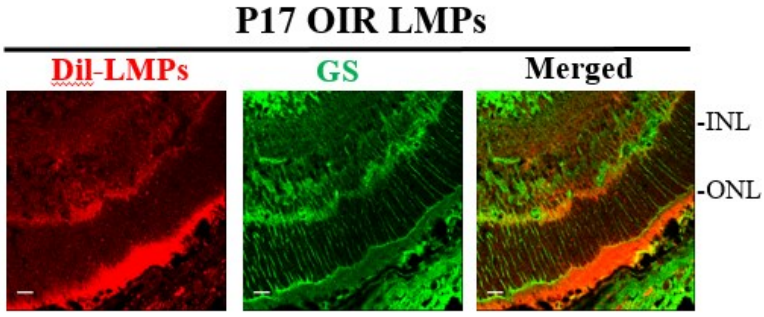
P17 OIR LMPs
Dil-LMPs
GS
Merged
-INL
-ONL

**B.**

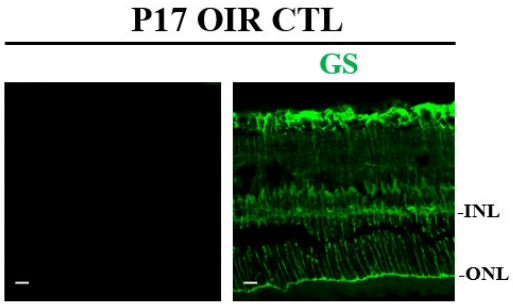
P17 OIR CTL
GS
-INL
-ONL

**C.**

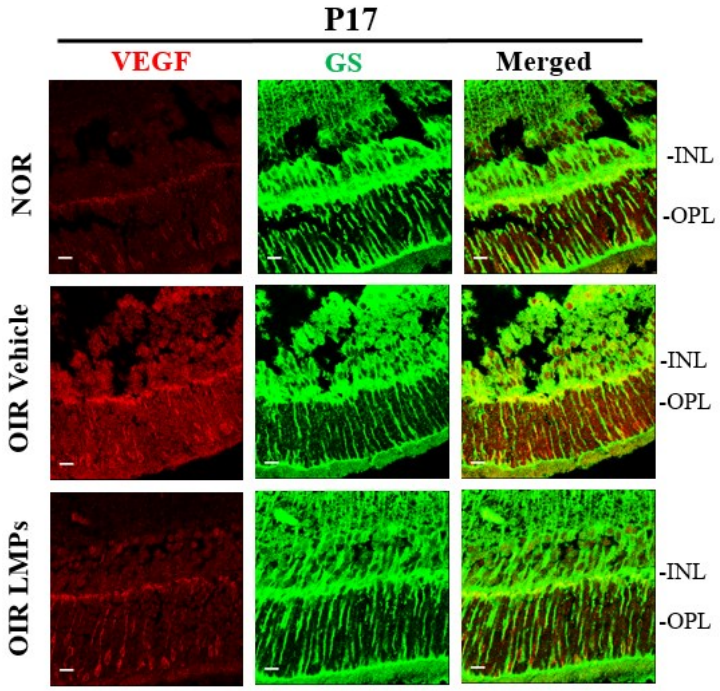
P17
VEGF
GS
Merged
NOR
OIR Vehicle
OIR LMPs
-INL
-OPL

**D.**

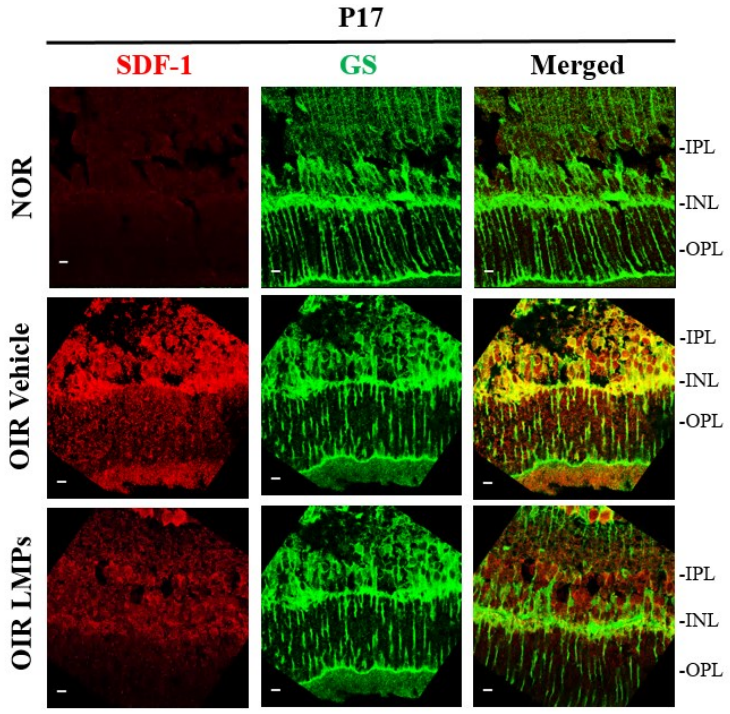


***Note.*** **A.** Representative immunofluorescent staining of P17 retinal sections of the OIR LMPs. The retinal sections were stained with glutamate synthetase (GS, green), indicating the uptake of Dil-LMPs (red) by Müller cells (green). **B.** Representative images of P17 retinal sections of the OIR CTL without Dil-LMPs injection. **C.** Representative immunofluorescent staining of P17 retinal sections. P17 retinal sections were stained with VEGF (red) and GS (green) in the NOR, OIR Vehicle, and OIR LMPs. **D.** Representative immunofluorescent staining of P17 retinal sections of NOR, OIR Vehicle, and OIR LMPs. The retinal sections were stained with SDF-1 (red) and GS

(green). IPL = inner plexiform layer; INL = inner nuclear layer; OPL = outer plexiform layer; ONL = outer nuclear layer. Original magnification: x 630. Scale bars =50 μm.

### 3.7 LMPS DOWNREGULATE ERK1/2 AND HIF-1A EXPRESSION IN MULLER CELLS *IN VIVO*

To study whether LMPs affected the expression of ERK1/2 and HIF-1α in the OIR mouse model, we used antibodies to determine the expression of ERK1/2 and HIF-1α in Müller cells *in vivo*.

First, we stained P17 retinal sections of NOR, OIR vehicle, and OIR LMPs with ERK1/2 and GS. ERK1/2 was expressed at a modest level in the GCL of NOR (see Figure 36A). Whereas its expression was substantially increased by hypoxia (OIR vehicle), as indicated by the increased red fluorescent intensity in the IPL and INL. In addition to the IPL and INL, ERK1/2 expression was also enhanced in the GCL. LMPs significantly downregulated ERK1/2 expression in the IPL and INL (see Figure 36A). When the sections were co-stained with GS, ERK1/2 was co-localized with GS in the IPL (the inner process of Müller cells) and INL (the somata of Müller cells), as evidenced by the presence of the merged color yellow (see Figure 36A). The expression of ERK1/2 in the GCL was not co-stained with GS, which suggested that ERK1/2 expressed in the GCL might attribute to astrocytes or RGCs instead of Müller cells (see Figure 36A). The ERK1/2 staining intensity in NOR retinal sections was similar to that of the OIR vehicle and OIR LMPs.

Next, we determined HIF-1α expression in Müller cells via staining of P17 retinal sections of NOR, OIR vehicle, and OIR LMPs with HIF-1α and GS. HIF-1α was barely detectable under normoxia; however, it was drastically upregulated in Müller cells under hypoxia (OIR vehicle) (see Figure 36B). Specifically, the expression of HIF-1α increased dramatically in the GCL and IPL.

LMPs suppressed the effect (see Figure 36B). When the sections were co-stained with GS, HIF-1α was co-localized with GS in the GCL and IPL, where the endfeet and inner processes of Müller cells localize, respectively (see Figure 36B). The HIF-1α staining intensity in the NOR retinal sections was similar to that of the OIR vehicle and OIR LMPs.

**Figure 36.** ***LMPs Downregulate ERK1/2 and HIF-1α Expression in Müller Cells In Vivo.***

**A.**

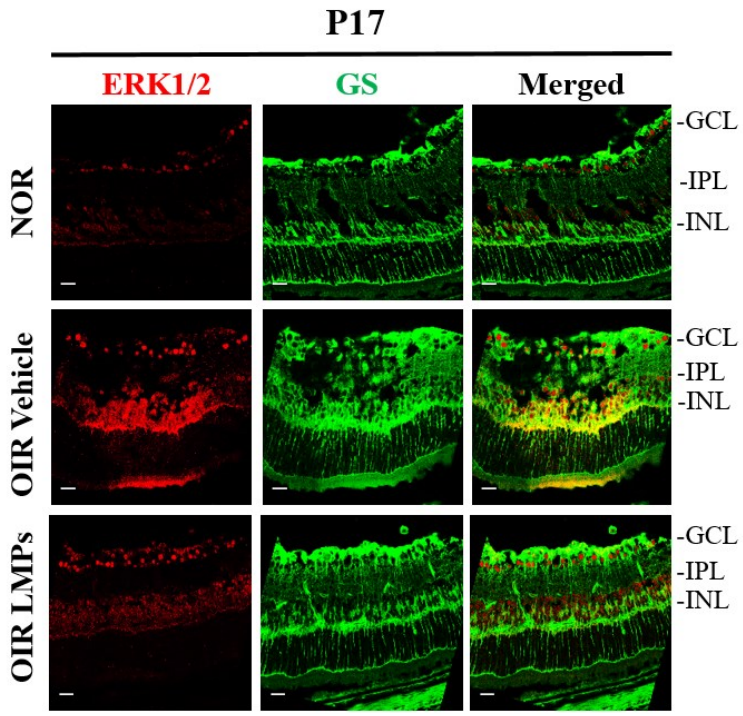


**B.**

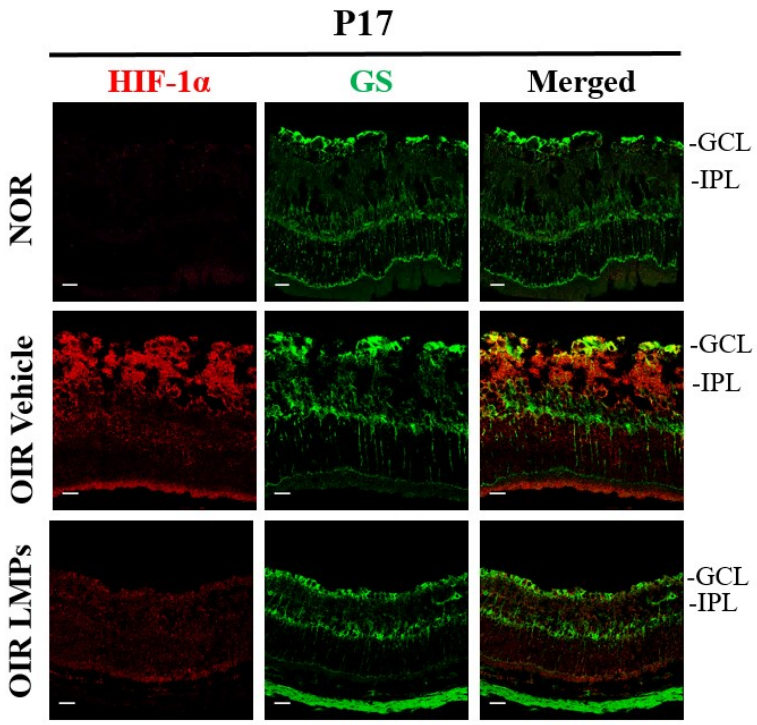


***Note.*** **A.** Representative images of NOR, OIR Vehicle, and OIR LMPs at P17. Retinal sections were stained with ERK1/2 (red) and GS (green). **B.** Representative immunofluorescent images of NOR, OIR Vehicle, and OIR LMPs at P17. Retinal sections were stained with HIF-1α (red) and GS (green). GCL = ganglion cell layer, IPL = inner plexiform layer, INL = inner nuclear layer. Original magnification: x 630. Scale bars =50 μm.

# Chapter 4.
# DISCUSSION

Müller cells, the primary macroglial cells, are essential for retinal homeostasis maintenance and neurons nourishment [45]. The present work is the first to show that human T lymphocyte-derived microparticles (LMPs) induced by an apoptotic reagent impede pathological retinal NV via targeting Müller cells in the OIR mouse model.

Previously, we demonstrated that LMPs are internalized by epithelial [145], endothelial [129], Lewis lung carcinoma cells [128], and macrophages [126]. Specifically, LMPs mediate the angiogenesis-inhibiting effects on Lewis lung carcinoma cells [128] and human retinal endothelial cells [129] via low-density lipoprotein receptor (LDLR) and macrophages through scavenger receptor CD36 [126]. In our current study, we focused on studying the effect of LMPs on Müller cells in the retina, due to the fact that Müller cells have been shown to be the major contributor of VEGF overproduction under pathological conditions [52, 132, 133]. LMPs were internalized by Müller cells *in vitro* (see Figure 27)

and *in vivo* (see Figure 35A). The expression of LDLR has been reported to be increased in Müller cells during retinal NV [146]. Here, we did not specifically study the uptake means of LMPs in Müller cells. However, considering the compositions of the plasma membrane of microparticles, which are composed of abundant lipids [147], as well as the physiological role of LDLR as the transporter of lipoproteins [148], it is conceivable that the uptake of LMPs by Müller cells is partly mediated through LDLR. Moreover, we do not exclude the possibility that other cells within the retina endocytose LMPs. In a recent publication, we demonstrated that LMPs are phagocytosed by macrophages through scavenger receptor CD36 [126]. In this regard, LMPs might be phagocytosed by microglial cells [149], astrocytes [150], and RPE cells [151] that also express scavenger receptor CD36 on the cell surface.

LMPs play a critical role in intercellular communication, acting as a mediator between parental cells and recipients, and consequently inducing a variety of cellular responses [125, 128, 129, 145]. In response to a broad spectrum of environmental changes or insults, Müller cells undergo activation (gliosis), which is presented by increased proliferation [48]. The lasting proliferation induces Müller cells to form glial scars, releasing a considerable number of growth factors and cytokines, which ultimately gives rise to secondary injury and accelerates the disease process [51]. Our present data revealed that LMPs reduced Müller cell proliferation dose-dependently (see Figure 28C). Moreover, LMPs prevented hypoxia-induced apoptosis at the concentration (10 μg/mL) that had a significant influence on Müller cell proliferation (see Figure 28C-D). In this regard, LMPs might serve as a potential therapy targeting overactivated Müller cells without causing a cytotoxic effect on cells that are critical for maintaining retinal homeostasis and neural functions. Moreover, the current results agree with our previous observations that LMPs can suppress excessive cell proliferation in non-malignant cells without causing cell death [125].

Inflammation is involved in the process of retinal NV [135]. At least three immune responses are demonstrated to be involved in this process: monocyte-derived macrophages, complements, and retinal microglia [76, 152]. An increased number of macrophages has been shown to invade into the hypoxic retina [76] and promote retinal NV [77]. Gao et al,. [78] demonstrated that the deletion of peripheral macrophages has no effect on the vaso-obliteration phase; however, it has a significant influence on pathological angiogenesis in the ischemic retinopathy mouse model. Clinical studies have indicated that VEGF and SDF-1 levels are significantly upregulated in the vitreous of stage 4 ROP patients characterized by retinal NV [93]. Besides the well-known pro-angiogenic effect [42], VEGF also serves as a potent chemoattractant for monocyte/macrophage recruitment [85]. SDF-1 participates in macrophage recruitment in ROP and other diseases [78, 96]. Our present data revealed that the expression of chemokines (VEGF and SDF-1) in the retina was diminished after a single intravitreal injection of LMPs (see Figures 35C and 35D). The infiltration-suppressive effect of LMPs on macrophages was illustrated and confirmed both *in vitro* (see Figure 29) and *in vivo* (see Figure 34A). Earlier, we showed that LMPs have no cytotoxic effect on macrophage viability [126], which excludes the possibility that LMPs eliminate macrophages. In addition, we also ruled out the possibility that LMPs diminished the density of residential microglia, as evidenced by the fact that most of the F4/80 positive cells were not co-stained with microglial specific marker TMEM119, and there were no apparent difference in microglial number in the LMPs-injected condition compared with the control (see Figure 34B-C). Our current data are in accordance with Davis et al., [75], showing that the increased number of macrophages in ROP during retinal NV is due to enhanced chemoattraction of peripheral macrophages instead of the proliferation of residential microglia.

An increasing body of evidence has demonstrated that M2 macrophages predominate in the retina during the development of pathological retinal NV, in which specific depletion of M2 macrophages significantly prevents aberrant retinal neovessels [73, 153]. Additionally, the pro-

angiogenic role of macrophages, especially M2 macrophages, has been confirmed in the development of choroidal NV [154, 155]. In a previous study, we showed that macrophages phagocytose LMPs via scavenger receptor CD36 [126]. Inhibition of CD36 abrogates the angiostatic effects of LMPs on choroidal NV [126]. Furthermore, LMPs exert an angiostatic effect via altering the phenotype of macrophages from M2 (pro-angiogenesis) to M1 (anti-angiogenesis) [126]. Here, we did not specifically study the phenotype regulation impact of LMPs on macrophages in the development of aberrant retinal NV. However, it is possible that LMPs regulate the phenotype of macrophages (from M2 to M1) during retinal NV. Taken together, this finding extends our knowledge about the influence of LMPs on macrophage activities, in which LMPs not only directly regulate the phenotype of macrophages but also indirectly modulate their recruitment.

Müller cells are the predominant source of various pro-inflammatory cytokines and growth factors, including VEGF and SDF-1, upon injuries [52, 132, 133, 156]. The contribution of VEGF to pathological retinal NV has been extensively studied [50]. Mounting evidence has pointed out that Müller cell-secreted VEGF significantly contributes to the formation of aberrant retinal vasculature [52, 132, 157]; however, it has a negligible effect on vascular development in the retina [158]. SDF-1 is an α-chemokine that exerts the chemoattractant effect exclusively through its ligand G-protein coupled receptor CXCR4 [95]. SDF-1 also promotes aberrant retinal NV and vascular leakage in the proliferative retinopathy mouse model [99]. The inhibition of SDF-1 significantly alleviates pathological retinal NV [99]. Here, we demonstrated that intravitreally injected-LMPs penetrated through the whole thickness of the retina and predominantly distributed in the INL and ONL (see Figure 35A). Our results also indicated that LMPs were internalized by Müller cells and reduced VEGF and SDF-1 expressions in Müller cells *in vivo* (see Figures 35C and 35D). Overall, the present findings further clarified the potential targets as well as the underlying effects of LMPs *in vivo.* LMPs not only affect direct angiogenesis-promoting cells (endothelial cells) [129] but also possess the capacity to target indirect angiogenesis-stimulating cells (Müller cells). However, we

should bear in mind that LMPs might interact with other cells within the retina that also participate in pathological retinal NV.

Previously, we reported that LMPs exert anti-angiogenic effects via targeting VEGF-related signaling pathways in diverse cell types, such as the upregulation of angiostatic receptor CD36 and downregulation of VEGFR2 in human umbilical vascular endothelial cells, reducing VEGF expression in Lewis lung carcinoma cells, and attenuating VEGF-induced ERK1/2 and Akt phosphorylation in human retinal endothelial cells [125, 128, 129]. Therefore, we investigated whether LMPs antagonized the upstreaming signaling events of VEGF and SDF-1 productions in Müller cells. Based on other publications [138, 139, 159], and our previous observations [125, 129], we surmise that LMPs affected two critical upstream regulators in Müller cells: ERK1/2 and HIF-1α.

ERK1/2, a mitogen-activated protein kinase, is essential for transducing external signals to the interior of the cell [160]. The activation of ERK1/2 is mediated via kinases-induced phosphorylation of either tyrosine (Tyr185) or threonine (Thr183) residues [160]. ERK1/2 is involved in a considerable number of cellular activities, including cell growth, proliferation, differentiation, and survival [160]. ERK1/2 activation is necessary for Müller cell proliferation [137]. Furthermore, the ERK1/2 signaling pathway participates in regulating VEGF secretion from Müller cells in diabetic retinopathy [138, 161]. Earlier, we showed that LMPs downregulate the expression of phosphorylated-ERK1/2, which is activated by VEGF-A in human retinal endothelial cells [129]. LMPs also inhibit human umbilical vascular endothelial cell proliferation via downregulating the expression of phosphorylated ERK1/2 [125]. Our previous observations suggest that LMPs can regulate the activation of ERK1/2 in different cells. In our current study, we showed that LMPs inhibited Müller cell proliferation dose-dependently (see Figure 28C). LMPs also downregulated the ERK1/2 protein in Müller cells *in vitro* (see Figure 32B) and *in vivo* (see Figure 36A). Although we did not specifically study the influence of LMPs on the phosphorylation process of ERK1/2 in Müller cells; based on our

previous findings [125, 129], it is reasonable to believe that LMPs inhibit Müller cell proliferation via downregulation of the phosphorylated-ERK1/2 in Müller cells.

The HIF-1 is a heterodimeric transcriptional factor that regulates cellular response under hypoxia [102]. HIF-1 belongs to the HIF family, which comprises two subunits: HIF-1α (120kD), an oxygen-regulated subunit; and HIF-1β (94kD), a stably-expressed subunit [102]. The protein expression of HIF-1α is dramatically enhanced under hypoxia [100]. Studies have shown that ERK1/2 activation promotes HIF-1α protein synthesis [100]. Additionally, ERK1/2 is capable of phosphorylating HIF-1α, which consequently increases the transcriptional activity of HIF-1α [162, 163]. The HIF-1 complex activates the transcription of target genes that contain HREs in the promoter region [102, 139]. Both VEGF and SDF-1 contain HREs in their promoter region and are transcriptionally activated by HIF-1 [139, 164]. Yoshida et al., [106] clearly demonstrated the contribution of HIF-1α to pathological retinal NV. They found that injection of cardiac glycoside digoxin either intraperitoneally or intraocularly reduce retinal HIF-1α expression, which results in the attenuation of pathological retinal NV by more than 70%. Similarly, Murilo et al., [157] showed that digoxin inhibits hypoxia-induced HIF-1α accumulation, majorly in the INL of the retina. Furthermore, Lin et al., [165] utilized a Müller cell-derived HIF-1α knockout mice and showed that HIF-1α generated from Müller cells have a negligible impact on retinal development, however, it significantly contributes to pathological retinal NV, retinal inflammation, and VEGF overproduction [165]. HIF-1α is barely detectable in all retinal layers under normal conditions [166]. In contrast, hypoxia significantly stimulates its expression in the inner retina [166]. Consistent with Theirsch et al., [166], the expression of HIF-1α was almost undetectable under normoxia (see Figure 36B) and was significantly increased by hypoxia in the IPL, where Müller cell inner processes locate (see Figure 36B). In contrast to Markeus et al., results [166], the intensity of HIF-1α in the INL (Müller cell somata) was not significantly enhanced. The difference in expressed location of HIF-1α might be attributed to the different hypoxic procedure time. Markeus et al,. [166] kept the mice under hypoxia

for only 6 h and sacrificed them immediately for HIF-1α detection. Whereas, in our condition, mice were kept under hypoxia for 5 days, which provide Müller cells with sufficient time to produce HIF-1α protein. And the phenomenon was suppressed by LMPs (see Figure 36B).

In our current study, we utilized the OIR mouse model, hoping to gain a better understanding of the underlying LMPs process. The OIR mouse model stands out as the most popular animal model for studying pathogenesis as well as therapeutic interventions of retinal NV; more than 11, 000 published articles adopted this model. However, we should keep in mind that this model is not perfect and contains several disadvantages, including the fact that (a) the mice are not born prematurely, which is different from that in humans; (b) the center of the retina is avascularized instead of peripheral as occurs in human ROP; and (c) retinal vasculature develops postnatally in mice, which is different from that in humans [36, 167].

The angiogenesis-inhibiting effect of LMPs was confirmed *in vivo*. LMPs significantly attenuated hypoxia-induced aberrant retinal NV (see Figure 33A-B). The impact of LMPs on retinal vascular development was tested earlier. Intravitreally injected-LMPs only have a modest effect on the development of retinal vasculature in rats [129]. Retinal NV is a sophisticatedly regulated process that involves the cooperation of retinal cells and non-retinal cells [168]. Earlier, we reported that LMPs impede the critical steps involved in angiogenesis [129]. LMPs significantly attenuate the proliferation of retinal endothelial cell and endothelial cell migration induced by VEGF [129]. Moreover, LMPs reduce the downstream signaling events of VEGF in endothelial cells [129]. Together, these suggest that the angiogenesis-inhibiting phenomenon that we observed in the current *in vivo* study could be a culmination of multiple events, including the direct and indirect effects of LMPs. The direct effects include the following: (a) reduce retinal endothelial cell migration due to the reduced production of VEGF in the hypoxic retina [129]; and (b) mitigate retinal endothelial cell proliferation [129]. The indirect effects include the following: (a) suppress the expression of angiogenesis-inducing

factors/chemokines in Müller cells (e.g., VEGF and SDF-1); (b) reduce macrophage recruitment, and (c) the reduced recruitment of the pro-angiogenic macrophages further results in decreased VEGF expression because macrophages are capable of producing VEGF [63].

In conclusion, we demonstrated that LMPs are capable of reducing Müller cell proliferation and preventing cell apoptosis induced by hypoxia. Intravitreally injected-LMPs were internalized by Müller cells and subsequently reduced the expression of angiogenic factors/chemokines (e.g., VEGF and SDF-1) in Müller cells. LMPs also downregulated the expression of ERK1/2 and HIF-1α in Müller cells. In addition, LMPs indirectly attenuated the infiltration of macrophages in the hypoxic retina. Together, this led to the alleviation of aberrant retinal NV (see Figure 37).

**Figure 37.** ***Schematic Model Depicting The Putative Mechanisms Concerned with The Angiogenesis-Inhibiting Effects of LMPs in the Mouse Model of Oxygen-Induced Ischemic Retinopathy.***

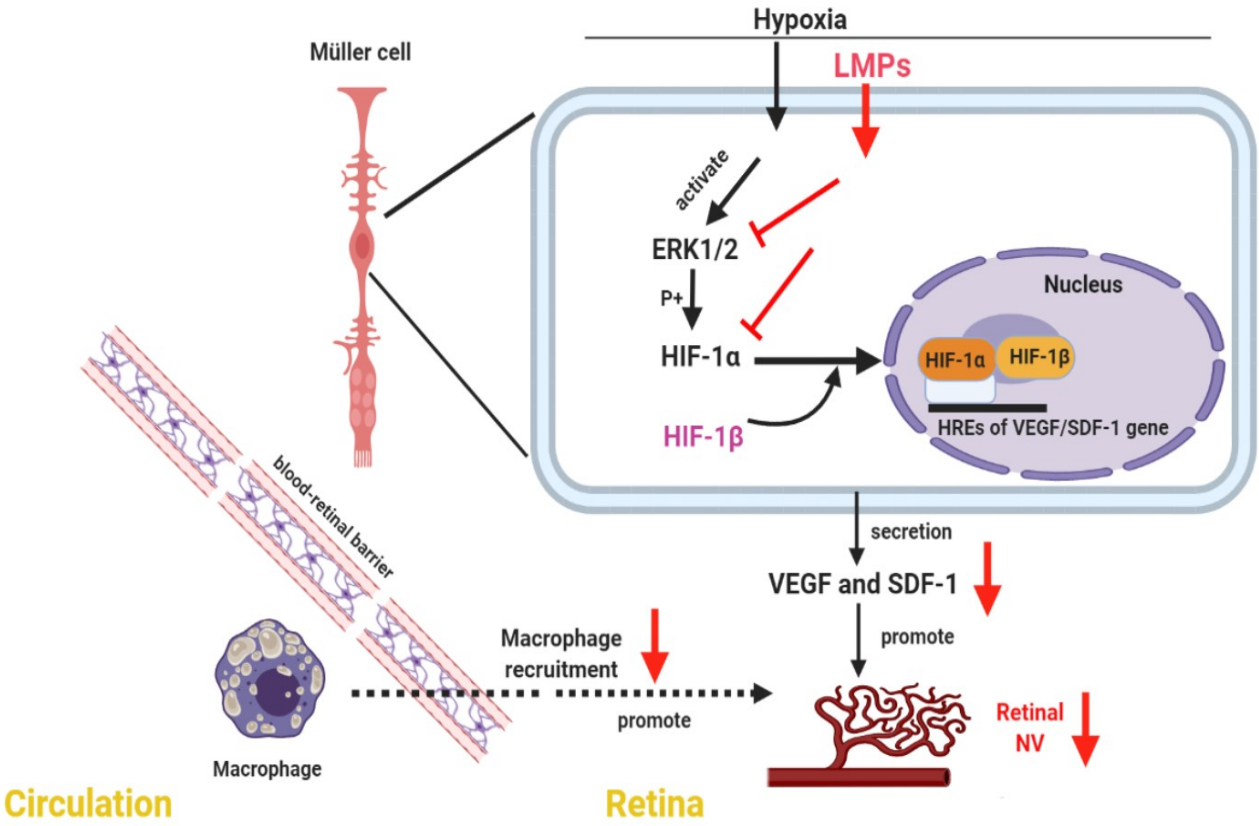


***Note.*** In the proposed model, intravitreal injection of LMPs is internalized by Müller cells. LMPs downregulate the expression of ERK1/2 and HIF-1α and reduce the expression of angiogenic factors/chemoattractants (VEGF and SDF-1) in Müller cells. LMPs also suppress the recruitment of macrophages to the hypoxic retina. All this leads to the alleviation of aberrant retinal NV.

ERK1/2: extracellular-signal-regulated kinases 1/2; HIF-1α: hypoxia-inducible factor-1α; HIF-1β: hypoxia-inducible factor-1β; HREs: hypoxia response elements; LMPs: lymphocytic microparticle; NV: neovascularization; P+: phosphorylation; SDF-1: stromal cell-derived factor-1; VEGF: vascular endothelial growth factor

# Chapter 5:
# CONCLUSION

In our group, we have been studying the effect of microparticles released from apoptosis-stimulated human T lymphocytes for many years. The study of lymphocytic microparticles was

initially driven by the observation of elevated levels of microparticles, which are released from lymphocytes in the plasma of patients associated with cardiovascular disease [110]. We showed that LMPs possess a strong anti-angiogenesis effect on various models, and the effect is not stimuli-dependent, in which microparticles generated from hyperoxia (95% $O_2$)-stimulated human T lymphocytes have comparable anti-angiogenesis effect [129]. The anti-proliferation effect of LMPs is not stimuli-dependent as well. Microparticles derived from human T lymphocytes stimulated with actinomycin D (apoptosis stimulus), phytohemagglutinin (PhA, cell division stimulus), or hyperoxia/hypoxia (oxidative stress stimuli) have comparable effect [169]. The anti-proliferation effect of LMPs is also parental cell-origin independent. Microparticles generated from CEM T lymphoblastic cells, Jurkat T lymphocytes, or human peripheral T lymphocytes possess a similar effect [169]. In contrast, the effect of microparticles might be cell-type dependent. Studies have shown that platelet-cell derived microparticles promote angiogenesis [114], whereas microparticles derived from endothelial cells suppress angiogenesis [115].

Compared to anti-VEGF mAbs, the following advantages show the feasibility of LMPs and their components (miRNAs) serving as an anti-angiogenic therapy targeting retinal NV diseases: (a) LMPs inhibit VEGF signaling [125, 129]; (b) LMPs selectively suppress rapidly proliferating cells, e.g., Müller cells (see Figure 28A) activated endothelial cells [125, 129], but do not cause cell death of these cells and do not affect the viability of neuronal cells [169]; (c) LMPs induce the expression of scavenger receptor CD36 (an anti-angiogenic factor) in endothelial cells [125]; (d) LMPs not only alter the phenotype of macrophages from pro-angiogenesis (M2) to anti-angiogenesis (M1) [126] but also suppress the recruitment of macrophages (see Figure 34A); and (e) LMPs have a longer half-life (~148h) in the eyes than that of anti-VEGF mAbs (~63h) (unpublished data). LMPs generated from human peripheral lymphocytes possess a potent inhibitory effect on endothelial cell activities (growth, proliferation, and migration), demonstrating the feasibility of personalized microparticles to inhibit aberrant angiogenesis as well as minimizing the immune response.

This study is aimed at expanding our understanding of the underlying anti-angiogenic mechanisms of LMPs as a novel therapeutic strategy for treating aberrant retinal NV diseases. Here, we only studied the short-term effect of LMPs *in vivo.* Further studies are required to investigate the long-term impact of LMPs and whether LMPs affect the visual functions *in vivo*. Additionally, future studies are needed to investigate the interaction of LMPs with other cells within the retina, such as astrocytes, microglial cells, and RPE cells, to enhance our understanding of the effects of LMPs on the retina.

BIBLIOGRAPHY

[1] Sung CH, Chuang JZ: The Cell Biology of Vision. J Cell Biol 2010, 190:953-63.

[2] Navarro R: The Optical Design of the Human Eye: a Critical Review. Journal of Optometry 2009, 2:3-18.

[3] Willoughby CE, Ponzin D, Ferrari S, Lobo A, Landau K, Omidi Y: Anatomy and Physiology of the Human Eye: Effects of Mucopolysaccharidoses Disease on Structure and Function -A Review. CLIN EXP OPHTHALMOL 2010, 38:2-11.

[4] Katherine Chuang MAF, and Lucian V. Del Priore: Potential of Gene Editing and Induced Pluripotent Stem Cells (iPSCs) in Treatment of Retinal Diseases. Yale J Biol Med 2017, 90:635-42.

[5] Klintworth GK: The Cornea Structure and Macromolecules in Health and Disease. Am J Pathol 1977, 89:718-808.

[6] MAURICE DM: The Cornea and the Sclera.

[7] Manik Goel RGP, Richard K. Lee and Sanjoy K. Bhattacharya: Aqueous Humor Dynamics: A Review. Open J Ophthalmol 2010, 4:52-9.

[8] Sturm RA, Larsson M: Genetics of Human Iris Colour and Patterns. Pigment Cell Melanoma Res 2009, 22:544-62.

[9] Borges- Giampani AS, Giampani J: Anatomy of Ciliary Body, Ciliary Processes, Anterior Chamber Angle and Collector Vessels. Glaucoma - Basic and Clinical Aspects, 2013.

[10] Julio Escribano MC-P: Bioinformatics and Reanalysis of Subtracted Expressed Sequence Tags from the Human Ciliary Body: Identification of Novel Biological Functions. Mol Vis 2002, 8:312-32.

[11] Nickla DL, Wallman J: The Multifunctional Choroid. Prog Retin Eye Res 2010, 29:144-68.

[12] Şt. Oprea CMP, F.M. Filipoiu, Raluca Tulin, Gabriela Diana Oprea: The Anatomy of the Choroid. Revista Română de Anatomie funcţională şi clinică, macro- şi microscopică şi de Antropologie 2016.

[13] Booij JC, Baas DC, Beisekeeva J, Gorgels TG, Bergen AA: The Dynamic Nature of Bruch's Membrane. Prog Retin Eye Res 2010, 29:1-18.

[14] Remington LA: Retina. Clinical Anatomy and Physiology of the Visual System, 2012. pp. 61-92.

[15] Reese BE: Development of the retina and optic pathway. Vision Res 2011, 51:613-32.

[16] Evelyne Sernagor SJEaROLW: Development of Retinal Ganglion Cell Structure and Function. Prog Retin Eye Res 2001, 20:139-74.

[17] Sanes JR, Masland RH: The Types of Retinal Ganglion Cells: Current Status and Implications for Neuronal Classification. Annu Rev Neurosci 2015, 38:221-46.

[18] Balasubramanian R, Gan L: Development of Retinal Amacrine Cells and Their Dendritic Stratification. Curr Ophthalmol Rep 2014, 2:100-6.

[19] Euler T, Haverkamp S, Schubert T, Baden T: Retinal Bipolar Cells: Elementary Building Blocks of Vision. Nat Rev Neurosci 2014, 15:507-19.

[20] Boije H, Shirazi Fard S, Edqvist PH, Hallbook F: Horizontal Cells, the Odd Ones Out in the Retina, Give Insights into Development and Disease. Front Neuroanat 2016, 10:77.

[21] Molday RS, Moritz OL: Photoreceptors at A Glance. J Cell Sci 2015, 128:4039-45.

[22] Strauss O: The Retinal Pigment Epithelium in Visual Function. Physiol Rev 2005, 85:845-81.

[23] Perkins BD, Fadool JM: Photoreceptor Structure and Development Analyses Using GFP Transgenes. Methods Cell Biol 2010, 100:205-18.

[24] Fronk AH, Vargis E: Methods for Culturing Retinal Pigment Epithelial Cells: A Review of Current Protocols and Future Recommendations. J Tissue Eng 2016, 7:2041731416650838.

[25] J.R. SparrrowD. Hicks aCPH: The Retinal Pigment Epithelium in Health and Disease. Curr Mol Med 2010, 10:802-23.

[26] Diala W Abu-Hassan TSAaMJK: The Trabecular Meshwork: A Basic Review of Form and Function. J Ocul Biol 2014, 2.

[27] Beebe DC: Development of the Ciliary Body: A Brief Review. Trans Ophathalmol Soc 1986, 105:123.

[28] Donaldson PJ, Grey AC, Maceo Heilman B, Lim JC, Vaghefi E: The Physiological Optics of the Lens. Prog Retin Eye Res 2017, 56:e1-e24.

[29] Bevalot F, Cartiser N, Bottinelli C, Fanton L, Guitton J: Vitreous Humor Analysis for the Detection of Xenobiotics in Forensic Toxicology: a review. Forensic Toxicol 2016, 34:12-40.

[30] Fruttiger M: Development of the Retinal Vasculature. Angiogenesis 2007, 10:77-88.

[31] Sun Y, Smith LEH: Retinal Vasculature in Development and Diseases. Annu Rev Vis Sci 2018, 4:101-22.

[32] Yoshikawa Y, Yamada T, Tai-Nagara I, Okabe K, Kitagawa Y, Ema M, Kubota Y: Developmental Regression of Hyaloid Vasculature is Triggered by Neurons. J Exp Med 2016, 213:1175-83.

[33] Ray F Gariano TWG: Retinal Angiogenesis in Development and Disease. Nature 2005, 438:960-6.

[34] Jing Chen LEHS: Retinopathy of Prematurity. Angiogenesis 2007, 10:133-40.

[35] Coorey NJ, Shen W, Chung SH, Zhu L, Gillies MC: The Role of Glia in Retinal Vascular Disease. Clin Exp Optom 2012, 95:266-81.

[36] Kim CB, D'Amore PA, Connor KM: Revisiting the Mouse Model of Oxygen-Induced Retinopathy. Eye Brain 2016, 8:67-79.

[37] Hellström A, Smith LEH, Dammann O: Retinopathy of Prematurity. The Lancet 2013, 382:1445-57.

[38] An International Classification of Retinopathy of Prematurity. II. The Classification of Retinal Detachment. The International Committee for the Classification of the Late Stages of Retinopathy of Prematurity. Arch Ophthalmol 1987, 105:906-12.

[39] Komal Agarwal SJ: Classification of Retinopathy of Prematurity: From Then Till Now. COMMUNITY EYE HEALTH JOURNAL 2018, 31.

[40] Liegl R, Hellstrom A, Smith LE: Retinopathy of Prematurity: The Need for Prevention. Eye Brain 2016, 8:91-102.

[41] Mutlu FM, Sarici SU: Treatment of Retinopathy of Prematurity: A Review of Conventional and Promising New Therapeutic Options. Int J Ophthalmol 2013, 6:228-36.

[42] Kim LA, D'Amore PA: A Brief History of Anti-VEGF for the Treatment of Ocular Angiogenesis. Am J Pathol 2012, 181:376-9.

[43] Falavarjani KG, Nguyen QD: Adverse Events and Complications Associated with Intravitreal Injection of Anti-VEGF Agents: A Review of Literature. Eye (Lond) 2013, 27:787-94.

[44] Tolentino M: Systemic and Ocular Safety of Intravitreal Anti-VEGF Therapies for Ocular Neovascular Disease. Surv Ophthalmol 2011, 56:95-113.

[45] Andreas Bringmann TP, Jens Grosche, Mike Francke, Peter Wiedemann, Serguei N Skatchkov, Neville N Osborne, Andreas Reichenbach: Muller Cells in the Healthy and Diseased Retina. Prog Retin Eye Res 2006, 25:397-424.

[46] NORENBURG RERMD: Müller Cell Localisation of Glutamine Synthetase in Rat Retina. Nature 1977, 268:654-5.

[47] Toft-Kehler AK, Skytt DM, Kolko M: A Perspective on the Muller Cell-Neuron Metabolic Partnership in the Inner Retina. Mol Neurobiol 2018, 55:5353-61.

[48] Bringmann A, Wiedemann, P.: Muller Glial Cells in Retinal Disease. Ophthalmologica 2012, 227:1-19.

[49] Wang M, Wong WT: Microglia-Muller Cell Interactions in the Retina. Adv Exp Med Biol 2014, 801:333-8.

[50] J S Penn AM, R B Caldwell, M Bartoli, R W Caldwell, M E Hartnett: Vascular Endothelial Growth Factor in Eye Disease. Prog Retin Eye Res 2008, 27:331-71.

[51] Eastlake K, Banerjee PJ, Angbohang A, Charteris DG, Khaw PT, Limb GA: Muller Glia as An Important Source of Cytokines and Inflammatory Factors Present in the Gliotic Retina during Proliferative Vitreoretinopathy. Glia 2016, 64:495-506.

[52] Jiang Y, Wang H, Culp D, Yang Z, Fotheringham L, Flannery J, Hammond S, Kafri T, Hartnett ME: Targeting Muller Cell-Derived VEGF164 to Reduce Intravitreal Neovascularization in The Rat Model of Retinopathy of Prematurity. IOVS 2014, 55:824-31.

[53] Juanjuan Wang XX, Michael H Elliott, Meili Zhu, Yun-Zheng Le: Muller Cell-Derived VEGF is Essential for Diabetes-Induced Retinal Inflammation and Vascular Leakage. Diabetes 2010, 59:2297-305.

[54] Gordon S, Taylor PR: Monocyte and macrophage heterogeneity. Nat Rev Immunol 2005, 5:953-64.

[55] Shapouri-Moghaddam A, Mohammadian S, Vazini H, Taghadosi M, Esmaeili SA, Mardani F, Seifi B, Mohammadi A, Afshari JT, Sahebkar A: Macrophage Plasticity, Polarization, and Function in Health and Disease. J Cell Physiol 2018, 233:6425-40.

[56] Italiani P, Boraschi D: From Monocytes to M1/M2 Macrophages: Phenotypical vs. Functional Differentiation. Front Immunol 2014, 5:514.

[57] Dedonder SE, Cheng C, Willard LH, Boyle DL, Ganta RR: Transmission electron microscopy reveals distinct macrophage- and tick cell-specific morphological stages of Ehrlichia chaffeensis. PLoS One 2012, 7:e36749.

[58] Wynn TA, Chawla A, Pollard JW: Macrophage biology in development, homeostasis and disease. Nature 2013, 496:445-55.

[59] Underhill AAaDM: Mechanisms of Phagocytosis in Macrophages. Annu Rev Immunol 1999, 17:593-623.

[60] Chenghai Li BL, Zonghan Dai, Yunxia Tao: Knockdown of VEGF Receptor-1 (VEGFR-1) Impairs Macrophage Infiltration, Angiogenesis and Growth of Clear Cell Renal Cell Carcinoma (CRCC). Cancer Biol Ther 2011, 12:872-80.

[61] Owen JL, Mohamadzadeh M: Macrophages and Chemokines as Mediators of Angiogenesis. Front Physiol 2013, 4:159.

[62] Unanue ER: Antigen-Presenting Function of Macrophages. Ann Rev Immunol 1984, 2:395-428.

[63] H L Naug JB, G A Gole, G Gobé: Vitreal Macrophages Express Vascular Endothelial Growth Factor in Oxygen-Induced Retinopathy. Clin Exp Ophthalmol 2000, 28:48-52.

[64] Shi C, Pamer EG: Monocyte Recruitment during Infection and Inflammation. Nat Rev Immunol 2011, 11:762-74.

[65] Griffith JW, Sokol CL, Luster AD: Chemokines and Chemokine Receptors: Positioning Cells for Host Defense and Immunity. Annu Rev Immunol 2014, 32:659-702.

[66] Miller MC, Mayo KH: Chemokines from a Structural Perspective. Int J Mol Sci 2017, 18.

[67] Lolis EJFaE: Structure,Function, And Inhibition of Chemokines. Annu Rev Pharmacol Toxicol 2002, 42:469-99.

[68] Turner MD, Nedjai B, Hurst T, Pennington DJ: Cytokines and Chemokines: At the Crossroads of Cell Signalling and Inflammatory Disease. Biochim Biophys Acta 2014, 1843:2563-82.

[69] Martinez FO, Gordon S: The M1 and M2 Paradigm of Macrophage Activation: Time for Reassessment. F1000Prime Rep 2014, 6:13.

[70] Nadine Jetten SV, Marion J Gijbels, Mark J Post, Menno P J De Winther, Marjo M P C Donners: Anti-Inflammatory M2, but Not Pro-Inflammatory M1 Macrophages Promote Angiogenesis In Vivo. Angiogenesis 2014, 17:109-18.

[71] Uzma Saqib SS, Kyoungho Suk, Owais Mohammad, Mirza S. Baig and Rajkumar Savai: Phytochemicals as Modulators of M1-M2 Macrophages in Inflammation. Oncotarget 2018, 9:17937-50.

[72] Michael H Davies JPE, Michael R Powers: Microglia and Macrophages are Increased in Response to Ischemia Induced Retinopathy in The Mouse Retina. Mol Vis 2006, 12:467-77.

[73] Yedi Zhou SY, Shintaro Nakao, Takeru Yoshimura, Yoshiyuki Kobayashi, Takahito Nakama, Yuki Kubo, Kohta Miyawaki, Muneo Yamaguchi, Keijiro Ishikawa, Yuji Oshima, Koichi Akashi,

Tatsuro Ishibashi: M2 Macrophages Enhance Pathological Neovascularization in The Mouse Model of Oxygen-Induced Retinopathy. IOVS 2015, 56:4767-77.

[74] Sha Gao CL, Yanji Zhu, Yanuo Wang, Ailing Sui, Yisheng Zhong, Bing Xie, Xi Shen: PEDF Mediates Pathological Neovascularization by Regulating Macrophage Recruitment and Polarization in The Mouse Model of Oxygen-Induced Retinopathy. Sci Rep 2017, 7:42846.

[75] Davies MH, Eubanks JP, Powers MR: Microglia and Macrophages are Increased in Response to Ischemia-Induced Retinopathy in The Mouse Retina. Mol Vis 2006, 12:467-77.

[76] Keiko Kataoka KMN, Hiroki Kaneko, Nico van Rooijen, Shu Kachi, Hiroko Terasaki: The Roles of Vitreal Macrophages and Circulating Leukocytes in Retinal Neovascularization. IOVS 2011, 52:1431-8.

[77] Matthew R Ritter EB, Stacey K Moreno, Edith Aguilar, Michael I Dorrell, Martin Friedlander: Myeloid Progenitors Differentiate into Microglia and Promote Vascular Repair in A Model of Ischemic Retinopathy. J Clin Invest 2006, 116:3266-76.

[78] Xiang Gao YW, XiaoQin Li, HuiYuan Hou, JingBo Su, LiBo Yao, Jian Zhang: Macrophages Promote Vasculogenesis of Retinal Neovascularization in An Oxygen-Induced Retinopathy Model in Mice. Cell Tissue Res 2016, 364:599-610.

[79] Kerbel RS: Tumor Angiogenesis. N Engl J Med 2008, 358:2039-49.

[80] Noonan DM, De Lerma Barbaro A, Vannini N, Mortara L, Albini A: Inflammation, Inflammatory Cells and Angiogenesis: Decisions and Indecisions. Cancer Metastasis Rev 2008, 27:31-40.

[81] Adair TH MJ: Chapter 1: Overview of Angiogenesis. San Rafael (CA): Morgan & Claypool Life Sciences 2010.

[82] Rajabi M, Mousa SA: The Role of Angiogenesis in Cancer Treatment. Biomedicines 2017, 5.

[83] Stringer CJRaSE: The Splice Variants of Vascular Endothelial Growth Factor (VEGF) and Their Receptors. J Cell Sci Ther 2001, 114:853-65.

[84] Edmund Tischer RM, Taymar Hartman, Maria Silva, Denis GospodarowiczS, John C. Fiddes, and Judith A. Abrahaml: The Human Gene for Vascular Endothelial Growth Factor. THE JOURNAL OF BIOLOGICAL CHEMISTRY 1991, 266:11947-54.

[85] Leek RD: Macrophage Infiltration Is Associated with VEGF and EGFR Expression in Breast Cancer. J Pathol 2000, 190:430-6.

[86] Hirotoki Ohkubo YI, Tsutomu Minamino, Koji Eshima, Ken Kojo, Shin-ichiro Okizaki, Mitsuhiro Hirata, Masabumi Shibuya, Masahiko Watanabe, Masataka Majima: VEGFR1-Positive Macrophages Facilitate Liver Repair and Sinusoidal Reconstruction After Hepatic Ischemia/Reperfusion Injury. PLoS One 2014, 9:e105533.

[87] Potente M, Gerhardt H, Carmeliet P: Basic and therapeutic aspects of angiogenesis. Cell 2011, 146:873-87.

[88] Blanco R, Gerhardt H: VEGF and Notch in Tip and Stalk Cell Selection. Cold Spring Harb Perspect Med 2013, 3:a006569.

[89] Jonathan Stone AI, Tamar Alon, Jacob Pe'er, Hadassah Gnessin, Tailoi Chan-Ling, and Eli Keshet: Development of Retinal Vasculature Is Mediated by HypoxiaInduced Vascular Endothelial Growth Factor (VEGF) Expression by Neuroglia The Journal of Neuroscience 1995, 15:4738-47.

[90] Smith LEH: Pathogenesis of retinopathy of prematurity. Semin Neonatol 2003, 8:469-73.

[91] Donahue ML, Phelps DL, Watkins RH, LoMonaco MB, Horowitz S: Retinal vascular endothelial growth factor (VEGF) mRNA expression is altered in relation to neovascularization in oxygen induced retinopathy. Curr Eye Res 1996, 15:175-84.

[92] Wang H: Anti-VEGF Therapy in the Management of Retinopathy of Prematurity: What We Learn from Representative Animal Models of Oxygen-Induced Retinopathy. Eye Brain 2016, 8:81-90.

[93] Sonmez K, Drenser KA, Capone A, Jr., Trese MT: Vitreous Levels of Stromal Cell-Derived Factor 1 and Vascular Endothelial Growth Factor in Patients with Retinopathy of Prematurity. Ophthalmology 2008, 115:1065-70 e1.

[94] Conrad C. Bleul RCF, Jose M. Casasnovas, Alessandro Aiuti, and Timothy A. Springer: A Highly Efficacious Lymphocyte Chemoattractant, Stromal Cell-derived Factor 1 (SDF-1). J Exp Med 1996, 184:1101-9.

[95] Magda Kucia KJ, Ryan Reca, Marcin Wysoczynski, Laura Bandura, Daniel J. Allendorf, Jin Zhang, Janina Ratajczak & Mariusz Z. Ratajczak: CXCR4–SDF-1 Signalling, Locomotion, Chemotaxis and Adhesion. J Mol Histol 2004, 35:233-45.

[96] Wan X, Xia W, Gendoo Y, Chen W, Sun W, Sun D, Cao C: Upregulation of Stromal Cell-Derived Factor 1 (SDF-1) Is Associated with Macrophage Infiltration in Renal Ischemia-Reperfusion Injury. PLoS One 2014, 9:e114564.

[97] Salcedo R, Oppenheim JJ: Role of Chemokines in Angiogenesis: CXCL12/SDF-1 and CXCR4 Interaction, A Key Regulator of Endothelial Cell Responses. Microcirculation 2003, 10:359-70.

[98] Elena De Falco DP, Anna Rita Torella, Stefania Straino, Maria Grazia Iachininoto, Alessia Orlandi, Silvia Truffa, Paolo Biglioli, Monica Napolitano, Maurizio C. Capogrossi, and Maurizio Pesce: SDF-1 Involvement in Endothelial Phenotype and Ischemia-Induced Recruitment of Bone Marrow Progenitor Cells. Blood 2004, 104:3472-82.

[99] Butler JM, Guthrie SM, Koc M, Afzal A, Caballero S, Brooks HL, Mames RN, Segal MS, Grant MB, Scott EW: SDF-1 Is Both Necessary and Sufficient to Promote Proliferative Retinopathy. J Clin Invest 2005, 115:86-93.

[100] Yee Koh M, Spivak-Kroizman TR, Powis G: HIF-1 Regulation: Not So Easy Come, Easy Go. Trends Biochem Sci 2008, 33:526-34.

[101] Rattner A, Williams J, Nathans J: Roles of HIFs and VEGF in Angiogenesis in the Retina and Brain. J Clin Invest 2019, 130:3807-20.

[102] Majmundar AJ, Wong WJ, Simon MC: Hypoxia-Inducible Factors and The Response to Hypoxic Stress. Mol Cell 2010, 40:294-309.

[103] Ramya Krishna Vadlapatla ADV, and Ashim K. Mitra: Hypoxia-Inducible Factor-1 (HIF-1): A Potential Target for Intervention in Ocular Neovascular Diseases. Curr Drug Targets 2013, 14:919-35.

[104] Krock BL, Skuli N, Simon MC: Hypoxia-Induced Angiogenesis: Good and Evil. Genes Cancer 2011, 2:1117-33.

[105] Hiroaki Ozaki AYY, Neil Delia, Keiko Ozaki, Jose D. Luna, Haruhiko Yamada, Sean F. Hackett, Naoyuki Okamoto, DonaldJ. Zack, Gregg L Semenza, and Peter A. Campochiaro: Hypoxia Inducible Factor-la Is Increased in Ischemic Retina: Temporal and Spatial Correlation with VEGF Expression. Invest Ophlhalmol Vis Sci 1999, 40:182-9.

[106] Yoshida T, Zhang H, Iwase T, Shen J, Semenza GL, Campochiaro PA: Digoxin Inhibits Retinal Ischemia-Induced HIF-1Alpha Expression and Ocular Neovascularization. FASEB J 2010, 24:1759-67.

[107] Masanobu Morita OO, Toshiharu Yamashita, Satoru Takahashi, Norio Suzuki, Osamu Nakajima, Shimako Kawauchi, Masatsugu Ema, Shigeki Shibahara, Tetsuo Udono, Koji Tomita, Makoto Tamai, Kazuhiro Sogawa, Masayuki Yamamoto and Yoshiaki Fujii-Kuriyama: HLF/HIF-2— is a key factor in retinopathy of prematurity in association with erythropoietin. EMBO J 2003, 22:1134-46.

[108] Miwa Y, Hoshino Y, Shoda C, Jiang X, Tsubota K, Kurihara T: Pharmacological HIF Inhibition Prevents Retinal Neovascularization with Improved Visual Function in a Murine Oxygen-Induced Retinopathy Model. Neurochem Int 2019, 128:21-31.

[109] Charlotte Lawsona DK, Elizabeth Findinga,b, Emily Ulfeldera,b, and Virginia Luis-Fuentes: Extracellular Vesicles: Evolutionarily Conserved Mediators of Intercellular Communication. Yale J Biol Med 2017, 90:481-91.

[110] Shantsila E, Kamphuisen PW, Lip GY: Circulating Microparticles in Cardiovascular Disease: Implications for Atherogenesis and Atherothrombosis. J Thromb Haemost 2010, 8:2358-68.

[111] van Niel G, D'Angelo G, Raposo G: Shedding light on the cell biology of extracellular vesicles. Nat Rev Mol Cell Biol 2018, 19:213-28.

[112] S ELA, Mager I, Breakefield XO, Wood MJ: Extracellular Vesicles: Biology and Emerging Therapeutic Opportunities. Nat Rev Drug Discov 2013, 12:347-57.

[113] Yuana Y, Sturk A, Nieuwland R: Extracellular Vesicles in Physiological and Pathological Conditions. Blood Rev 2013, 27:31-9.

[114] Hyun Kyung Kim KSS, Jun-Ho Chung, Kyoung Rhan Lee and Se-Na Lee: Platelet Microparticles Induce Angiogenesis In Vitro. Br J Haematol 2003, 124:376-84.

[115] Mezentsev A, Merks RM, O'Riordan E, Chen J, Mendelev N, Goligorsky MS, Brodsky SV: Endothelial Microparticles Affect Angiogenesis In Vitro: Role of Oxidative Stress. Am J Physiol Heart Circ Physiol 2005, 289:H1106-14.

[116] Safaei R, Larson BJ, Cheng TC, Gibson MA, Otani S, Naerdemann W, Howell SB: Abnormal Lysosomal Trafficking and Enhanced Exosomal Export of Cisplatin in Drug-Resistant Human Ovarian Carcinoma Cells. Mol Cancer Ther 2005, 4:1595-604.

[117] Bebawy M, Combes V, Lee E, Jaiswal R, Gong J, Bonhoure A, Grau GE: Membrane Microparticles Mediate Transfer of P-Glycoprotein to Drug Sensitive Cancer Cells. Leukemia 2009, 23:1643-9.

[118] Dalli J, Norling LV, Renshaw D, Cooper D, Leung KY, Perretti M: Annexin 1 Mediates the Rapid Anti-Inflammatory Effects of Neutrophil-Derived Microparticles. Blood 2008, 112:2512-9.

[119] Gasser O, Schifferli JA: Activated Polymorphonuclear Neutrophils Disseminate Anti-Inflammatory Microparticles by Ectocytosis. Blood 2004, 104:2543-8.

[120] Angelillo-Scherrer A: Leukocyte-Derived Microparticles in Vascular Homeostasis. Circ Res 2012, 110:356-69.

[121] Ziad Mallat BndH, Jeanny Ohan, Guy Lese`che, Jean-Marie Freyssinet, Alain Tedgui: Shed Membrane Microparticles With Procoagulant Potential in Human Atherosclerotic Plaques A Role for Apoptosis in Plaque Thrombogenicity. Circulation 1999, 99:348-53.

[122] Vanwijk MJ, Svedas E, Boer K, Nieuwland R, Vanbavel E, Kublickiene KR: Isolated Microparticles, but not Whole Plasma, from Women with Preeclampsia Impair Endothelium-Dependent Relaxation in Isolated Myometrial Arteries from Healthy Pregnant Women. Am J Obstet Gynecol 2002, 187:1686-93.

[123] Angela Tesse MCMn, Be´ne´dicte Hugel, Karel Chalupsky, Christian D. Muller, Ferhat Meziani, Delia Mitolo-Chieppa, Jean-Marie Freyssinet, Ramaroson Andriantsitohaina: Upregulation of Proinflammatory Proteins Through NF-kB Pathway by Shed Membrane Microparticles Results in Vascular Hyporeactivity. Arterioscler Thromb Vasc Biol 2005, 25:2522-7.

[124] Chun Yang WX, Qian Qiu, Houda Tahiri, Carmen Gagnon, Guoxiang Liu, Pierre Hardy: Generation of Lymphocytic Microparticles and Detection of Their Proapoptotic Effect on Airway Epithelial Cells. Journal of visualized experiments : JoVE 2015:e52651.

[125] Chun Yang BRM, Tang Zhu, Carmen Gagnon, Josiane Lafleur, Swathi Seshadri, Pierre Lachapelle, Jean-Claude Lavoie, Sylvain Chemtob, Pierre Hardy: Lymphocytic Microparticles Inhibit Angiogenesis by Stimulating Oxidative Stress and Negatively Regulating VEGF-Induced Pathways. Am J Physiol Regul Integr Comp Physiol 2008, 294:R467-76.

[126] Houda Tahiri SO, Chun Yang, François Duhamel, Suzanne Samarani, Ali Ahmad, Mark Vezina, Martin Bussières, Elvire Vaucher, Przemyslaw Sapieha, Gilles Hickson, Karim Hammamji, Réjean Lapointe, Francis Rodier, Sophie Tremblay, Isabelle Royal, Jean-François Cailhier, Sylvain Chemtob, Pierre Hardy Lymphocytic Microparticles Modulate Angiogenic Properties of Macrophages in Laser-Induced Choroidal Neovascularization. Sci Rep 2016, 6:37391.

[127] Qiu Q, Yang C, Xiong W, Tahiri H, Payeur M, Superstein R, Carret AS, Hamel P, Ellezam B, Martin B, Vezina M, Sapieha P, Liu G, Hardy P: SYK is a Target of Lymphocyte-Derived Microparticles in the Induction of Apoptosis of Human Retinoblastoma Cells. Apoptosis 2015, 20:1613-22.

[128] Yang Chun GC, Hou Xin, Hardy Pierre: Low Density Lipoprotein Receptor Mediates Anti-VEGF Effect of Lymphocyte T-Derived Microparticles in Lewis Lung Carcinoma Cells. Cancer Biol Ther 2014, 10:448-56.

[129] Chun Yang WX, Qian Qiu, Zhuo Shao, David Hamel, Houda Tahiri, Grégoire Leclair, Pierre Lachapelle, Sylvain Chemtob, Pierre Hardy: Role of Receptor-Mediated Endocytosis in The Antiangiogenic Effects of Human T Lymphoblastic Cell-Derived Microparticles. Am J Physiol Regul Integr Comp Physiol 2012, 302:R941-9.

[130] Hume MGHaRI: Dil and DiO: Versatile Fluorescent Dyes for Neuronal Labelling and Pathway Tracing. The Cell 1989, 12:2236-89.

[131] L E Smith EW, A McLellan, S K Kostyk, R D'Amato, R Sullivan, P A D'Amore: Oxygen-Induced Retinopathy in The Mouse. IOVS 1994, 35:101-11.

[132] Haibo Wang GWS, Zhihong Yang, Yanchao Jiang, Manabu McCloskey, Kenneth Greenberg, Pete Geisen, William D Culp, John Flannery, Tal Kafri, Scott Hammond, M Elizabeth Hartnett: Short Hairpin RNA-Mediated Knockdown of VEGFA in Muller Cells Reduces Intravitreal Neovascularization in A Rat Model of Retinopathy of Prematurity. Am J Pathol 2013, 183:964-74.

[133] Yanyan Bai J-xM, Junjing Guo, Juanjuan Wang, Meili Zhu, Ying Chen, Yun-Zheng Le: Muller Cell-Derived VEGF Is A Significant Contributor to Retinal Neovascularization. J Pathol 2009, 219:446-54.

[134] Munoz-Sanchez J, Chanez-Cardenas ME: The Use of Cobalt Chloride as a Chemical Hypoxia Model. J Appl Toxicol 2019, 39:556-70.

[135] Susumu Ishida TU, Kenji Yamashiro, Yuichi Kaji, Shiro Amano, Yuichiro Ogura, Tetsuo Hida, Yoshihisa Oguchi, Jayakrishna Ambati, Joan W Miller, Evangelos S Gragoudas, Yin-Shan Ng, Patricia A D'Amore, David T Shima, Anthony P Adamis: VEGF164-Mediated Inflammation Is Required for Pathological, but Not Physiological, Ischemia-Induced Retinal Neovascularization. J Exp Med 2003, 198:483-9.

[136] Masato Murakami YZ, Masanori Hirashima, Toshio Suda, Yohei Morita, Jun Ooehara, Hideo Ema, Guo-Hua Fong, Masabumi Shibuya: VEGFR1 Tyrosine Kinase Signaling Promotes Lymphangiogenesis as well as Angiogenesis Indirectly via Macrophage Recruitment. Arterioscler Thromb Vasc Biol 2008, 28:658-64.

[137] Jing Wang CH, Tian Zhou, Zijing Huang, Lingli Zhou, Xialin Liu NGF Increases VEGF Expression and Promotes Cell Proliferation via ERK1/2 and AKT Signaling in Müller Cells. Mol Vis 2016, 22:254-63.

[138] Xiaofeng Ye HR, Meng Zhang, Zhongcui Sun, Alice C Jiang, Gezhi Xu: ERK1/2 Signaling Pathway in The Release of VEGF from Muller Cells in Diabetes. IOVS 2012, 53:3481-9.

[139] Ceradini DJ, Kulkarni AR, Callaghan MJ, Tepper OM, Bastidas N, Kleinman ME, Capla JM, Galiano RD, Levine JP, Gurtner GC: Progenitor Cell Trafficking is Regulated by Hypoxic Gradients through HIF-1 Induction of SDF-1. Nat Med 2004, 10:858-64.

[140] Stahl A, Chen J, Sapieha P, Seaward MR, Krah NM, Dennison RJ, Favazza T, Bucher F, Lofqvist C, Ong H, Hellstrom A, Chemtob S, Akula JD, Smith LE: Postnatal Weight Gain Modifies Severity and Functional Outcome of Oxygen-Induced Proliferative Retinopathy. Am J Pathol 2010, 177:2715-23.

[141] Robertson RT, Levine ST, Haynes SM, Gutierrez P, Baratta JL, Tan Z, Longmuir KJ: Use of Labeled Tomato Lectin for Imaging Vasculature Structures. Histochem Cell Biol 2015, 143:225-34.

[142] Gordon JMAaS: F4/80, A Monoclonal Antibody Directed Specifically against the Mouse Macrophage. Eur J Immunol 1981, 11:805-15.

[143] Ryuichi Wada CJT, and Richard L. Proia: Microglial Activation Precedes Acute Neurodegeneration in Sandhoff Disease and Is Suppressed by Bone Marrow Transplantation. PNAS 2000, 97:10954-9.

[144] Bennett ML, Bennett FC, Liddelow SA, Ajami B, Zamanian JL, Fernhoff NB, Mulinyawe SB, Bohlen CJ, Adil A, Tucker A, Weissman IL, Chang EF, Li G, Grant GA, Hayden Gephart MG,

Barres BA: New tools for studying microglia in the mouse and human CNS. Proc Natl Acad Sci U S A 2016, 113:E1738-46.

[145] Qian Qiu WX, Chun Yang, Xiaotian Dai, Xiaoping Dan, Zaixing Yang, Yan Jiao, Yang Xiang, Guoxiang Liu, Pierre Hardy: Lymphocyte-Derived Microparticles Induce Apoptosis of Airway Epithelial Cells Through Activation of p38 MAPK and Production of Arachidonic Acid. Apoptosis 2014, 19:1113-27.

[146] María C Sánchez PFB, Jose D Luna, Susana G Ortiz, Patricio C Juarez, Clelia M Riera, Gustavo A Chiabrando: Low-Density Lipoprotein Receptor-Related Protein-1 (LRP-1) Expression in A Rat Model of Oxygen-Induced Retinal Neovascularization. Exp Eye Res 2006, 83:1378-85.

[147] Record M, Silvente-Poirot S, Poirot M, Wakelam MJO: Extracellular Vesicles: Lipids as Key Components of Their Biogenesis and Functions. J Lipid Res 2018, 59:1316-24.

[148] Jeon H, Blacklow SC: Structure and Physiologic Function of the Low-Density Lipoprotein Receptor. Annu Rev Biochem 2005, 74:535-62.

[149] Coraci IS, Husemann J, Berman JW, Hulette C, Dufour JH, Campanella GK, Luster AD, Silverstein SC, El Khoury JB: CD36, a Class B Scavenger Receptor, Is Expressed on Microglia in Alzheimer's Disease Brains and Can Mediate Production of Reactive Oxygen Species in Response to β-Amyloid Fibrils. Am J Clin Pathol 2002, 160:101-12.

[150] Bao Y, Qin L, Kim E, Bhosle S, Guo H, Febbraio M, Haskew-Layton RE, Ratan R, Cho S: CD36 is Involved in Astrocyte Activation and Astroglial Scar Formation. J Cereb Blood Flow Metab 2012, 32:1567-77.

[151] Sandra W. Ryeom JRSaRLS: CD36 Participates in the Phagocytosis of Rod Outer Segments by Retinal Pigment Epithelium. J Cell Sci 1996, 109:387-95.

[152] Ryoji Yanai AT, Kip M Connor: Complement Involvement in Neovascular Ocular Diseases. Adv Exp Med Biol 2012, 946:161-83.

[153] Zhou YD, Yoshida S, Peng YQ, Kobayashi Y, Zhang LS, Tang LS: Diverse roles of macrophages in intraocular neovascular diseases: a review. Int J Ophthalmol 2017, 10:1902-8.

[154] Tsutsumi C, Sonoda KH, Egashira K, Qiao H, Hisatomi T, Nakao S, Ishibashi M, Charo IF, Sakamoto T, Murata T, Ishibashi T: The Critical Role of Ocular-Infiltrating Macrophages in the Development of Choroidal Neovascularization. J Leukoc Biol 2003, 74:25-32.

[155] Sakurai E, Anand A, Ambati BK, van Rooijen N, Ambati J: Macrophage Depletion Inhibits Experimental Choroidal Neovascularization. Invest Ophthalmol Vis Sci 2003, 44:3578-85.

[156] Liu T, Tang X, Yao L, Song H: Expression and Significance of SDF-1 and its Receptor CXCR4 in the Retina of Pregnant Rats after Optic Nerve Injury. Eur J Inflamm 2018, 16.

[157] Murilo Rodrigues XX, Kathleen Jee, Savalan Babapoor-Farrokhran, Fabiana Kashiwabuchi, Tao Ma, Imran Bhutto, Syed Junaid Hassan, Yassine Daoud, David Baranano, Sharon Solomon, Gerard Lutty, Gregg L. Semenza, Silvia Montaner, and Akrit Sodhi: VEGF Secreted by Hypoxic Müller Cells Induces MMP-2 Expression and Activity in Endothelial Cells to Promote Retinal Neovascularization in Proliferative Diabetic Retinopathy. Diabetes 2013, 62:3863-73.

[158] Silke Becker HW, Aaron B Simmons, Thipparat Suwanmanee, Gregory J Stoddard, Tal Kafri, M Elizabeth Hartnett: Targeted Knockdown of Overexpressed VEGFA or VEGF164 in Muller Cells Maintains Retinal Function by Triggering Different Signaling Mechanisms. Sci Rep 2018, 8:2003.

[159] Michael T Dellinger RAB: Phosphorylation of Akt and ERK1/2 Is Required for VEGF-A/VEGFR2-Induced Proliferation and Migration of Lymphatic Endothelium. PLoS One 2011, 6:e28947.

[160] Jr RR: ERK1/2 MAP Kinases: Structure, Function, and Regulation. Pharmacol Res 2012, 66:105-43.

[161] Xiaofeng Ye GX, Qing Chang, Jiaweng Fan, Zhongcui Sun, Yaowu Qin, Alice C Jiang: ERK1/2 Signaling Pathways Involved in VEGF Release in Diabetic Rat Retina. IOVS 2010, 51:5226-33.

[162] E. MINET GM, D.MOTTET,M.RAES, and C. MICHIELS: Transduction Pathways Involved In Hypoxia-Inducible Factor-1 Phosphorylation and Activation. FREE RADICAL BIO MED 2001, 31:847-55.

[163] Darren E. Richard EB, Emmanuel Gothie, Danie` le Roux, and Jacques Pouysse´gur: p42/p44 Mitogen-Activated Protein Kinases Phosphorylate Hypoxia-Inducible Factor 1A (HIF-1a) and Enhance the Transcriptional Activity of HIF-1. J Biol Chem 1999, 274:32631-7.

[164] E Berra GP, J Pouysségur: MAP Kinases and Hypoxia in The Control of VEGF Expression. Cancer Metastasis Rev 2000, 19:139-45.

[165] M Lin YC, J Jin, Y Hu, K K Zhou, M Zhu, Y-Z Le, J Ge, R S Johnson, J-X Ma: Ischaemia-Induced Retinal Neovascularisation and Diabetic Retinopathy in Mice with Conditional Knockout of Hypoxia-Inducible Factor-1 in Retinal Muller Cells. Diabetologia 2011, 54:1554-66.

[166] Thiersch M, Lange C, Joly S, Heynen S, Le YZ, Samardzija M, Grimm C: Retinal Neuroprotection by Hypoxic Preconditioning Is Independent of Hypoxia-Inducible Factor-1 Alpha Expression in Photoreceptors. Eur J Neurosci 2009, 29:2291-302.

[167] Scott A, Fruttiger M: Oxygen-Induced Retinopathy: A Model for Vascular Pathology in the Retina. Eye (Lond) 2010, 24:416-21.

[168] Das A, McGuire PG: Retinal and Choroidal Angiogenesis: Pathophysiology and Strategies for Inhibition. Prog Retin Eye Res 2003, 22:721-48.

[169] Yang C, Xiong W, Qiu Q, Tahiri H, Superstein R, Carret AS, Sapieha P, Hardy P: Anti-Proliferative and Anti-Tumour Effects of Lymphocyte-Derived Microparticles Are Neither Species- Nor Tumour-Type Specific. J Extracell Vesicles 2014, 3.

# Annexe I

Project II:

**Temozolomide-Loaded Lymphocytic Microparticles to Treat Glioblastoma Stem-Like Cells**

This annexe includes:

1) Presentation of the project and the work has been done by the author.

To further explore the possibilities of LMPs as a potent angiogenesis-inhibitor, we utilized an angiogenesis-characterized model: glioblastoma stem cell model.

## 1. INTRODUCTION

Glioblastoma multiforme (GBM), also termed glioblastoma, is the most malignant form of tumor in the central nervous system [1]. The overall survival rate of postdiagnosis patients is less than 15 months despite receiving the full regimens [1].

Cancer stem cell theory has been popular for years. Cancer stem-like cells are a small population of undifferentiated cancer cells characterized by unlimited self-renewal capacity and potent differentiation properties [2]. These cells not only possess stemness characteristics but also contain normal stem cell functions, such as active DNA damage repair, anti-apoptotic pathways, and expression of multi-drug transporters on the membrane [2]. Moreover, they play an essential role in giving rise to malignancies, driving infinite tumor growth, inducing drug resistance, and exerting the pro-angiogenic and pro-metastatic properties [2]. Cancer stem-like cells have been successfully isolated from human GBM tissues [3], and human cell lines [4] via using the stem cell marker CD133, also termed prominin-1 [5]. Bao et al., [6] demonstrated GBM stem-like cells (GSCs) express a significantly higher level of vascular endothelial growth factor (VEGF), which promotes endothelial cell migration and tube formation. Anti-VEGF treatment with Bevacizumab strongly reduces vascular leakage and vascular density in GBM models; however, it increases tumor cell invasion [7]. These data suggest that the angiogenesis mechanisms of cancer stem-like cells might differ from angiogenesis-induced by differentiated cells. Additionally, there is a need for investigating therapeutic approaches with superior efficiency targeting angiogenesis-induced by cancer stem-like cells.

Temozolomide (TMZ) is the first-line chemotherapy for GBM treatment approved by the FDA in early 2005 [8]. TMZ elicits cytotoxicity via the addition of methyl group to guanine site of $O^6$ and $N^7$ and adenosine site of $N^3$ during DNA replication [9]. This process causes the formation of mismatched DNA pairs, which results in DNA single- or double-strand break and eventually cell apoptosis [8]. However, the increased incidence of TMZ resistance underlies one of the major obstacles for GBM treatment [10]. Studies reported two primary TMZ resistant mechanisms: one is the $O^6$-methylguanine-DNA methyltransferase (MGMT)-dependent mechanism; the other is MGMT-independent mechanisms [10]. Increasing bodies of evidence showed that cancer stem-like cells in GBM play a crucial role in MGMT-independent TMZ resistance [11, 12]. Moreover, studies demonstrated that GSCs possess stronger resistance to TMZ as compared with differentiated GBM cancer cells [13-15].

Extracellular vesicles (EVs) are lipid bilayer-wrapped vesicles of different sizes that are released from cells [16]. EVs has received considerable attention not only due to their intercellular communicator characteristic but also a promising alternative to conventional approaches as drug delivery systems with certain advantages: (1) bypasses phagocytosis and immune activation due to the endogenous inert characteristic; (2) stability in the circulation; (3) protect internal contents from exogeneous interruption due to their natural properties; (4) greater delivery efficiency and less off-target effects; (5) capability to cross certain physical barriers, such as the blood-brain barrier (BBB) [17, 18]. Taking these facilities into account, EVs has emerged as a promising carrier for drug delivery to treat brain diseases.

Microparticles, also termed microvesicles, are a subgroup of EVs originated from outward budding of the plasma membrane [16]. Lymphocytic microparticles (LMPs) are small membrane vesicles generated from apoptotic human CEM T lymphocytes [19]. Previously we have reported that LMPs possess strong anti-tumor and anti-angiogenic effects in different models [20-22]. Therefore, we investigated whether LMPs exert cytotoxicity to GSCs, whether encapsulation of chemotherapy

TMZ within LMPs could increase the sensitivity of GSCs to TMZ, and whether these outcomes are associated with angiogenesis inhibitory effect.

## 2. MATERIALS AND METHODS

### 2.1 U87 cancer stem-like cell culture

The human U87 cell line was purchased from American Type Culture Collection (ATCC). U87 cells were cultured for three days in the specific neural stem cell medium: Dulbecco's Modified Eagle Medium/F12 (DMEM/F12, Gibco) supplemented with recombinant human epidermal growth factor (EGF, 20 ng/mL, Peprotech), recombinant human fibroblast growth factor-basic (bFGF, 20 ng/mL, Peprotech), B27 with insulin (1:50, Thermo Scientific), recombinant human leukemia inhibiting factor (LIF, 1000 U/mL, Peprotech), and 1% of penicillin/streptomycin, before processing to fluorescence-activated cell sorting (FACS).

### 2.2 U87 cancer stem-like cells sorted by FACS

For U87 stem-like cell sorting. Briefly, U87 cells were cultured in the neural stem cell medium as abovementioned for three days to expand cancer stem-like cells. After three days of incubation, tumorspheres were collected and centrifuged at the speed of 300 g for 5 min to precipitate the tumorspheres. Supernatant was aspirated, and the pellet was dissociated by Accutase. FACS buffer (phosphate-buffered saline (PBS) + 1% fetal bovine serum (FBS)) was added to the cells. Samples were centrifuged and resuspended in 45 μL of FACS buffer, followed by incubation with 5 μL of AlexaFluor 488-conjugated anti-CD133 monoclonal antibody (1:10, R&D systems) on ice for 20 min and protection from light. After incubation, samples were centrifuged and resuspended in 200 μL FACS buffer per sample. U87 cells without staining were used as a negative control. Cells sorted

positive with CD133 antibody were cultured in the neural stem cell medium. While cells sorted negative with CD133 antibody were cultured in DMEM supplemented with 10% FBS. Images of the tumorspheres were taken daily by a Zeiss microscope. The diameter of the tumorspheres was also measured, and the width of the tumorspheres less than 200 μm were collected for the following experiments.

**2.3 Immunofluorescent staining**

Immunofluorescent staining was used to confirm the sorted-U87 cells cultured in the neural stem cell medium were GSCs. Tumorspheres were fixed with 4% PFA, blocked 1 h at room temperature with medium containing 5% normal goat serum (NGS), 2% bovine serum albumin (BSA), 0.3% TritonX-100/PBS, and 0.3M Glycine. Primary and secondary antibodies were diluted in PBS contained 0.3% TritonX-100/PBS and 2% BSA. Tumorspheres were incubated at 4℃ overnight with a polyclonal antibody against CD133 (1:500, rabbit, Abcam) and a polyclonal antibody against GFAP (1:200, rabbit, Abcam). After primary incubation, tumorspheres were incubated for 2 h at room temperature with goat-anti-rabbit AlexaFluor 488 (1:1000, Life Technologies) and goat-anti-rabbit AlexaFluor 594 (1:1000, Life Technologies). The cell nucleus was identified by DAPI (1:5000) staining. Images (3 images/condition) were taken by the DMi8 Leica microscope (Concord).

For differentiated U87 cells, they were fixed with 4% PFA, blocked 1 h at room temperature with medium containing 5% NGS, 2% BSA, 0.3% TritonX-100/PBS, and 0.3M Glycine. Primary and secondary antibodies were diluted in PBS that contained 0.3% TritonX-100/PBS and 2% BSA. Cells were incubated for 2 h at room temperature with a polyclonal antibody against CD133 (1:500, rabbit, Abcam) and a polyclonal antibody against GFAP (1:200, rabbit, Abcam). After primary incubation, cells were incubated for 2 h at room temperature with goat-anti-rabbit AlexaFluor 488 (1:1000, Life Technologies) and goat-anti-rabbit AlexaFluor 594 (1:1000, Life Technologies).

DAPI (1:5000) was used to identify the cell nucleus. Images (3 images/condition) were taken by the DMi8 Leica microscope (Concord).

**2.4 Cell viability assay**

Unsorted U87, CD133 positive U87, and CD133 negative U87 cells were treated with different concentrations of LMPs (5, 10, 20, 30, 50, and 100 μg/mL). The cell viability of the cells abovementioned was determined by MTT assay. The MTT working solution was prepared by adding MTT powder (5 mg/mL, Sigma Aldrich) in PBS, followed by dissolving the MTT solution in the water bath of 60℃ for 1 min. The dissolved MTT solution was filtered with a 0.22 μm filter (Sigma Aldrich) under the hood, covered with an aluminum foil, and stored at -20℃ for long-term usage.

Briefly, unsorted U87 cells, CD133 positive U87 cells, and CD133 negative U87 cells (1.5 x $10^5$ cells/mL) were cultured in the 24-well plate overnight. Cells were treated with different concentrations of LMPs (5, 10, 20, 30, 50, and 100 μg/mL) for 24, 48, and 72 h, followed by incubation with MTT working solution for 3 h in the humidified incubator under standard conditions (37℃, 5% $CO_2$, 21% $O_2$).

For CD133 positive U87 cells: After 3 h of incubation, the plate was centrifuged at 500 g for 5 min to precipitate the spheres. The MTT working solution was carefully removed. Formazan was dissolved by adding 150 μL of acidified isopropanol solvent (1 mL 1N HCl in 20 mL isopropanol) for 15 min at 37℃, followed by transferring 100 μL of the dissolvent to a 96-well black plate for reading (absorbance: 560 nm, reference: 650 nm; Clariostar).

For CD133 negative U87 and unsorted U87 cells: The cultured medium was discarded, followed by adding 150 μL of acidified isopropanol solvent (1 mL 1N HCl in 20 mL isopropanol) to each

well for 15 min at 37°C to dissolve the formazan. 100 µL of the dissolvent was transferred to a 96-well black plate for reading (absorbance: 560 nm, reference: 650 nm; Clariostar).

### 2.5 Real-time cell apoptosis and necrosis

The cell apoptosis and necrosis of CD133 positive U87 cells treated with different concentrations of LMPs were determined by RealTime Glio Annexin and Necrosis assay (Promega). Briefly, CD133 positive U87 cells (5 x $10^4$ cells/mL) were seeded in the 96-well plate with 100 µL of neural stem cell medium. Different concentrations of LMPs (5, 10, 20, 30, 50, 100 µg/mL) were added to each well for 24, 48, and 72 h. Detection reagent was prepared according to the manufacture's protocol, and 100 µL of detection reagent was added to each well. The plate was read (Clariostar) at 1, 24, 48, and 72 h, respectively.

## 3. RESULTS

### Isolation of Glioblastoma Stem-Like Cells from U87 Cell Line

Our previous results indicated that LMPs possess potent anti-tumor effects on various types of cancer cells, such as retinoblastoma [23], Lewis lung carcinoma [21], breast cancer [24], and lung cancer cells [24]. Therefore, we investigated whether LMPs exerted a cytotoxic effect on GSCs.

Cancer stem-like cells were isolated from the human U87 cell line. U87 cells were cultured in neural stem cell medium for three days to expand the population of stem-like cells. Images taken by the Zeiss microscopy indicated that the cells cultured in the neural stem cell medium instead of regular DMEM supplemented with 10% FBS, grew into a sphere-like morphology after two days (Annexe Figure 1A). On day 3, cells were collected for stem-like cell sorting via FACS. The GSCs

were identified by the CD133 antibody, a neural stem cell marker that has been used to identify cancer stem-like cells in GBM [3]. FACS results demonstrated that more than 95% of cells were CD133 positive, and less than 5% of cells were CD133 negative (Annexe Figure 1B). Both CD133 positive and negative cells were collected for the following experiments.

According to the study conducted by Sheila et al,. [3], GSCs only display the expression CD133 and lack of glial fibrillary acidic protein (GFAP) expression, which is a character of differentiated glial cells. To confirm that the sorted CD133 positive U87 cells did not differentiate during the following culture, we used immunofluorescent staining to identify the purity of the cells. Immunofluorescent staining images indicated that CD133 positive U87 cells were grown into sphere-like morphology and expressed CD133 exclusively; the expression of GFAP was not detected in CD133 positive U87 cells (Annexe Figure 1C). In contrast, CD133 negative U87 cells did not grow into sphere-like morphology; they were attached to the culture plate and grew into spindle-shaped (Annexe Figure 1D).

**A.**

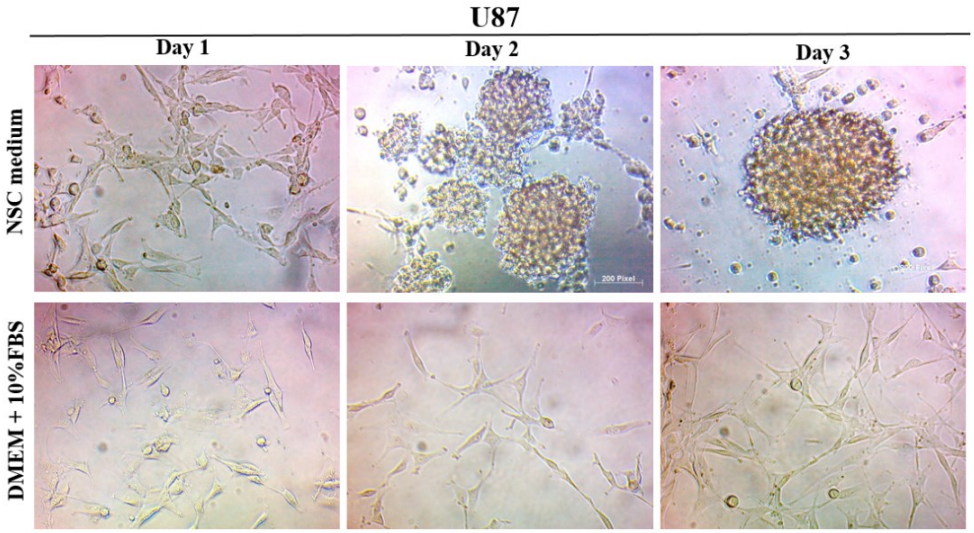

**B.**

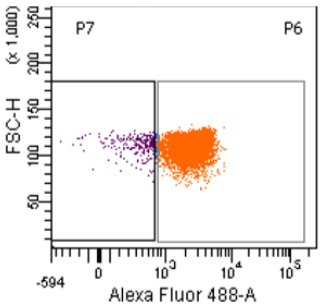


Tube: sample1

| Population | #Events | %Parent | %Total |
|---|---|---|---|
| All Events | 10,000 | #### | 100.0 |
| P1 | 249 | 2.5 | 2.5 |
| P3 | 7,288 | 72.9 | 72.9 |
| P4 | 7,212 | 99.0 | 72.1 |
| P5 | 7,108 | 98.6 | 71.1 |
| P6 | 6,806 | 95.8 | 68.1 |
| P7 | 266 | 3.7 | 2.7 |

**C.**

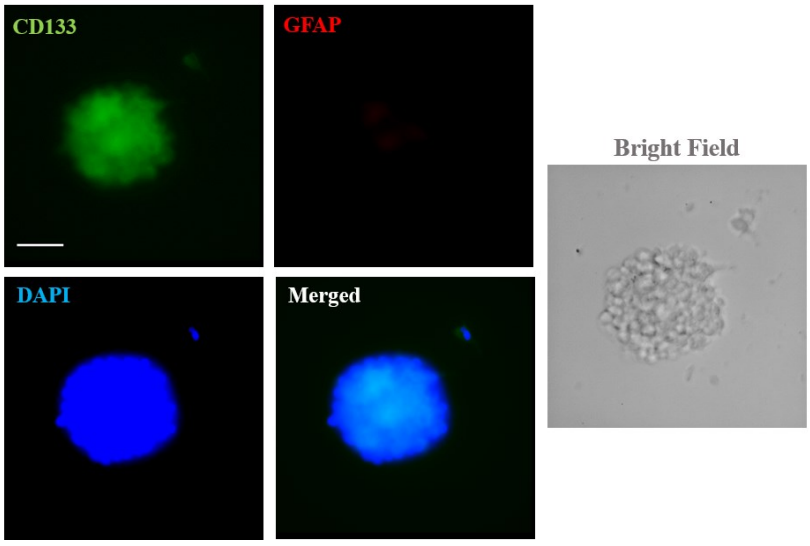


**D.**

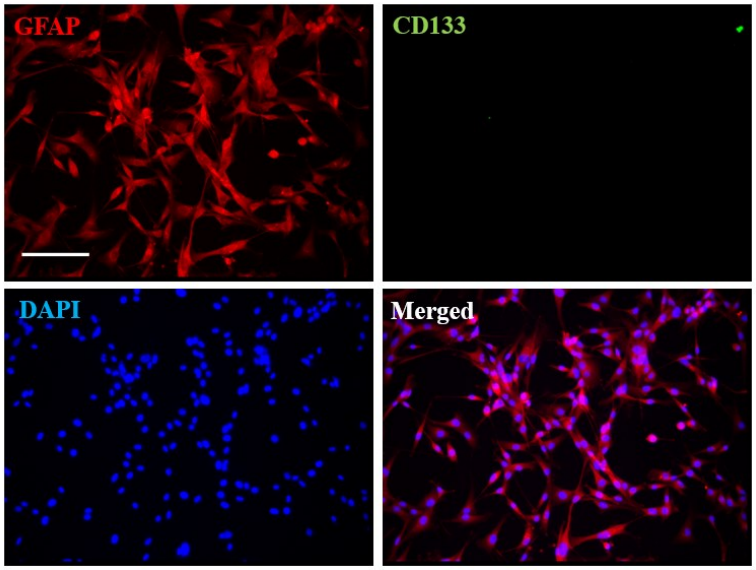

**Annexe Figure 1. Isolation of glioblastoma stem-like cells from U87 cell line. A.** Representative images of U87 cells cultured in neural stem cell medium or regular DMEM supplemented with 10% FBS. **B.** Percentage of CD133 positive and negative U87 cells sorted by FACS analysis. **C.** Representative immunofluorescent staining images of CD133 positive U87 cells. Cells were stained with CD133 (green), GFAP (red), and DAPI (blue). **D.** Representative immunofluorescent staining images of CD133 negative U87 cells. Cells were stained with CD133 (green), GFAP (red), and DAPI (blue). Original magnification: x 200. Scale bar: 100 μm.

**LMPs Inhibit CD133 Positive U87 Cell Viability Dose-Dependently and Time-Dependently**

To investigate whether LMPs induced a cytotoxic effect on CD133 positive U87 cells, we treated the cells with different concentrations of LMPs (5, 10, 20, and 30 μg/mL) for 24, 48, and 72 h. The results of the MTT assay demonstrated that LMPs inhibited CD133 positive U87 cell viability dose-dependently and time-dependently (Annexe Figure 2A-C). Previously, we have observed that LMPs exert the anti-tumor effect within a range of concentration (unpublished data). Above the maximum level, LMPs increase cell viability of cancer cells instead of reducing it (unpublished data). Therefore, we questioned whether a higher concentration of LMPs increased the cell viability of cancer stem cells in U87. CD133 positive U87 cells were incubated with higher concentrations of LMPs (50 and 100 μg/mL) for 72 h. However, results indicated that LMPs induced an even more potent cytotoxic effect on CD133 positive U87 cells as compared with the lower doses (Annexe Figure 2D). The morphologies of CD133 positive U87 cells were captured at 72 h after incubating with different concentrations of LMPs (Annexe Figure 2E). As indicated in the Annexe Figure 2E, CD133 positive U87 cells grew into large spheroid in control (CTL). However, the size of the spheroids was smaller upon LMPs treatment. When the concentration of LMPs reached 100 μg/mL, there were barely spheroid detectable under the microscope (Annexe Figure 2E)

**A.**

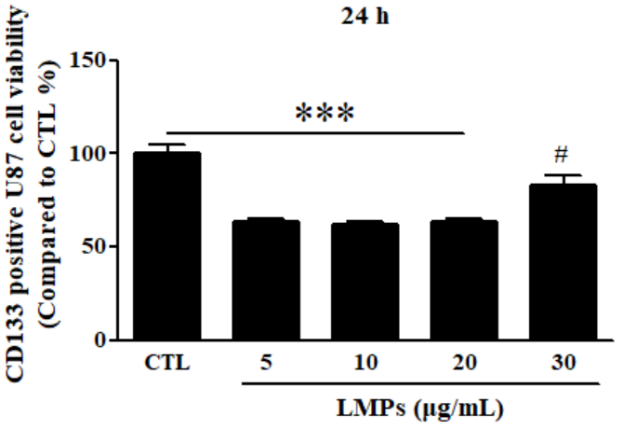
24 h
CD133 positive U87 cell viability
(Compared to CTL %)
150
100
50
0
***
#
CTL
5
10
20
30
LMPs (μg/mL)

**B.**

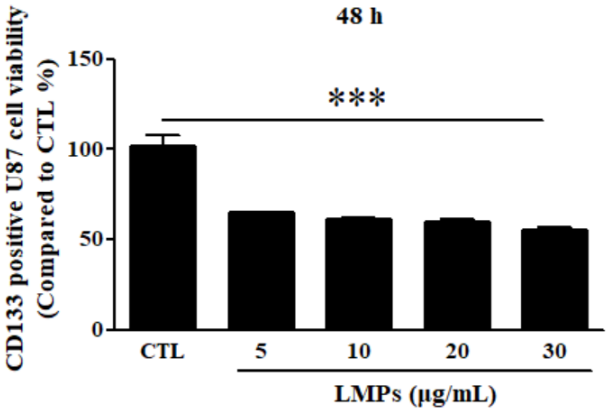
48 h
CD133 positive U87 cell viability
(Compared to CTL %)
150
100
50
0
***
CTL
5
10
20
30
LMPs (μg/mL)

**C.**

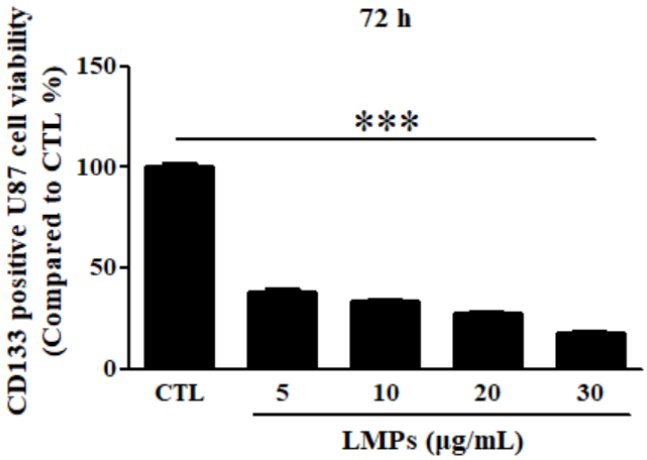
72 h
CD133 positive U87 cell viability
(Compared to CTL %)
150
100
50
0
***
CTL
5
10
20
30
LMPs (μg/mL)

**D.**

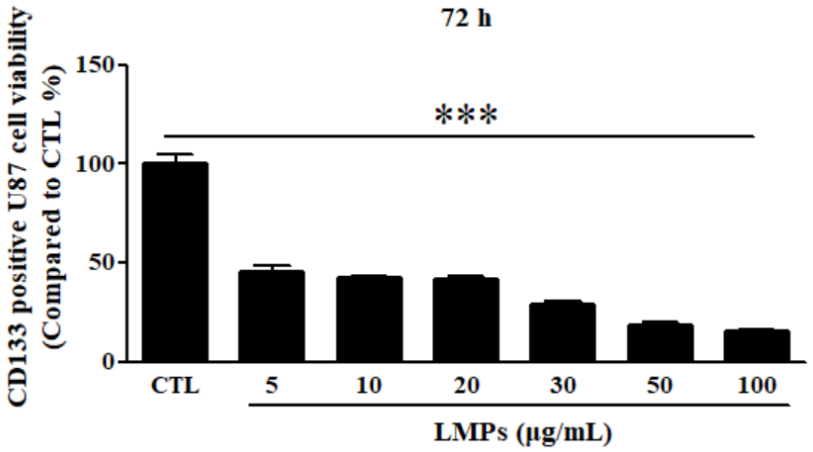


**E.**

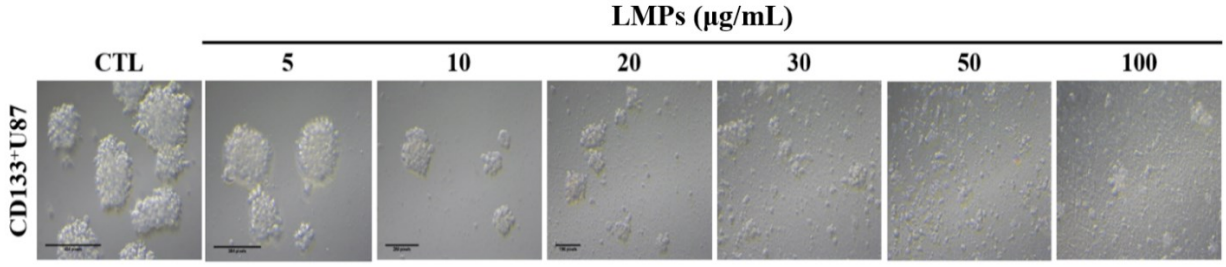


**Annexe Figure 2. LMPs inhibit CD133 positive U87 cell viability dose-dependently and time-dependently. A-C: Cell viability of CD133 positive U87 cell treated with different concentrations of LMPs (5, 10, 20, 30 μg/mL) at 24, 48, and 72 h. A.** Cell viability of CD133 positive U87 cells at 24 h. #$P < 0.01$, ***$P < 0.001$ vs. CTL. **B.** Cell viability of CD133 positive U87 cells at 48 h. ***$P < 0.001$ vs. CTL. **C.** Cell viability of CD133 positive U87 cells at 72 h. ***$P < 0.001$ vs. CTL. Cell growths were all presented as the percentage of CTL. **D.** CD133 positive U87 cells treated with different concentrations of LMPs (5, 10, 20, 30, 50, 100 μg/mL) for 72 h. Cell growth was presented as the percentage of CTL. ***$P < 0.001$ vs. CTL. **E.** Representative images of CD133 positive U87 cells at 72 h after incubating with different concentrations of LMPs. Original magnification x 200.

**LMPs Induce Cell Death of CD133 Positive U87 Cells**

The observed reduction of cell growth in CD133 positive U87 cells could be caused by decreased cell proliferation or increased cell death (apoptosis or necrosis). To determine whether LMPs induced cell apoptosis or necrosis in CD133 positive U87 cells, we used real-time cell apoptosis/necrosis kit to determine the cell death of CD133 positive U87 treated with different concentrations of LMPs. Results demonstrated that low concentrations of LMPs (5, 10, 20, and 30 μg/mL) induced significant cell apoptosis in CD133 positive U87 cells (Annexe Figure 3A-C). Instead of inducing cell apoptosis, high concentrations of LMPs (50 and 100 μg/mL) significantly induced cell necrosis (Annexe Figure 3D-F).

**A.**

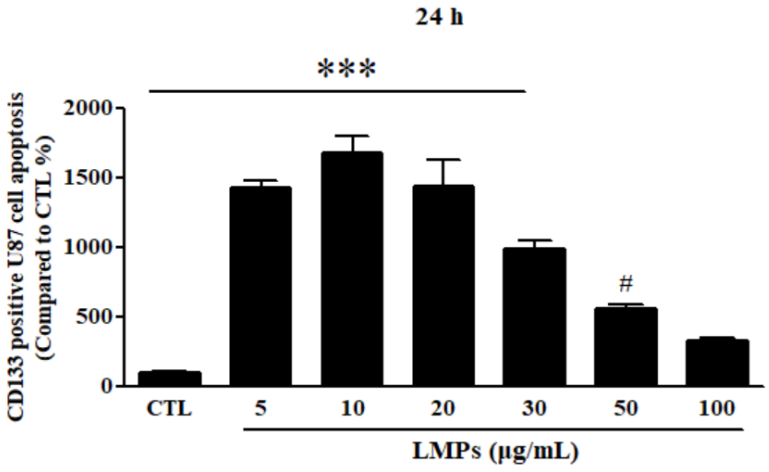

**B.**

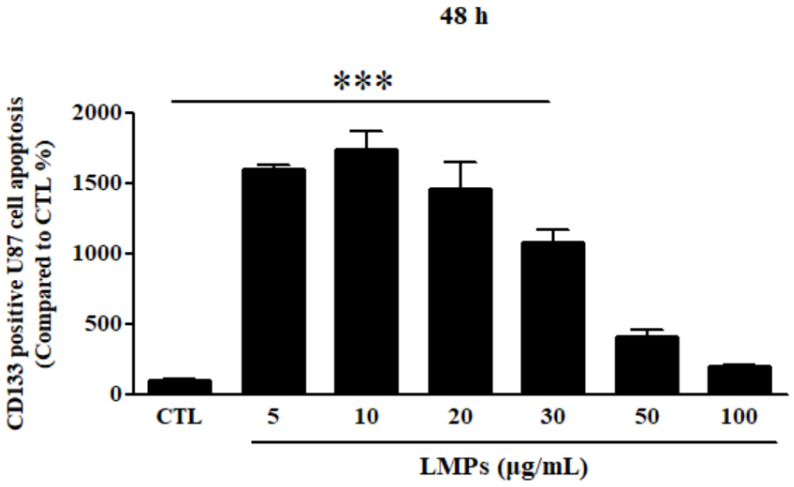
48 h
***
CD133 positive U87 cell apoptosis
(Compared to CTL %)
2000
1500
1000
500
0
CTL
5
10
20
30
50
100
LMPs (μg/mL)

**C.**

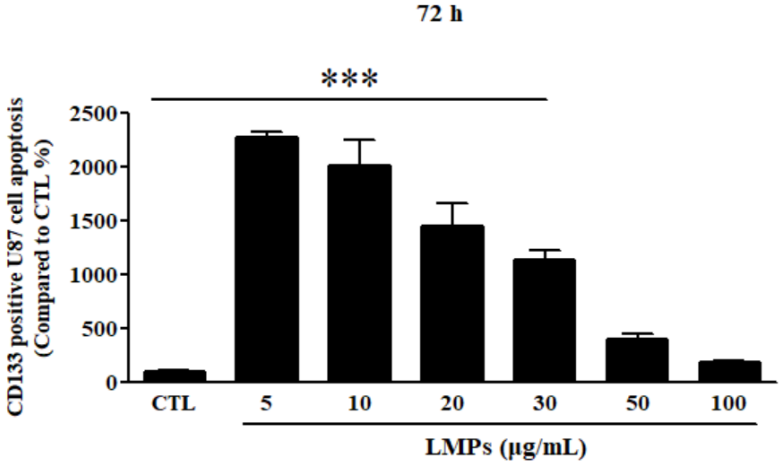
72 h
***
CD133 positive U87 cell apoptosis
(Compared to CTL %)
2500
2000
1500
1000
500
0
CTL
5
10
20
30
50
100
LMPs (μg/mL)

**D.**

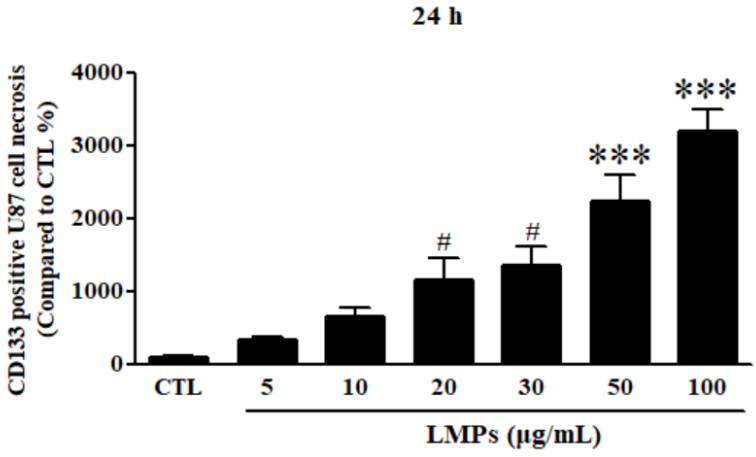
24 h
CD133 positive U87 cell necrosis
(Compared to CTL %)
4000
3000
2000
1000
0
#
#
***
***
CTL
5
10
20
30
50
100
LMPs (μg/mL)

**E.**

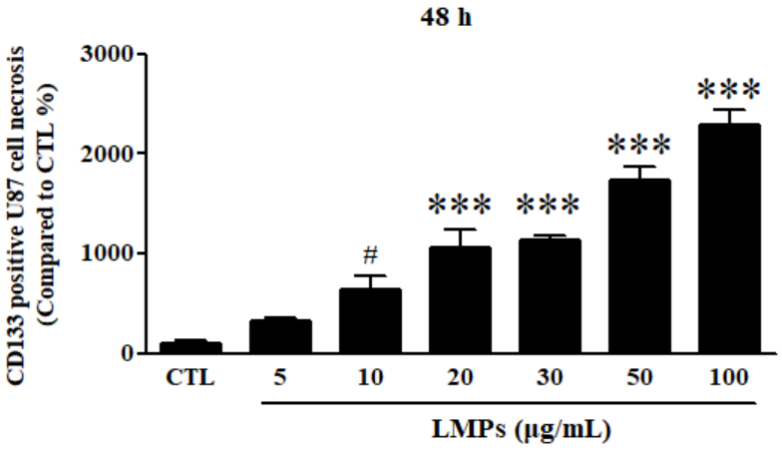


**F.**

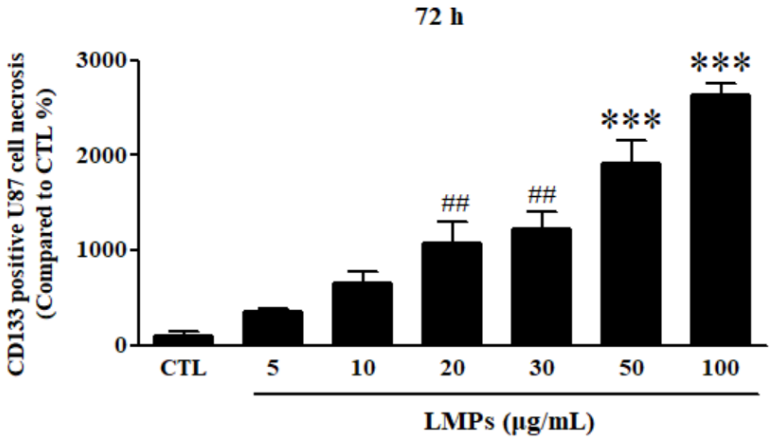


**Annexe Figure 3. LMPs induce cell death of CD133 positive U87 Cells. A-C: Cell apoptosis of CD133 positive U87 cells treated with different concentrations of LMPs (5, 10, 20, 30, 50, and 100 μg/mL) at 24, 48, and 72 h. D-F: Cell necrosis of CD133 positive U87 cells treated with different concentrations of LMPs (5, 10, 20, 30, 50, and 100 μg/mL) at 24, 48, and 72 h.** **A.** Cell apoptosis of CD133 positive U87 cells at 24 h. Cell apoptosis was presented as the percentage of CTL. #$P < 0.05$, ***$P < 0.001$ vs. CTL. **B.** Cell apoptosis of CD133 positive U87 cells at 48 h. Cell apoptosis was presented as the percentage of CTL. ***$P < 0.001$ vs. CTL. **C.** Cell apoptosis of CD133 positive U87 cells at 72 h. Cell apoptosis was presented as the percentage of CTL. ***$P < 0.001$ vs. CTL. **D.** Cell necrosis of CD133 positive U87 cells at 24 h. Cell necrosis was presented as the percentage of CTL. #$P < 0.05$, ***$P < 0.001$ vs. CTL. **E.** Cell necrosis of CD133 positive U87 cells at 48 h. Cell necrosis was presented as the percentage of CTL. #$P < 0.05$, ***$P < 0.001$ vs. CTL. **F.** Cell necrosis of CD133 positive U87 cells at 72 h. Cell necrosis was presented as the percentage of CTL. ##$P < 0.01$, ***$P < 0.001$ vs. CTL.

**No Difference between CD133 Positive or Negative U87 Cells upon LMPs Treatment**

Studies have demonstrated that cancer stem cells in GBM behave differently as compared with differentiated GBM cells [25]. Furthermore, increasing bodies of evidence have reported that cancer stem cells in GBM are much more resistant to TMZ compared to differentiated GBM cancer cells [13, 14]. Therefore, we questioned whether CD133 negative U87 cells responded differently upon LMPs treatment.

CD133 negative U87 cells were collected from FACS cell sorting and cultured in regular DMEM supplemented with 10% FBS. Different concentrations of LMPs (5, 10, 20, 30, 50, and 100 μg/mL) were used to treat CD133 negative U87 cells for 72 h. Cell growth was determined by MTT assay. Results showed that cells were much more sensitive in response to LMPs, as evidenced by the lowest concentration of LMPs (5 μg/mL) reduced by more than 70% of cell growth (Annexe Figure 4A). Similar to the response manner of CD133 positive U87 cells, LMPs dose-dependently suppressed CD133 negative U87 cell growth (Annexe Figure 4A). The morphologies of CD133 negative U87 cells were captured at 72 h after treating with different concentrations of LMPs (5, 10, 20, 30, 50, and 100 μg/mL) (Annexe Figure 4B). As shown in Annexe Figure 4B, CD133 negative U87 cells in CTL were attached to the culture plate and grew into a spindle shape. Upon LMPs treatment, cells were less well-organized and grew sparsely.

To gain a better insight into the effect of LMPs, we mimic the *in vivo* condition, which is the mixture of cancer stem cells and differentiated cancer cells [1]. We cultured the unsorted U87 cells in the NSC medium, which contained both cancer stem cells and differentiated cells of U87. Cell growth was measured by MTT assay. The results revealed that LMPs reduced cell growth dose-dependently (Annexe Figure 4C). The morphologies of U87 treated with different concentrations of LMPs (5, 10, 20, 30, 50, and 100 μg/mL) were captured at 72 h (Annexe Figure 4D). As shown in the Annexe Figure 4D, the unsorted U87 cells, which were cultured in NSC medium, grew into

a sphere-like shape in the center surrounded by spindle shape cells in the peripheral in CTL group. However, there were significantly less sphere-like cells that grew in the center upon LMPs treatment, even at the lowest concentration (5 µg/mL). As the concentration of LMPs increased, U87 cells that grew into spindle shape were less well-organized. When the concentration reached 100 µg/mL, cell debris was detectable under the microscope (Annexe Figure 4D).

**A.**

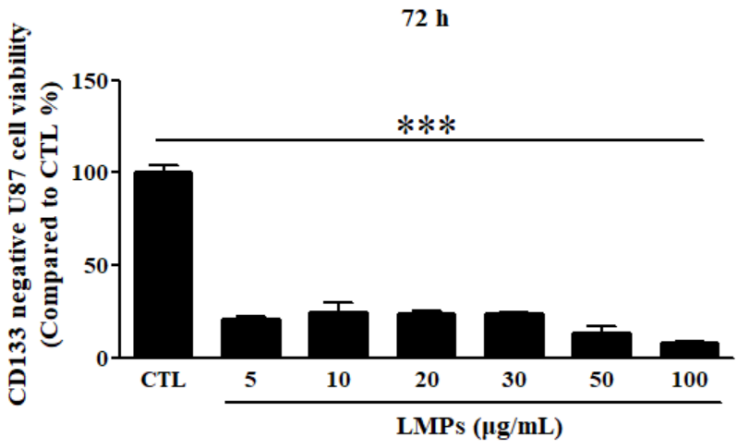


**B.**

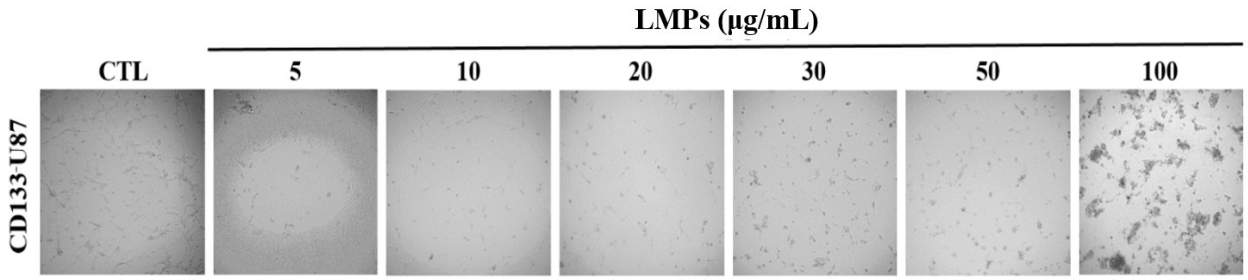

**C.**

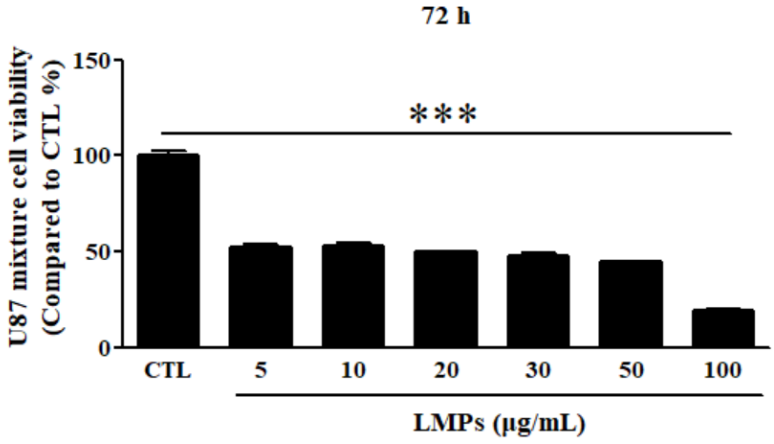


**D.**

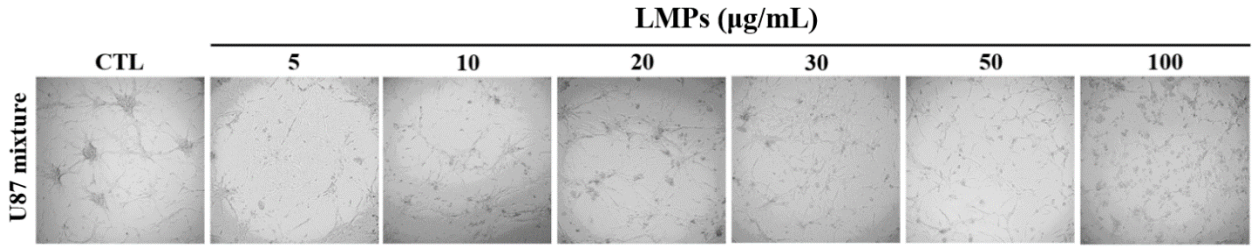


**Annexe Figure 4. No difference between CD133 positive or negative U87 cells upon LMPs treatment. A.** Cell growth of CD133 negative U87 cells incubated with indicated concentrations of LMPs (5, 10, 20, 30, 50, and 100 μg/mL) at 72 h. Cell growth was presented as the percentage of CTL. ***$P < 0.001$ vs. CTL. **B.** Representative images of different concentrations of LMPs-treated CD133 negative U87 cells. **C.** Cell growth of unsorted U87 cells cultured in neural stem cell medium (a mixture of CD133 positive and CD133 negative U87 cells) was determined by MTT assay. Cells were incubated with different concentrations of LMPs (5, 10, 20, 30, 50, and 100 μg/mL) for 72 h. Cell growth was presented as the percentage of CTL. ***$P < 0.001$ vs. CTL. **D.** Representative images of unsorted U87 cells (cultured in NSC medium) treated with different concentrations of LMPs (5, 10, 20, 30, 50, and 100 μg/mL). Original magnification x 200.

## 4. DISCUSSION AND CONCLUSION

Our present study provides evidence of LMPs as a potent inhibitor for glioblastoma stem-like cells.

A small population of cells (< 1%) within the brain possesses the capacity of self-renewal and property of differentiation, which is known as stem cells [26]. However, the yield of cancer stem-like cells in GBM has a significant difference, ranging from 0.3% to 25.1% [3, 4]. The difference may be caused by the isolation techniques as well as the diversity of the isolation samples, in which some use human GBM cell line [4]; others use human GBM tissues [3] to isolate cancer stem-like cells. Here, we showed that after expanding human GBM cell line U87 cells in the NSC medium for three days before isolation, we were able to collect more than 95% of CD133 positive U87 cancer stem-like cells (Annexe Figure 1B). Furthermore, we confirmed the purity of CD133 positive U87 cells by immunofluorescent staining, in which the cells were non-adherent, grew into sphere-like morphology, and lacked of GFAP expression (a cell maker for differentiated glial cells) (Annexe Figure 1C). Our results are in line with Yu et al [4] findings.

LMPs possess potent anti-tumor effects on Lewis lung carcinoma and retinoblastoma cells [21, 23]. In the Lewis lung carcinoma model [21], results revealed that LMPs dose-dependently suppress carcinoma cell viability, and LMPs (20 μg/mL) reduce cell viability by 50% [21]. Here, we showed that LMPs (5 μg/mL) reduced cell growth of different subtypes of U87 cells by 50% (Annexe Figure 2 and Figure 4). The difference response sensitivity upon LMPs treatment may be attributed to the diversity of tumor-types and differences of the incubation time, where Lewis lung carcinoma cells were incubated only for 24 h, while U87 cells were stimulated with LMPs for 72 h. Furthermore, we showed that LMPs at the concentration of 5 μg/mL increased 149 fold of cell apoptosis of CD133 positive U87 cells after 24 h of incubation, and more than 200 fold at 72 h as compared with control (Annexe Figure 3). However, we did not observe the similar effects of LMPs

on Lewis lung carcinoma cells or retinoblastoma cells at the same concentration, in which there is no significance of cell apoptosis [21, 23]. These results demonstrated that human U87 cells are much sensitive to LMPs as compared with other cancer cell types, and this might be attributed to the aggressiveness of GBM cells.

In our previous study, we have shown that the anti-proliferation effects of LMPs on tumor cells are stimulus-independent as well as cell type-independent [24]. LMPs significantly reduced cell proliferation of human breast cancer, cervical cancer, lung carcinoma, neuroblastoma cells, as well as mouse neuroblastoma cells in a dose-dependent manner [24]. Moreover, the mechanisms of anti-proliferative effects on tumor cells exerted by LMPs were studied. We demonstrated that LMPs induce cell cycle arrest in the $G_0/G_1$ phase, whereas the percentage of the cells in the $G_2$/M phase drastically declined [24]. Although we showed that LMPs have cytotoxic effects on different types of tumor cells, however, LMPs have no detrimental impact on neural cells [24]. These data suggested that LMPs are only toxic to malignant cells.

Studies have shown that CD133 positive and negative cells from GBM possess diverse growing patterns and molecular profiles [25]. In addition, Fu et al,. [14] demonstrated that differentiated GBM cells are much more sensitive to TMZ chemotherapy than cancer stem cells. These results provide evidence that cancer stem-like cells and differentiated cancer cells in GBM behave differently, and cancer stem cells in GBM may underlie the center of chemotherapy resistance [2]. However, our results were in contrast to others. Both CD133 positive and negative U87 cells responded to LMPs, in which LMPs inhibited cell growth dose-dependently (Annexe Figure 2 and Figure 4). However, CD133 negative U87 cells were more sensitive than CD133 positive U87 upon LMPs treatment.

In conclusion, our current data suggest that LMPs are potent anti-tumor reagent treating GBM, as supported by (1) LMPs inhibited cell viability of differentiated cells and stem-like cells of U87

in a dose-dependent fashion; (2) LMPs at low concentration induced significant cell apoptosis of cancer stem cells, and at high concentration induced significant cell necrosis of cancer stem cell in human U87. Further studies are needed to investigate whether LMPs increase the sensitivity of cancer stem cells to TMZ chemotherapy.

**Bibliography**

[1] Agnihotri S, Burrell KE, Wolf A, Jalali S, Hawkins C, Rutka JT, Zadeh G: Glioblastoma, a brief review of history, molecular genetics, animal models and novel therapeutic strategies. Arch Immunol Ther Exp (Warsz) 2013, 61:25-41.

[2] Lathia JD: Cancer stem cells in glioblastoma. GENES & DEVELOPMENT 2015, 29:1203-17.

[3] Sheila K. Singh IDC, Mizuhiko Terasaki, Victoria E. Bonn, Cynthia Hawkins, Jeremy Squire, and Peter B. Dirks: Identification of a Cancer Stem Cell in Human Brain Tumors. Cancer Reaserch 2003, 63:5821-8.

[4] Yu SC, Ping YF, Yi L, Zhou ZH, Chen JH, Yao XH, Gao L, Wang JM, Bian XW: Isolation and characterization of cancer stem cells from a human glioblastoma cell line U87. Cancer Lett 2008, 265:124-34.

[5] Ahmed SI, Javed G, Laghari AA, Bareeqa SB, Farrukh S, Zahid S, Samar SS, Aziz K: CD133 Expression in Glioblastoma Multiforme: A Literature Review. Cureus 2018, 10:e3439.

[6] Bao S, Wu Q, Sathornsumetee S, Hao Y, Li Z, Hjelmeland AB, Shi Q, McLendon RE, Bigner DD, Rich JN: Stem Cell-Like Glioma Cells Promote Tumor Angiogenesis Through Vascular Endothelial Growth Factor. Cancer Res 2006, 66:7843-8.

[7] Keunen O, Johansson M, Oudin A, Sanzey M, Rahim SA, Fack F, Thorsen F, Taxt T, Bartos M, Jirik R, Miletic H, Wang J, Stieber D, Stuhr L, Moen I, Rygh CB, Bjerkvig R, Niclou SP: Anti-VEGF Treatment Reduces Blood Supply and Increases Tumor Cell Invasion in Glioblastoma. Proc Natl Acad Sci 2011, 108:3749-54.

[8] Newlands ES, Stevens MFG, Wedge SR, Wheelhouse RT, Brock C: Temozolomide: A Review of Its Discovery, Chemical Properties, Pre-Clinical Development and Clinical trials. Cancer Treat Rev 1997, 23:35-61.

[9] Ulasov IV, Sonabend AM, Nandi S, Khramtsov A, Han Y, Lesniak MS: Combination of adenoviral virotherapy and temozolomide chemotherapy eradicates malignant glioma through autophagic and apoptotic cell death in vivo. Br J Cancer 2009, 100:1154-64.

[10] Jiapaer S, Furuta T, Tanaka S, Kitabayashi T, Nakada M: Potential Strategies Overcoming the Temozolomide Resistance for Glioblastoma. Neurol Med Chir (Tokyo) 2018, 58:405-21.

[11] Eyler CE, Rich JN: Survival of the fittest: cancer stem cells in therapeutic resistance and angiogenesis. J Clin Oncol 2008, 26:2839-45.

[12] Blough MD, Beauchamp DC, Westgate MR, Kelly JJ, Cairncross JG: Effect of aberrant p53 function on temozolomide sensitivity of glioma cell lines and brain tumor initiating cells from glioblastoma. J Neurooncol 2011, 102:1-7.

[13] Yan Y, Xu Z, Dai S, Qian L, Sun L, Gong Z: Targeting autophagy to sensitive glioma to temozolomide treatment. J Exp Clin Cancer Res 2016, 35:23.

[14] FU Jun LZ-g, LIU Xiao-mei, CHEN Fu-rong, SHI Hong-liu, PANG Jesse Chung-sean, NG Ho-keung and CHEN Zhong-ping: Glioblastoma stem cells resistant to temozolomide-induced autophagy. Chinse Medical Jounal 2009, 122:1255-9.

[15] Buccarelli M, Marconi M, Pacioni S, De Pascalis I, D'Alessandris QG, Martini M, Ascione B, Malorni W, Larocca LM, Pallini R, Ricci-Vitiani L, Matarrese P: Inhibition of autophagy increases susceptibility of glioblastoma stem cells to temozolomide by igniting ferroptosis. Cell Death Dis 2018, 9:841.

[16] Raposo G, Stoorvogel W: Extracellular vesicles: exosomes, microvesicles, and friends. J Cell Biol 2013, 200:373-83.

[17] Fuhrmann G, Serio A, Mazo M, Nair R, Stevens MM: Active loading into extracellular vesicles significantly improves the cellular uptake and photodynamic effect of porphyrins. Journal of controlled release : official journal of the Controlled Release Society 2015, 205:35-44.

[18] Yang T, Martin P, Fogarty B, Brown A, Schurman K, Phipps R, Yin VP, Lockman P, Bai S: Exosome delivered anticancer drugs across the blood-brain barrier for brain cancer therapy in Danio rerio. Pharm Res 2015, 32:2003-14.

[19] Chun Yang WX, Qian Qiu, Houda Tahiri, Carmen Gagnon, Guoxiang Liu, Pierre Hardy: Generation of Lymphocytic Microparticles and Detection of Their Proapoptotic Effect on Airway Epithelial Cells. Journal of visualized experiments : JoVE 2015:e52651.

[20] Chun Yang WX, Qian Qiu, Zhuo Shao, David Hamel, Houda Tahiri, Grégoire Leclair, Pierre Lachapelle, Sylvain Chemtob, Pierre Hardy: Role of Receptor-Mediated Endocytosis in The Antiangiogenic Effects of Human T Lymphoblastic Cell-Derived Microparticles. Am J Physiol Regul Integr Comp Physiol 2012, 302:R941-9.

[21] Yang Chun GC, Hou Xin, Hardy Pierre: Low Density Lipoprotein Receptor Mediates Anti-VEGF Effect of Lymphocyte T-Derived Microparticles in Lewis Lung Carcinoma Cells. Cancer Biol Ther 2014, 10:448-56.

[22] Houda Tahiri SO, Chun Yang, François Duhamel, Suzanne Samarani, Ali Ahmad, Mark Vezina, Martin Bussières, Elvire Vaucher, Przemyslaw Sapieha, Gilles Hickson, Karim Hammamji, Réjean Lapointe, Francis Rodier, Sophie Tremblay, Isabelle Royal, Jean-François Cailhier, Sylvain Chemtob, Pierre Hardy Lymphocytic Microparticles Modulate Angiogenic Properties of Macrophages in Laser-Induced Choroidal Neovascularization. Sci Rep 2016, 6:37391.

[23] Qiu Q, Yang C, Xiong W, Tahiri H, Payeur M, Superstein R, Carret AS, Hamel P, Ellezam B, Martin B, Vezina M, Sapieha P, Liu G, Hardy P: SYK is a Target of Lymphocyte-Derived Microparticles in the Induction of Apoptosis of Human Retinoblastoma Cells. Apoptosis 2015, 20:1613-22.

[24] Yang C, Xiong W, Qiu Q, Tahiri H, Superstein R, Carret AS, Sapieha P, Hardy P: Anti-Proliferative and Anti-Tumour Effects of Lymphocyte-Derived Microparticles Are Neither Species- Nor Tumour-Type Specific. J Extracell Vesicles 2014, 3.

[25] Beier D, Hau P, Proescholdt M, Lohmeier A, Wischhusen J, Oefner PJ, Aigner L, Brawanski A, Bogdahn U, Beier CP: CD133(+) and CD133(-) glioblastoma-derived cancer stem cells show

differential growth characteristics and molecular profiles. Cancer Res 2007, 67:4010-5.

[26] Cindi M. Morshead BAR, Constance C. Craig, Michael W. McBurney, William A. Staines, Dante Morassutti, Samuel Weiss, and Derek van der Kooy: Neural Stem Cells in the Adult Mammalian Forebrain: A Relatively Quiescent Subpopulation of Subependymal Cells Cell Press 1994, 13:1071-82.

# Annexe II

*MicroRNA-181a Inhibits Ocular Neovascularization by Interfering with VEGF Expression*

By Chun Yang *et al*.,

Paper published in Cardiovascular Therapeutics

June 2018

DR CHUN YANG (Orcid ID : 0000-0002-2648-9444)

Article type : Original Research Article

# Title: MicroRNA-181a Inhibits Ocular Neovascularization by Interfering with VEGF Expression

**Running head**: miR-181a inhibits neovascularization

Chun Yang[1], Houda Tahiri[1], Chenrongrong Cai[1], Muqing Gu[2], Carmen Gagnon[1], Pierre Hardy [1 *]

[1]Departments of Pediatrics, Physiology and Pharmacology, University of Montreal, Montreal, Quebec, Canada.

[2]Department of Gynecological Endocrinology, Beijing Obstetrics and Gynecology Hospital, Capital Medical University, Beijing, China.

**Corresponding author:**

Dr. P. Hardy; Departments of Pediatrics, Research Center of CHU Sainte-Justine, 3175 Côte-Sainte-Catherine, Montreal, H3T 1C5, Canada. E-mail: pierre.hardy@recherche-ste-justine.qc.ca

Phone: (514) 345-4931 (ext. 3656), Fax: (514) 345-4801

**Keywords:** miR-181a, anti-angiogenesis, ocular neovascularization, extracellular miRNAs (ex-miRNAs)

**Abstract**

**Aim:** Excess angiogenesis or neovascularization plays a key role in the pathophysiology of several ocular diseases such as retinopathy of prematurity, diabetic retinopathy and exudative age-related macular degeneration. MicroRNA-181a (miR-181a) was found highly expressed in retina and choroidal tissues. This study intends to investigate the role of miR-181a in the regulation of ocular neovascularization in different pathophysiological conditions.

**Method:** We performed the RNA sequence to identify the microRNAs components of anti-angiogenic lymphocyte-derived microparticles (LMPs). The effect of miR-181a on human retinal endothelial cells proliferation was assessed *in vitro*. The impact of miR-181a on angiogenesis was confirmed using *in vitro* angiogenesis assay, *ex vivo* choroidal explant and *in vivo* retinal neovascularization. The expression of major angiogenic factors was assessed by real-time qPCR.

**Results:** RNA sequence revealed that miR-181a is selectively enriched in LMPs. Importantly, the inhibition of miR-181a significantly abrogated the effect of LMPs on endothelial viability, but overexpression of miR-181a reduced endothelial cell viability in a dose-dependent manner. miR-181a strongly inhibited *in vitro* angiogenesis and *ex vivo* choroidal neovascularization. The strong anti-angiogenic effect of miR-181a was also displayed on the retinal neovascularization of the *in vivo* mouse model of oxygen-induced retinopathy. In keeping with its effect, several angiogenesis-related genes were dysregulated in the miR-181a overexpressed endothelial cells.

**Conclusion:** These data may open unexpected avenues for the development of miR-181a as a novel therapeutic strategy that would be particularly useful and relevant for the treatment of neovascular diseases.

**Keywords:** miR-181a, anti-angiogenesis, neovascularization, extracellular miRNAs (ex-miRNAs), angiogenic factor, endothelial cell

## Introduction

Excess angiogenesis or neovascularization (NV) plays a key role in the pathophysiology of several ocular diseases such as retinopathy of prematurity, wet form of age-related macular degeneration (AMD) and diabetic retinopathy [1]. The angiogenesis is regulated by a large number of angiogenesis-related factors and determined by a relative balance between pro- and anti-angiogenic factors [2]. The angiogenesis-related factors form a well-coordinated and functional network of molecules affecting the angiogenesis process, thus an effective therapy

may require targeting multiple components of the angiogenic pathway. Endothelial cells are involved in many aspects of vascular biology by producing different factors that regulate cell adhesion, cell proliferation, and vascular tone [3]. The signaling of vascular endothelial growth factor (VEGF) is one of the most potent pathways and is almost exclusively found in endothelial cells. Importantly, a large number of microRNAs (miRNAs) are responsible for angiogenesis and are expressed in endothelial cells [4-6]. MiRNAs are a group of endogenous small non-coding regulatory RNAs (~ 22 nucleotides) silencing their target genes at the post-transcriptional level [7,8]. Each miRNA regulates the expression of multiple protein-coding genes and therefore miRNA-based therapy provides the rationale basis for effective anti-angiogenic treatment [9].

The extracellular microvesicles (EVs) are biologic effectors to influence various physiological and pathological functions of recipient cells [10-12]. We have demonstrated that EVs derived from apoptotic human T-lymphocytes (LMPs) possess strong anti-angiogenic properties in *in vivo* corneal neovascularization, tumor neovascularization[13,14] and limit neovascularization of oxygen-induced retinopathy (OIR) and neovascularization in a laser-induced murine choroidal neovacularization (CNV) model [13-18]. Nonetheless, the potent anti-angiogenic components of LMPs have not been well explored. Selective disposal of some miRNAs in EVs has been suggested to mediate both short-range and distant communication between various cells, and could impact diverse physiological and pathological processes [19-21]. The main goal of this study is to investigate the miRNAs that mediate the anti-angiogenic effect of LMPs.

## Methodology

### Cell culture

Human retinal endothelial cells (HREC) were obtained from Applied Cell Biology Research Instituteand cultured as recommended. Human umbilical vein endothelial cell lines (HUVEC) were purchased from ATCC, and were maintained according to standard procedures.

### LMPs production

Human CEM T cells were purchased from ATCC and grown in X-VIVO medium (Cambrex). LMPs were generated and characterized as described previously [13].

**RNAisolation from LMPs**

RNAs were isolated from LMPs using the miRNeasy Mini Kit (Qiagen) according to the manufacturer's protocol. Quality Threshold and the concentrations were determined using NanoDrop ND-1000 (NanoDrop Technologies). High RNA quality of isolated RNA was confirmed for all samples using the BioAnalyzer 2100 (Agilent Technologies).

**Expression profiling—Illumina BeadChips**

Expression profiling of RNAs in LMPs with three biological replicates was performed using the Illumina MiSeqBeadChips (Illumina Inc) where 200ng of total RNA was processed according to the supplier's protocol. The percentage of reads that fall on miRNA, rRNA, lincRNA, etc. was computerized based on gencode v19 annotations, and the features found in gencode were quantified using Cufflinks. Following read trimming and alignment, counts for all samples were extracted using HTSeq-count and the miR base definition of known miRNAs (IRIC's Genomics Core Facility, University of Montreal).

**Proliferation assay**

Human retinal endothelial cells (HREC) were transfected with 20nM of miR-181a inhibitor (hsa-miR-181a-5p inhibitor, Thermo Fisher Scientific) via liposomes CLS-3 (8 uM, a gift from Dr. Jeanne Leblond-Chain, University of Montreal) before incubation with LMPs (10μg/ml). After 48 hours treatment, cell proliferation was evaluated by [$^{3}$H]-thymidine incorporation assay as we described previously[13].

In a different experiment, endothelial cells were transfected with indicated concentrations of mirVana™ miRNA mimics (10, 25, 40 and 50 nM) for 48hours. The mimics of miR-181a-5p (hsa-181a-5p) and miRscr (negative control #1) were purchased from Thermo Fisher Scientific. Thecells were subjected to a proliferation assay.

**Apoptosis assay**

Cells were seeded in 96-well plate. The next day, cells were exposed to lenti-control (ABM) or Lenti-miR181a-5p (ABM) at MOI of 10 in the presence of polybrene (Sigma) at 8μg/ml or staurosporine (Cat. No.S4400, Sigma) as positive control in the presence of the RealTime-GloAnnexin V Apoptosis Assay Reagent (Promega) according to the protocol. The luminescence was collected kinetically with Clariostar (BMG Labtech) plate reader. The relative luminescence unit was presented.

**Endothelial cell tube formation assay**

The endothelial cell tube formation assay was performed as described [22]. The mimic of hsa-miR-181a-5p (mirVana® miRNA mimic), and mirVana™ miRNA mimic, Negative Control were purchased from Thermo Fisher Scientific. HREC were transfected with 50 nM mimic of miR-181a-5p or miRscr. 24 hours later, cells were seeded on Matrigel™ (BD Biosciences). The images were taken after 17-hour seeding using fluorescence microscopy (Eclipse E800, Nikon Corp).

**Treatment of choroidal explants and measurement of neovascularization**

The human RPE-removed choroidal explants were prepared according to our previously described procedure [16,17]. Briefly, choroidal explants were cultured in growth factor–reduced basement membrane matrix5 days. On day 6, explants were transduced with lenti-control and lenti-miR-181a-5p ($10^6$ U/ml) for 72 hours. Photographs of individual explants were taken at the end of treatment and the neovessel areas were determined.

**Oxygen-induced retinopathy mouse model (OIR) and retina NV quantification**

The OIR model is generated based on the established method [23]. Briefly, the postnatal day P12 OIR mice were randomly divided into 2 groups and each group (n=7 mice) and received intravitreal injections of 1 μL of$10^{10}$U/ml of lenti-miR-181a-5p in one eye and lenti-control in the contralateral eye respectively. At P17, retinal flatmounts were prepared as described previously [24]. Of note, to avoid the influence of postnatal body weight and postnatal weight gain on the severity of retinal NV in OIR model [25,26], we measured mice body weight before and after lentivirus treatments. The P12 OIR mice with body weight lower than 5g or over 7g were discarded, and the mice at P17 with body weights between 5 and 7.5 g were kept for retinal NV analysis. Vessels in flat-mounted retinas were stained with red fluorescent isolectin B4and the area of neovascular tufts were measured as described [27]. Neovascularizations were quantified by comparing the number of pixels in the neovascular tuft areas with the total number of pixels in the retina using the SWIFT-NV method [24,28].

**Quantitative RT-PCR**

Total RNA was extracted from HREC cells using an RNA extraction kit (Qiagen). Synthesis of cDNAs and quantitative analysis of gene expression were performed as we described previously [29]. β-actin was used as internal control.PCR primers targeting human MAPK1,

Bcl-2, VEGF and β-actin were synthesized by Alpha DNA (Montreal, Canada) as follows: MAPK1**:**forward 5′-GGCCCCTGAAAGAATAAACCC-3′; reverse 5′-CGAAGGATGGCCAACTCAATC-3′; Bcl-2: forward 5′-GGTGAACTGGGGGAGGATTG-3′, reverse 5′-GTGCCGGTTCAGGTACTCAG-3′; VEGF:forward 5′-CTACCTCCACCATGCCAAGT-3′; reverse 5′-GCAGTAGCTGCGCTGATAGA-3′; β-actin: forward 5'-CTGCGGCATTCACGAAACTAC-3', reverse 5'-ATCTCTTTCTGCATCCTGTCCG-3'.The method of analyzing the expression of mouse VEGFα and 18s in OIR mice retina was described previously [16].

**Statistical analysis**

All experiments were repeated independently at least 3 times in duplicate or triplicate. Values are presented as means ± SEM. Statically significant differences between two groups were analyzed by Student's t test. One-way ANOVA followed by post-hoc Bonferroni tests was performed for comparison among means. Statistical significance was set at $P < 0.05$.

**Results**

**1. Inhibition of miR-181a significantly attenuated the effect of LMPs on HREC cell proliferation.**

We have previously reported that LMPs exert a strong inhibitory effect on proliferation of endothelial and cancer cells [13,15,30]. We have also demonstrated that LMPs significantly reduced the proliferation of human retinal endothelial cell (HREC) in a dose-dependent manner [15]. As a first step in identifying miRNAs that are enriched in LMPs, we isolated the total RNAs from LMPs and performed RNAs sequence. The resulting data suggested that miRNAs are selectively incorporated into LMPs in which miR-181a is one of the most abundant miRNAs (**Table 1)**. Thus, we speculated that miR-181a may play a role inmediating the effect of LMPs on endothelial cells. To prove this hypothesis, we used the inhibitor of miR-181a to block the activity of miR-181a when HREC cells were incubated with LMPs. The results of cell proliferation assay suggested that the inhibitor of miR-181a significantly, not dramatically, attenuated the effect of LMPs (**Figure 1A**). The same phenomenon was observed in the proliferation assay of human umbilical vein endothelial cells (HUVECs) **(Figure1B**).

**2. miR-181a inhibited endothelial cell proliferation.**

The synthetic mimic of miR-181a-5p was used to test anti-proliferative activity in HREC. The miR-181a-5p inhibited cell proliferation in a dose-dependent manner, producing up to 50% inhibition compared to a negative control miRNA (miRscr) (**Figure 2A**). miR-181a-5p was also overexpressed in the human umbilical vein endothelial cell (HUVEC) with lentiviral vector (lenti-miR-181a-5p), and cell growth was assessed by MTT assay. The cell growth of the HUVEC cells infected with lenti-miR-181a-5p was reduced in a dose-dependent manner (**Figure 2B**). Given the significant reduced cell growth by miR-181a, it is plausible to question whether miR-181a-5p affects cell apoptosis. To address this question, we performed the cell apoptosis assay on the HREC cells overexpressing miR-181a by lentiviral vector. The lenti-miR-181-5p at the MOI of 10did not significantly induce HREC cell death (**Figure 2C,** *p*0.114), although this dose of lenti-miR-181a-5p significantly suppressed cell growth.

**3. miR-181a inhibited angiogenesis *in vitro and ex vivo*.**

We performed an endothelial cell tube formation assayto assess the anti-angiogenic effect of miR-181a-5p*in vitro*. HREC transfected with mimic of miR-181a-5p showed dramatically decreased tube formation: a 70% decrease, compared to HREC transfected with miRscr mimic (**Figure 3A, 3B**). We also investigated the effects of miR-181a on neovessel sprouting from cultured human choroidal explants. The human choroidal explants were transduced with lenti-control and lenti-miR-181a-5p. The neovascularized areas were strongly suppressed by miR-181a**,** with a reduction of 84.1±6.6%, compared to the control group (**Figure 3C, 3D**).

**4. miR-181a inhibits retinal neovascularization in the mouse model of oxygen-induced retinopathy.**

To extend our investigation of the *in vivo* effect of miR-181a, we used an oxygen-induced retinopathy mouse model (OIR, a well-established animal model of ischemia-induced retinal neovascularization). Along with the in vitro and ex vivo effects, intravitreal injections of lenti-miR-181a-5p significantly decreased the retinal neovascularization areas, by 52% compared to the lenti-control group (**Figure 4A, 4B**). In line with this observation, the retinal VEGF expression was significantly decreased in the miR-181a treated OIR mice (**Figure 4C**).

**5. miR-181a altered the expression of angiogenic factors in endothelial cells.**

To better understand how miR-181a produces its anti-angiogenic effect in endothelial cells, we performed quantitative PCR to analyze the expression of the target genes of miR-181a-5p in the HREC cell transduced with lenti-miR-181a-5p. These genes were selected based on the published papers [31-33] and database of TargetScanHuamn 7.1 (http://www.targetscan.org/), miRTarBase (http://mirtarbase.mbc.nctu.edu.tw/). They are involved in endothelial biological processes associated with angiogenesis, such as the cell cycle, cell migration, cell growth and proliferation [33].They are the mitogen-activated protein kinase 1 (MAPK1) [32], B-cell lymphoma 2 (Bcl2) [31], and VEGF [33]. Compared to those in HREC cells transduced with lenti-control, the mRNA levels of these genes were all significantly reduced by miR-181a-5p (**Figure 5**).

**DISCUSSION**

There is mounting evidence that extracellular microvesicles (EVs) provide a means of intercellular communication both in physiological and pathological conditions, by local and systemic intercellular exchange of biological information [34]. LMPs are membrane-derived EVs derived from human apoptotic T cells [13].The strong anti-angiogenic effect of LMPs has been demonstrated *in vitro*, *ex vivo*, as well as in several *in vivo* models [13-15]. It is well documented that EVs harbour a concentrated set of phospholipids, cytokines, proteins, RNAs, DNA, etc., and can influence diverse biological functions [35]. Since the discovery of miRNAs secreting within EVs (ex-miRNAs) in 2008, ex-miRNAs have been of interest to molecular biologists [19,20]. Our RNA sequence analysis revealed for the first time that miR-181a is one of the most abundant ex-miRNAs in the LMPs. This finding is supported by the fact that miR-181a was found highly expressed in the thymus, the primary lymphoid organ where maturation of T lymphocytes occurs in the early stages of T-cell differentiation [20,36-39]. Even though enriched in LMPs, miR-181a is one of the hundreds miRNAs expressed in LMPs. The inhibition of miRNA-181a caused only partial attenuation of the effect of LMPs (**Figure 1**), which suggested that miR-181a may not be the only active component. LMPs are heterogenic components containing lipids, proteins, DNAs and RNAs in addition to miRNAs [35]. The strong anti-angiogenic effects of LMPs may resulted from the synergistic effects of many different components in LMPs, thus more in-depth studies are needed to explore the other active factors.

The members of the miR-181 family are evolutionarily conserved across almost all vertebrates, suggesting their functional importance [37,40]. Numerous studies have reported the involvement of miR-181a in important cell functions such as growth, proliferation, death, survival, maintenance, vascular cell signaling and blood vessel formation [9]. Recently, the roles of miR-181a in the regulation of endothelial cell function, in vascular development, and in tumor angiogenesis have been studied in several *in vitro* and *in vivo* models [41-45]. Nonetheless, contradictory roles of miR-181a in modulating angiogenesis have been reported. Terek's group reported that miR-181a is overexpressed in chondrosarcoma by hypoxia and VEGF [44], and miR-181a promotes tumor angiogenesis through directly targeting G-protein signaling 16 and consequently increasing CXC chemokine receptor 4 signaling [45]. Conversely, the anti-angiogenic property of miR-181a was identified from 2 independent studies. First, Eom et al. found that miR-181a may inhibit mouse endothelial cells through negatively regulating VEGF receptor signaling [46], and then Li et al. demonstrated that ectopic miR-181a reduced *in vivo* angiogenesis via reduction of matrix metalloproteinase-14 expression in aggressive breast cancer cell lines [47]. These controversial findings may suggest that the anti-angiogenesis effect of miR-181a is cell- or tissue-specific.

Ocular angiogenesis is a major cause of many ocular diseases and blindness. It is a significant contributing factor in diabetic retinopathy, exudative AMD, corneal neovascularization, retinopathy of prematurity, neovascular glaucoma, etc. The ocular expression of miR-181a has been studied in the mouse and in the human eye. In the mouse, miR-181a was identified as strongly expressed in the retina [48]; in the human eye, miR-181a was abundantly expressed in the retina and RPE/choroid tissues [49]. One *in vitro* study revealed that hypoxia increased the expression of miR-181a in choroidal endothelial cells, and suggested an anti-angiogenic role of miR-181a through inhibiting cell migration and proliferation [50]. However, the role of miR-181a in pathophysiological angiogenesis *in vivo* has not been verified. Our current data generated from *in vitro*, *ex vivo* (choroidal neovascularization), and *in vivo* retinal neovascularization model (OIR), strongly support the anti-angiogenic role of miR-181a (**Figures 2-5**). Of special note, we observed that the concentration is critical for the anti-proliferation effect of miR-181a on endothelial cells, because the high dose of miR-181a (≥ 100nM of miR-181a-5p mimic) lost its effect on endothelial cell growth *in vitro.* Instead, endothelial cell growth was slightly increased, although not significant ($p$0.372 vs. control) (**Supplementary Figure S1**). Similar results were also observed in miR-181a treated HUVEC cells, breast cancer cells (MCF-7, MDA-MB-231), retinoblastoma cells (Y-79), and glioblastoma cells (U87, Gl261) when the

concentration of lenti-miR-181a is high (MOI ≥100) (data not shown).The possible explanation is that miR-181a may target multiple mRNAs within a cell, which means miR-181a may **be** both an agonist and an antagonist of a pathway. Thus, the final effect of a miR-181a may depend on the transcriptome of the cell and the behavior of the targets as well.

In pathological conditions, there is an imbalance of proangiogenic and anti-angiogenic factors secreted by retinal endothelial cells, and the over-expression of VEGF plays an important role in the pathogenesis of ocular angiogenesis [51]. Recent studies have shown a reciprocity relationship between the angiogenic activity of VEGF and Bcl2**;** the latter is an anti-oxidant and anti-apoptotic resident mitochondrial protein [52]. Nor et al. demonstrated that VEGF-mediated angiogenesis is associated with enhanced endothelial cell survival and induction of Bcl-2 expression [53]. Moreover, Biroccio et al. reported that Bcl-2 enhanced VEGF expression and neovascularization *in vivo* [54]. In the eyes, Bcl-2 expression in the endothelium plays a significant role during postnatal retinal vascularization [55]. Bcl-2 deficiency attenuated ischemia-driven retinal neovascularization during OIR and pathological choroidal neovascularization [55,56]. Therefore, modulation of Bcl–2 expression plays a central role during angiogenesis. Notably, miR-181a was found to play a direct role in controlling mitochondrial function by directly regulating expression of Bcl-2 [43]. During the whole senescence process of primary human umbilical vein endothelial cells (HUVEC), miR-181a was found highly expressed [57], but Bcl-2 is downregulated in the senescence HUVEC cells [58]. Although the combination of TargetScan and miRNAmap software does not predict that VEGF is the putative target gene of miR-181a, a correlation between the overexpression of miR-181a and VEGF was reported [33]. In keeping with this observation, we also showed that the expression of Bcl-2 and VEGF was significantly downregulated by overexpression of miR-181a in HREC cells (**Figure 5**).

In addition to Bcl2, direct targeting of miR-181a to MAPK1 (also named ERK5, or BMK1) was confirmed by luciferase reporter gene assays [32]. MAPK1 is expressed in a variety of tissues and its transcript is abundant in heart, placenta, lung, kidney, skeletal muscle and endothelial cells [59,60]. It can be activated by a range of growth factors, cytokines and cellular stresses. MAPK1-deficient mice and targeted deletion of MAPK1 in an adult mice model suggested an important role of MAPK1 in controlling angiogenesis [61-63]. Since VEGF functions as a potent activator for MAPK1 in endothelial cells, MAPK1 is likely responsible for transmitting VEGF-dependent anti-apoptotic signals [63]. One study also indicated the role of MAPK1 signaling in diabetic angiopathy [64]. Herein, we observed that in HREC cells, overexpression of miR-181a strongly inhibited MAPK1 expression, which

indicated that the anti-angiogenic effect of miR-181a may have resulted from interfering with the MAPK1/VEGF signaling. Thus, it is possible that miR-181a modulation of MAPK1 signaling may present a therapeutic window for aberrant ocular neovascularization.

In conclusion, we demonstrated for the first time that miR-181a exerts a strong anti-neovascularization effect in ocular angiogenesis models**;** in addition, miR-181a specifically targeted a set of angiogenic and cell growth-related genes. These data suggest that miR-181a may be developed as a new therapeutic strategy for treating ocular angiogenesis-related diseases.

**Disclosures:**

*Ethics:*

1. Human eyes were obtained from the Eye Bank of Canada. The approval of the human clinical study protocol and informed consent was obtained from CHU Sainte-Justine ethics committee, Ref # 3949, and our research adhered to the tenets of the Declaration of Helsinki.
2. All animal experiments were approved by the Animal Care Committee of CHU Sainte-Justine (Montreal, QC, Canada).

*Funding*: This work was supported by an operating grant to Pierre Hardy from the Canadian Institutes of Health Research (362383).

*Disclosures:* There is no conflict of interest (either financial or personal), the manuscript has not been published previously and is not being considered concurrently for another publication, and all authors and acknowledged contributors have read and approved the manuscript.

*Author contributions:*

Chun Yang: Concept/design, Drafting article, Critical revision of article, Statistics.
Houda Tahiri: Data analysis/interpretation.
Chenrongrong Cai: Data analysis, Data collection.
Muqing Gu: Data collection.
Carmen Gagnon: Statistics, Data analysis.
Pierre Hardy: Concept/design, Critical revision of article, Approval of article, Funding secured by.

**References:**

Reference:

1. Agrawal S, Chaqour B. MicroRNA signature and function in retinal neovascularization. World J Biol Chem. 2014;5(1):1-11.
2. Folkman J. Angiogenesis. Annu Rev Med. 2006;57:1-18.
3. Eelen G, de Zeeuw P, Simons M, Carmeliet P. Endothelial cell metabolism in normal and diseased vasculature. Circ Res. 2015;116(7):1231-1244.
4. Kuehbacher A, Urbich C, Zeiher AM, Dimmeler S. Role of Dicer and Drosha for endothelial microRNA expression and angiogenesis. Circ Res. 2007;101(1):59-68.
5. Suarez Y, Fernandez-Hernando C, Yu J, et al. Dicer-dependent endothelial microRNAs are necessary for postnatal angiogenesis. Proc Natl Acad Sci U S A. 2008;105(37):14082-14087.
6. Poliseno L, Tuccoli A, Mariani L, et al. MicroRNAs modulate the angiogenic properties of HUVECs. Blood. 2006;108(9):3068-3071.
7. Bartel DP. MicroRNAs: genomics, biogenesis, mechanism, and function. Cell. 2004;116(2):281-297.
8. Carthew RW, Sontheimer EJ. Origins and Mechanisms of miRNAs and siRNAs. Cell. 2009;136(4):642-655.
9. Landskroner-Eiger S, Moneke I, Sessa WC. miRNAs as modulators of angiogenesis. Cold Spring Harb Perspect Med. 2013;3(2):a006643.
10. Yanez-Mo M, Siljander PR, Andreu Z, et al. Biological properties of extracellular vesicles and their physiological functions. J Extracell Vesicles. 2015;4:27066.
11. Lee Y, El Andaloussi S, Wood MJ. Exosomes and microvesicles: extracellular vesicles for genetic information transfer and gene therapy. Hum Mol Genet. 2012;21(R1):R125-134.
12. Shen J, Yang X, Xie B, et al. MicroRNAs regulate ocular neovascularization. Mol Ther. 2008;16(7):1208-1216.
13. Yang C, Mwaikambo BR, Zhu T, et al. Lymphocytic microparticles inhibit angiogenesis by stimulating oxidative stress and negatively regulating VEGF-induced pathways. Am J Physiol Regul Integr Comp Physiol. 2008;294(2):R467-476.
14. Yang C, Gagnon C, Hou X, Hardy P. Low density lipoprotein receptor mediates anti-VEGF effect of lymphocyte T-derived microparticles in Lewis lung carcinoma cells. Cancer Biol Ther. 2010;10(5):448-456.

15. Yang C, Xiong W, Qiu Q, et al. Role of receptor-mediated endocytosis in the antiangiogenic effects of human T lymphoblastic cell-derived microparticles. Am J Physiol Regul Integr Comp Physiol. 2012;302(8):R941-949.

16. Tahiri H, Omri S, Yang C, et al. Lymphocytic Microparticles Modulate Angiogenic Properties of Macrophages in Laser-induced Choroidal Neovascularization. Sci Rep. 2016;6:37391.

17. Tahiri H, Yang C, Duhamel F, et al. p75 neurotrophin receptor participates in the choroidal antiangiogenic and apoptotic effects of T-lymphocyte-derived microparticles. Invest Ophthalmol Vis Sci. 2013;54(9):6084-6092.

18. Qiu Q, Yang C, Xiong W, et al. SYK is a target of lymphocyte-derived microparticles in the induction of apoptosis of human retinoblastoma cells. Apoptosis. 2015;20(12):1613-1622.

19. Iguchi H, Kosaka N, Ochiya T. Secretory microRNAs as a versatile communication tool. Commun Integr Biol. 2010;3(5):478-481.

20. Turchinovich A, Tonevitsky AG, Burwinkel B. Extracellular miRNA: A Collision of Two Paradigms. Trends Biochem Sci. 2016;41(10):883-892.

21. Ostenfeld MS, Jeppesen DK, Laurberg JR, et al. Cellular disposal of miR23b by RAB27-dependent exosome release is linked to acquisition of metastatic properties. Cancer Res. 2014;74(20):5758-5771.

22. DeCicco-Skinner KL, Henry GH, Cataisson C, et al. Endothelial cell tube formation assay for the in vitro study of angiogenesis. J Vis Exp. 2014;(91):e51312.

23. Smith LE, Wesolowski E, McLellan A, et al. Oxygen-induced retinopathy in the mouse. Invest Ophthalmol Vis Sci. 1994;35(1):101-111.

24. Stahl A, Connor KM, Sapieha P, et al. Computer-aided quantification of retinal neovascularization. Angiogenesis. 2009;12(3):297-301.

25 Vanhaesebrouck S, Daniels H, Moons L, Vanhole C, Carmeliet P, De Zegher F: Oxygen-induced retinopathy in mice: amplification by neonatal IGF-I deficit and attenuation by IGF-I administration. Pediatr Res. 2009;65:307-310.

26 Stahl A, Chen J, Sapieha P, et al. Postnatal weight gain modifies severity and functional outcome of oxygen-induced proliferative retinopathy. Am J Patho. 2010;177:2715-2723.

27. Shen J, Xie B, Dong A, Swaim M, Hackett SF, Campochiaro PA. In vivo immunostaining demonstrates macrophages associate with growing and regressing vessels. Invest Ophthalmol Vis Sci. 2007;48(9):4335-4341.

28. Joyal JS, Sitaras N, Binet F, et al. Ischemic neurons prevent vascular regeneration of neural tissue by secreting semaphorin 3A. Blood. 2011;117(22):6024-6035.
29. Yang C, Xiong W, Qiu Q, et al. Anti-proliferative and anti-tumour effects of lymphocyte-derived microparticles are neither species- nor tumour-type specific. J Extracell Vesicles. 2014;3.
30. Yang C, Xiong W, Qiu Q, et al. Generation of lymphocytic microparticles and detection of their proapoptotic effect on airway epithelial cells. J Vis Exp. 2015;(96):e52651.
31. Ouyang YB, Lu Y, Yue S, Giffard RG. miR-181 targets multiple Bcl-2 family members and influences apoptosis and mitochondrial function in astrocytes. Mitochondrion. 2012;12(2):213-219.
32. He Q, Zhou X, Li S, et al. MicroRNA-181a suppresses salivary adenoid cystic carcinoma metastasis by targeting MAPK-Snai2 pathway. Biochim Biophys Acta. 2013;1830(11):5258-5266.
33. Cuevas A, Saavedra N, Cavalcante MF, Salazar LA, Abdalla DS. Identification of microRNAs involved in the modulation of pro-angiogenic factors in atherosclerosis by a polyphenol-rich extract from propolis. Arch Biochem Biophys. 2014;557:28-35.
34. S ELA, Mager I, Breakefield XO, Wood MJ. Extracellular vesicles: biology and emerging therapeutic opportunities. Nat Rev Drug Discov. 2013;12(5):347-357.
35. Muralidharan-Chari V, Clancy JW, Sedgwick A, D'Souza-Schorey C. Microvesicles: mediators of extracellular communication during cancer progression. J Cell Sci. 2010;123(Pt 10):1603-1611.
36. Neilson JR, Zheng GX, Burge CB, Sharp PA. Dynamic regulation of miRNA expression in ordered stages of cellular development. Genes Dev. 2007;21(5):578-589.
37. Chen CZ, Li L, Lodish HF, Bartel DP. MicroRNAs modulate hematopoietic lineage differentiation. Science. 2004;303(5654):83-86.
38. Cichocki F, Felices M, McCullar V, et al. Cutting edge: microRNA-181 promotes human NK cell development by regulating Notch signaling. J Immunol. 2011;187(12):6171-6175.
39. Ebert PJ, Jiang S, Xie J, Li QJ, Davis MM. An endogenous positively selecting peptide enhances mature T cell responses and becomes an autoantigen in the absence of microRNA miR-181a. Nat Immunol. 2009;10(11):1162-1169.
40. Seoudi AM, Lashine YA, Abdelaziz AI. MicroRNA-181a - a tale of discrepancies. Expert Rev Mol Med. 2012;14:e5.

41. Kazenwadel J, Michael MZ, Harvey NL. Prox1 expression is negatively regulated by miR-181 in endothelial cells. Blood. 2010;116(13):2395-2401.

42. Erusalimsky JD, Kurz DJ. Cellular senescence in vivo: its relevance in ageing and cardiovascular disease. Exp Gerontol. 2005;40(8-9):634-642.

43. Rippo MR, Olivieri F, Monsurro V, Prattichizzo F, Albertini MC, Procopio AD. MitomiRs in human inflamm-aging: a hypothesis involving miR-181a, miR-34a and miR-146a. Exp Gerontol. 2014;56:154-163.

44. Sun X, Wei L, Chen Q, Terek RM. MicroRNA regulates vascular endothelial growth factor expression in chondrosarcoma cells. Clin Orthop Relat Res. 2015;473(3):907-913.

45. Sun X, Charbonneau C, Wei L, Chen Q, Terek RM. miR-181a Targets RGS16 to Promote Chondrosarcoma Growth, Angiogenesis, and Metastasis. Mol Cancer Res. 2015;13(9):1347-1357.

46. Eom S, Kim Y, Kim M, et al. Transglutaminase II/microRNA-218/-181a loop regulates positive feedback relationship between allergic inflammation and tumor metastasis. J Biol Chem. 2014;289(43):29483-29505.

47. Li Y, Kuscu C, Banach A, et al. miR-181a-5p Inhibits Cancer Cell Migration and Angiogenesis via Downregulation of Matrix Metalloproteinase-14. Cancer Res. 2015;75(13):2674-2685.

48. Karali M, Peluso I, Marigo V, Banfi S. Identification and characterization of microRNAs expressed in the mouse eye. Invest Ophthalmol Vis Sci. 2007;48(2):509-515.

49. Karali M, Persico M, Mutarelli M, et al. High-resolution analysis of the human retina miRNome reveals isomiR variations and novel microRNAs. Nucleic Acids Res. 2016;44(4):1525-1540.

50. Han F, Wu Y, Jiang W. MicroRNA-18a Decreases Choroidal Endothelial Cell Proliferation and Migration by Inhibiting HIF1A Expression. Med Sci Monit. 2015;21:1642-1647.

51. Pauleikhoff D, Bertram B, Holz FG, et al. Anti-VEGF therapy of neovascular age-related macular degeneration: therapeutic strategies status December 2012. Klin Monbl Augenheilkd. 2013;230(2):170-177.

52. Vaux DL, Cory S, Adams JM. Bcl-2 gene promotes haemopoietic cell survival and cooperates with c-myc to immortalize pre-B cells. Nature. 1988;335(6189):440-442.

53. Nor JE, Christensen J, Mooney DJ, Polverini PJ. Vascular endothelial growth factor (VEGF)-mediated angiogenesis is associated with enhanced endothelial cell survival and induction of Bcl-2 expression. Am J Pathol. 1999;154(2):375-384.

54. Biroccio A, Candiloro A, Mottolese M, et al. Bcl-2 overexpression and hypoxia synergistically act to modulate vascular endothelial growth factor expression and in vivo angiogenesis in a breast carcinoma line. FASEB J. 2000;14(5):652-660.

55. Wang S, Sorenson CM, Sheibani N. Attenuation of retinal vascular development and neovascularization during oxygen-induced ischemic retinopathy in Bcl-2-/- mice. Dev Biol. 2005;279(1):205-219.

56. Zaitoun IS, Johnson RP, Jamali N, et al. Endothelium Expression of Bcl-2 Is Essential for Normal and Pathological Ocular Vascularization. PloS One. 2015;10(10):e0139994.

57. Yentrapalli R, Azimzadeh O, Kraemer A, et al. Quantitative and integrated proteome and microRNA analysis of endothelial replicative senescence. J Proteomics. 2015;126:12-23.

58. Staszel T, Zapala B, Polus A, et al. Role of microRNAs in endothelial cell pathophysiology. Pol Arch Med Wewn. 2011;121(10):361-366.

59. Lee JD, Ulevitch RJ, Han J. Primary structure of BMK1: a new mammalian map kinase. Biochem Biophys Res Commun.1995;213(2):715-724.

60. Yan C, Takahashi M, Okuda M, Lee JD, Berk BC. Fluid shear stress stimulates big mitogen-activated protein kinase 1 (BMK1) activity in endothelial cells. Dependence on tyrosine kinases and intracellular calcium. J Biol Chem. 1999;274(1):143-150.

61. Roberts OL, Holmes K, Muller J, Cross DA, Cross MJ. ERK5 and the regulation of endothelial cell function. Biochem Soc Trans. 2009;37(Pt 6):1254-1259.

62. Regan CP, Li W, Boucher DM, Spatz S, Su MS, Kuida K. Erk5 null mice display multiple extraembryonic vascular and embryonic cardiovascular defects. Proc Natl Acad Sci U S A. 2002;99(14):9248-9253.

63. Hayashi M, Kim SW, Imanaka-Yoshida K, et al. Targeted deletion of BMK1/ERK5 in adult mice perturbs vascular integrity and leads to endothelial failure. J Clin Invest. 2004;113(8):1138-1148.

64. Wu Y, Feng B, Chen S, Chakrabarti S. ERK5 Regulates glucose-induced increased fibronectin production in the endothelial cells and in the retina in diabetes. Invest Ophthalmol Vis Sci. 2012;53(13):8405-8413.

**Table 1. The read counts of most abundant miRNAs in LMPs.** A table of small section from an Excel spread-sheet summarizing the analysis results of most abundant miRNA expression in LMPs.

| miRNAs | LMPs 1 | LMPs 2 | LMPs 3 | mean |
|---|---|---|---|---|
| no_feature (total) | 7538929 | 5742559 | 4875163 | 6052217 |
| **hsa-mir-181a-1** | **12490** | **7564** | **10006** | **10 020** |
| **hsa-mir-181a-2** | **12110** | **7202** | **9672** | **9 661** |
| hsa-let-7f-2 | 8612 | 4963 | 6235 | 6 603 |
| hsa-let-7f-1 | 8438 | 4847 | 6095 | 6 460 |
| hsa-mir-92a-1 | 7344 | 5852 | 5200 | 6 132 |
| hsa-mir-92a-2 | 7154 | 5694 | 5013 | 5 954 |
| hsa-mir-20a | 5356 | 2809 | 4060 | 4 075 |
| hsa-let-7g | 3490 | 2278 | 2332 | 2 700 |
| hsa-mir-148a | 3108 | 2244 | 2201 | 2 518 |
| hsa-mir-363 | 2636 | 1918 | 2664 | 2 406 |
| hsa-mir-21 | 2828 | 1814 | 2423 | 2 355 |

**Legend**

**Figure 1. Inhibition of miR-181a significantly attenuated the effect of LMPs on HREC cell proliferation.**The human retinal endothelial cells (HREC) **(A)** or human umbilical vein endothelial cells (HUVEC) **(B)** were transfected with 50nM of miR-181a inhibitor via liposomes CLS-3 before incubation with LMPs (10μg/ml). After 48 hours of treatment, cell proliferation was assessed and values were presented as percentages of control. **A.** ***$p$0.0001 vs. CTL, $^{\neq}p$0.044 vs. LMPs. **B.** **$p$0.002 vs. CTL, $^{\neq}p$0.012 vs. LMPs.

**Figure 2. miR-181a inhibited endothelial cell proliferation and cell growth. A.** Human retinal endothelial cells (HREC) were transfected with mimic of miR-181a-5p at indicated concentrations for 48 hours using lipofectamine 2000. Cell proliferation was assessed and values were normalized to cell proliferation of control cells and plotted as mean ± SE. *(***$p$<0.0001 vs. miRscr). **B.** miR-181a-5p was overexpressed in human umbilical vein endothelial cells (HUVEC) by lentiviral vector with different MOI (multiplicity of infection).

Data were normalized to cell viability of control cells (infected with lenti-control and plotted as mean ± SE. *(*p*0.048; ***p*0.0027 vs. lenti-control). **C.** HREC cell apoptosis was assessed by Real Time-Glo Annexin V Apoptosis Assay. (*p*0.114 vs. lenti-control).

**Figure 3. miR-181a inhibited angiogenesis *in vitro and ex vivo*. A.** Representative images of tube formation assay after HREC transfected with mimic of 50 nMof miR-181a-5p or miRscr. 24 hours after the transfection, HREC cells were seeded on Matrigel. The images were taken after 17 hours of seeding using fluorescence microscopy. **B.** The tube formation was quantified by calculating the cumulative length of the tube of each image. Data are plotted as mean ± SE, ****p*<0.0001 vs. miRscr. **C.** Representative images of human choroidal angiogenesis. The human choroidal explants were cultured in normal medium for 5 days for neovessel growth, and then tranduced with lenti-control and lenti-miR-181a-5p. The images were taken 3 days after lentivirus infections. **D.** The neovascularized areas in each condition were calculated and presented as a percentage of control (CTL, set as 100%). Data are plotted as mean ± SE, ***p*0.011vs. lenti-control.

**Figure 4. miR-181a inhibited *in vivo* retinal neovascularization of oxygen-induced retinopathy (OIR) in mice. A**. The images of retinal flatmounts from OIR mice were taken at postnatal day 17 (P17) after intravitreal injections at P12 with 1μl of $10^{10}$U/ml of lenti-control or lenti-miR-181a-5p. **B**. Retinal surface area covered by tufts (neovascularized area) was measured and quantified as a percentage of the entire retinal area, and these values were presented as relative to the lenti-control group, which was set as 100%. **p0.027* vs. lenti-control. **C.** Total RNAs were isolated from retina tissues of OIR mice at P17 and subjected to quantitative RT-PCR. VEGF values were normalized to values for β-actin mRNA and presented as percentages of lenti-control group. **p*0.035 vs. control.

**Figure 5. miR-181a suppressed the expression of MAPK1, BCL2, and VEGF in HREC cells.** 50nM of miRscr and miR-181a-5p mimics were delivered into HREC cells respectively. 36 hours later the total RNAs were isolated and the indicated genes of interest were analyzed by quantitative RT-PCR. β-actin was used as an internal control gene.The values were presented as percentages of miRscr. **p*0.029, ***p*0.076, ***p*0.014, vs. miRscr. MAPK1**:** mitogen-activated protein kinase 1; Bcl2**:** B-cell lymphoma 2; VEGF**:** vascular endothelial growth factor.

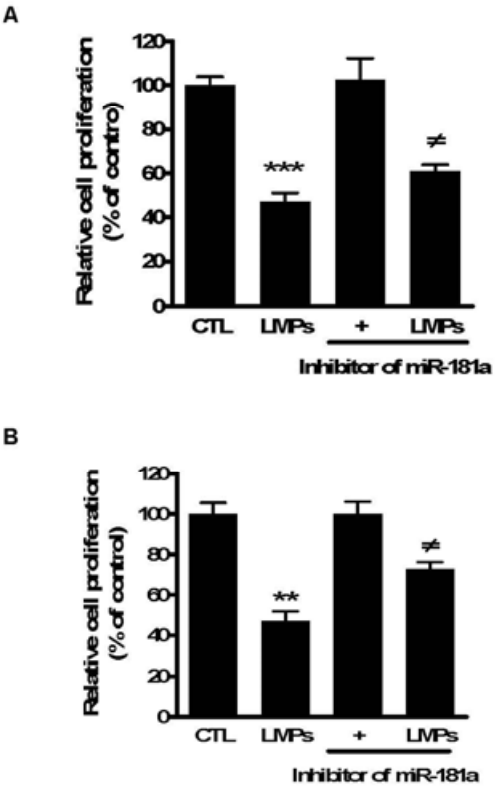


**Figure 1**

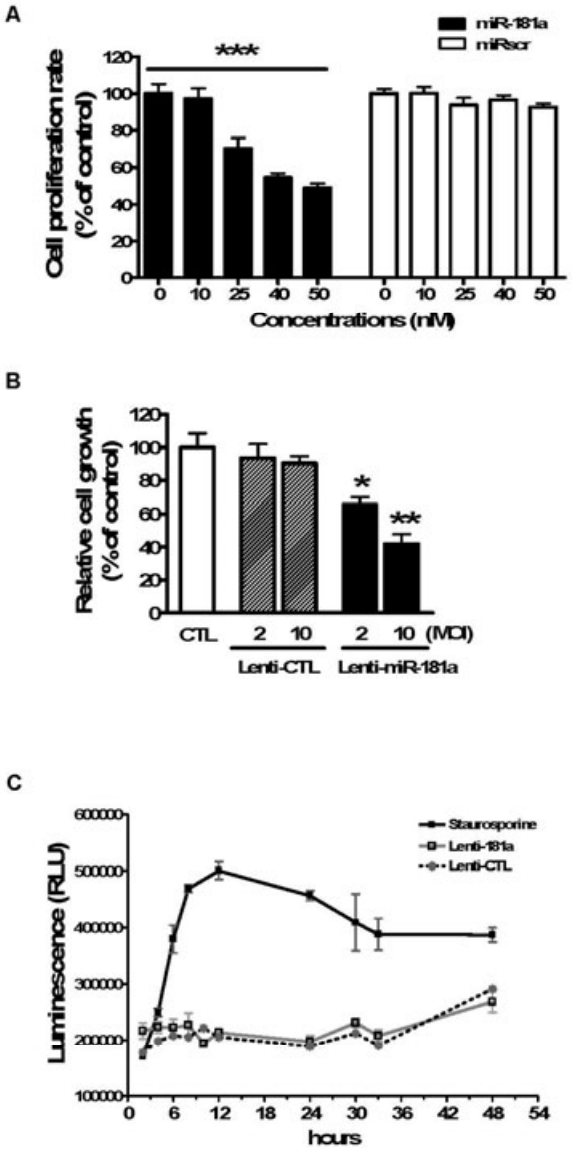


Figure 2

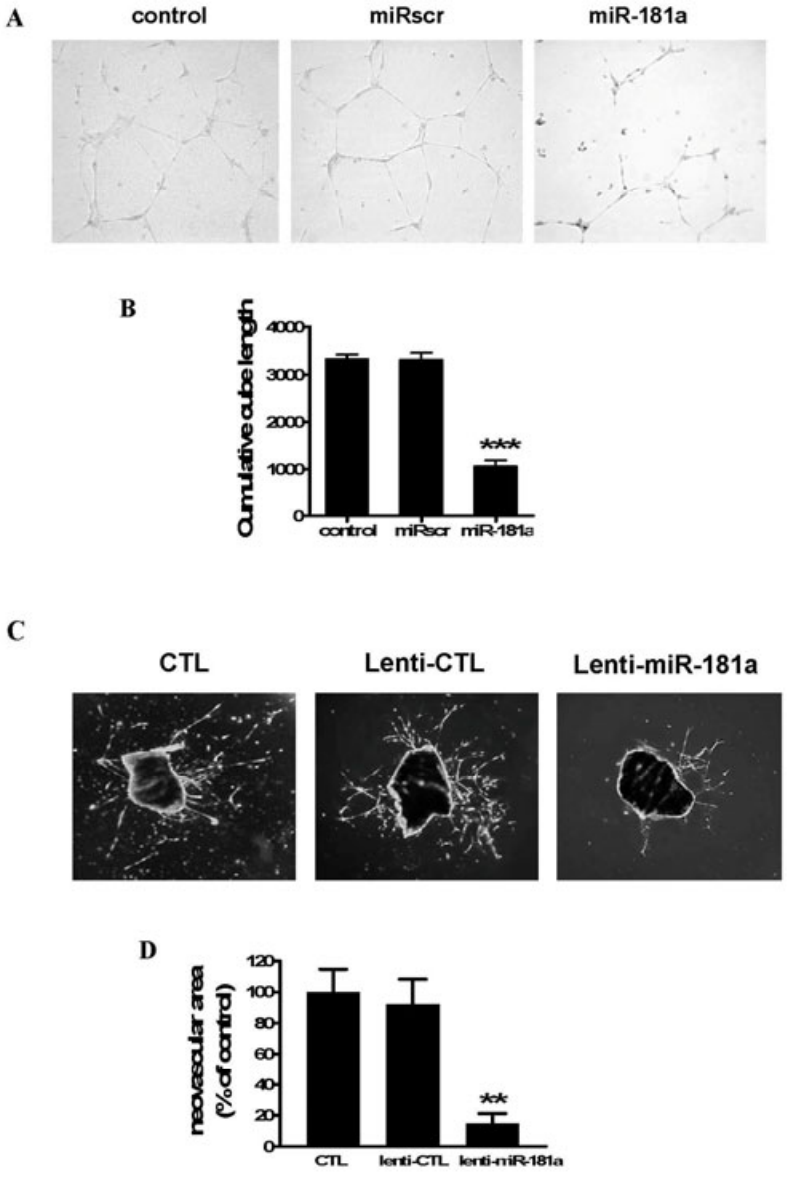


**Figure 3**

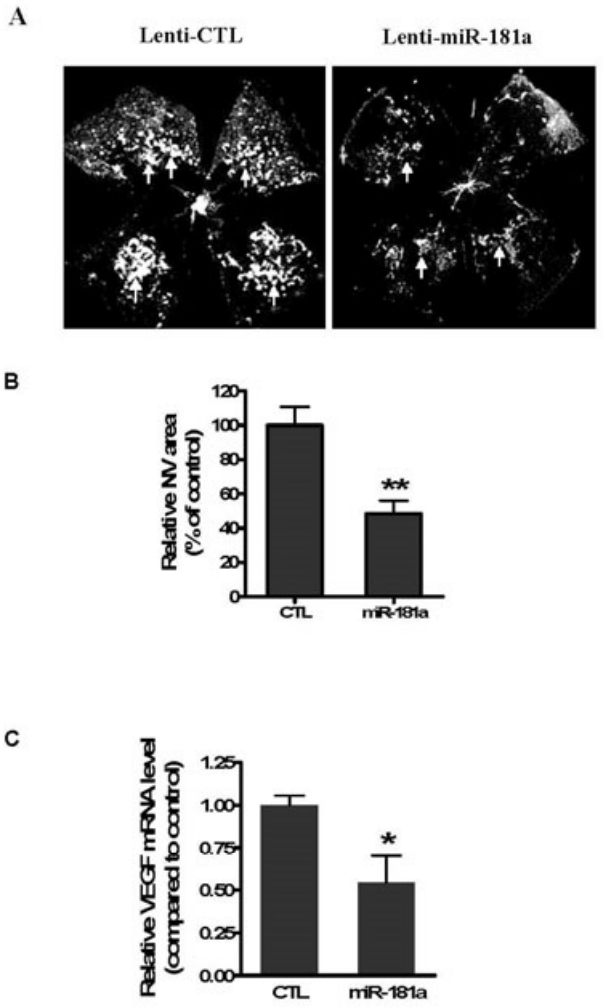


**Figure 4**

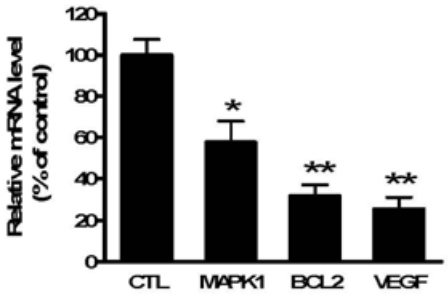


**Figure 5**